NMR Spectroscopic Studies on

Phosphoramidite Palladium Complexes:

Structures, Intermediates and Interaction Patterns

Dissertation

zur Erlangung des Doktorgrades

der Naturwissenschaften (Dr. rer. nat.)

an der Fakultät für Chemie und Pharmazie

der Universität Regensburg

vorgelegt von

Evelyn Hartmann

aus Schwandorf

2012

Die vorliegende Dissertation beruht auf Arbeiten, die im Zeitraum von November 2008 bis Mai 2012 am Institut für organische Chemie der Universität Regensburg unter der Leitung von Prof. Dr. Ruth Gschwind durchgeführt wurden.

Promotionsgesuch eingereicht am 04 .06.2012

Prüfungsausschuss:	Prof. Dr. Axel Jacobi von Wangelin	Vorsitzender
	Prof. Dr. Ruth M. Gschwind	1. Gutachter
	Prof. Dr. Kirsten Zeitler	2. Gutachter
	Prof. Dr. Otto S. Wolfbeis	3. Prüfer

Ich bin dann mal weg.

An dieser Stelle möchte ich allen danken, die zum Gelingen dieser Arbeit beigetragen haben. An erster Stelle sei hier meine Doktormutter Frau Prof. Dr. Ruth Gschwind erwähnt, der ich für die interessante und anspruchsvolle Themenstellung sowie die intensiven Diskussionen und letztendlich das Vertrauen in meine Arbeit danken möchte. Außerdem möchte ich mich recht herzlich bei Prof. Dr. Kirsten Zeitler für die Übernahme des Zweitgutachtens bedanken, sowie bei Prof. Dr. Otto Wolfbeis und Prof. Dr. Axel Jacobi von Wangelin für die Bereitschaft zur Ausübung des Amtes des Drittprüfers bzw. des Vorsitzenden.

Ich möchte mich auch recht herzlich bei allen Kollaborationspartnern bedanken, allen voran Dr. Katrin Schober. Desweiteren gilt mein Dank Dr. Tobias Thaler und Prof. Dr. Paul Knochel für die erfolgreiche Zusammenarbeit auf dem Thema der Negishi Kreuzkupplung sowie Thomas Hofbeck, Dr. Tobias Fischer und Prof. Dr. Hartmut Yersin für die interessante Kollaboration auf dem Gebiet der OLED-Emitter.

Mein ganz besonderer Dank gilt aber meinen lieben Kollegen am Arbeitskreis. Zum einen möchte ich mich bei euch dafür bedanken, dass ihr mir stets mit Rat und Tat kompetent zur Seite gestanden seid. Zum anderen habt ihr erheblich dazu beigetragen, dass der Spaßfaktor in den letzten vier Jahren durch die eine oder andere Pause, gut gepflegte, langjährige Traditionen oder durch spontane, verrückte Einfälle nicht zu kurz gekommen ist. Vielen lieben Dank daher an Dr. Guido Federwisch, Dr. Roland Kleinmaier und Dr. Tobias Gärtner, an Dr. Katrin Schober, Dr. Markus Schmid und Dr. Matthias Fleischmann, an Diana Drettwan, Maria Neumeier und Christian Feldmeier, Nils Sorgenfrei, Michael Haindl und Carina Koch, an Felicitas von Rekowski, Michael Hammer und unser neuestes AK-Mitglied Hanna Bartling.

Ein herzliches Dankeschön geht auch an die gesamte NMR-Abteilung, Fritz Kastner, Dr. Thomas Burgemeister und Dr. Ilya Shenderovich, Annette Schramm und Georgine Stühler für ihre Hilfsbereitschaft, wenn das Spektrometer mal wieder nicht so wollte wie ich wollte. Ich möchte auch Nikola Kastner-Pustet und Ulrike Weck für ihre freundliche Unterstützung in allen technischen und bürokratischen Fragen danken.

Zu guter Letzt möchte ich noch meinem Bruder Erwin recht herzlich danken für seine uneingeschränkte Unterstützung während der letzten Jahre. Ein herzliches Dankeschön geht auch an all meine Freunde, real oder imaginär, vor allem an Flow sowie an das gesamte Team der „13“ für die vielen schönen Abende, welche stets für die nötige Abwechslung sorgten.

Table of Contents

1 Introduction and Outline

Stereoselective functionalization of organic molecules is of great importance to modern synthesis. The accurate preparation of pharmaceutically active molecules is essential to ensure appropriate biological activity. Thereby, diastereoselective approaches are required for an efficient set-up of multiple stereocentres. In the field of asymmetric catalysis palladium-catalyzed C-C bond forming reactions find broad application in modern synthesis, such as in terms of the Stille or Sonogashira coupling reactions or the Heck, Negishi and Suzuki cross-couplings, which have recently been awarded with the Nobel Prize in 2010.

The key for a successful stereoselective functionalization of an organic molecule lies in the correct choice of a chiral ligand to control and direct the regio-, diastereo- and enantioselectivity. Therefore, a significant progress in the use of chiral monodentate phosphorligands could be observed in the last few years. Due to their high synthetic availability, high resistance to oxidation and low costs phosphoramidites have become an attractive alternative to the classical bidentate ligands - such as DIOP- and BINAP-derivatives - in asymmetric catalysis. In addition the modular structure of this privileged class of ligands enables an easy fine-tuning for specific carbon-carbon and carbon-heteroatom bond forming reactions.

Despite the broad applications of monodentate phosphoramidite ligands the secret of their success in asymmetric catalysis is not fully understood so far. Therefore the focus of this thesis centers upon structural investigations on different phosphoramidite palladium complexes, their ability to form inter- and intraligand interactions and the elucidation of intermediates in the Umpolung reaction.

In chapter 2 the general ability - or rather the affinity – for aggregation of three different phosphoramidite ligands and of their Cu-, Pd- and Ir-complexes is described. ^{1}H DOSY measurements were used to investigate temperature dependent aggregation trends in order to discuss similarities and differences between the obtained aggregation curves. A new fast and easy method for the optimization of catalysis in terms of reaction temperature in an early development state and its applicability is presented.

In chapter 3 the pseudo-bidentate character of two monodentate phosphoramidite ligands within palladium complexes is proven. For that purpose the *trans*-*cis*-isomerization driven by the formation of weak attractive interligand interactions is investigated on the

example of palladium complexes using homo- and heterocombinations of different phosphoramidite ligands. Complex structures are clarified upon the combinations of various 1D and 2D NMR spectra. Intra- and interligand CH-π and π-π interactions are resolved by a combination of NOESY spectra and chemical shift analysis. The retention of the general complex structure upon ligand variation is proven and the formation of interaction surfaces capable for CH-π andπ-π interactions is proposed. In addition the influence of the formation of weak interactions on rotational processes within the complexes is addressed.

In chapter 4 a new method for the quantitative determination of interligand interactions within transition metal complexes is presented. The proof of concept is given on the example of two phosphoramidite palladium complexes. In addition the structural differences in interaction pattern leading to the differences in interaction strength are discussed in detail upon NOESY spectra and chemical shift analysis.

In chapter 5 the reaction mechanism of the palladium catalyzed Umpolung reaction is investigated. Based on $^{1}H^{31}P$ HMBC and using a combination of various other 2D NMR spectra the complex structures of the intermediates in the different steps of the catalytic cycle are characterized. The focus of this study lies on the mechanistic differences using two diastereomeric phosphoramidite ligands providing different enantioselectivities in the investigated Umpolung reaction.

In chapter 6 the sterocontrol of a highly diastereoselective Csp^3-Csp^2 Negishi cross-coupling reaction is investigated. By using $^{1}H^{31}P$ HMBC spectra the selectivity determining palladium intermediate could be identified and, furthermore, by using proton decoupled 1D phosphor spectroscopy the complex structure of this intermediate was clarified.

In chapter 7 the aggregation trends of the highly efficient triplet emitter *fac*-Ir(ppy)$_3$ which finds broad application in organic light emitting diodes (OLEDs) is presented. By ^{1}H DOSY measurements the temperature and solvent dependency of the aggregation behavior of *fac*-Ir(ppy)$_3$ was investigated. In addition the different contributions of CH-π/π-π interactions versus dipole-dipole interactions verified by disaggregation studies are discussed.

2 Aggregation Studies on Phosphoramidite Ligands and their Transition Metal Complexes

^{1}H DOSY Spectra of Ligands for Highly Enantioselective Reactions – A Fast and Simple NMR Method to Optimize Catalytic Reaction Conditions

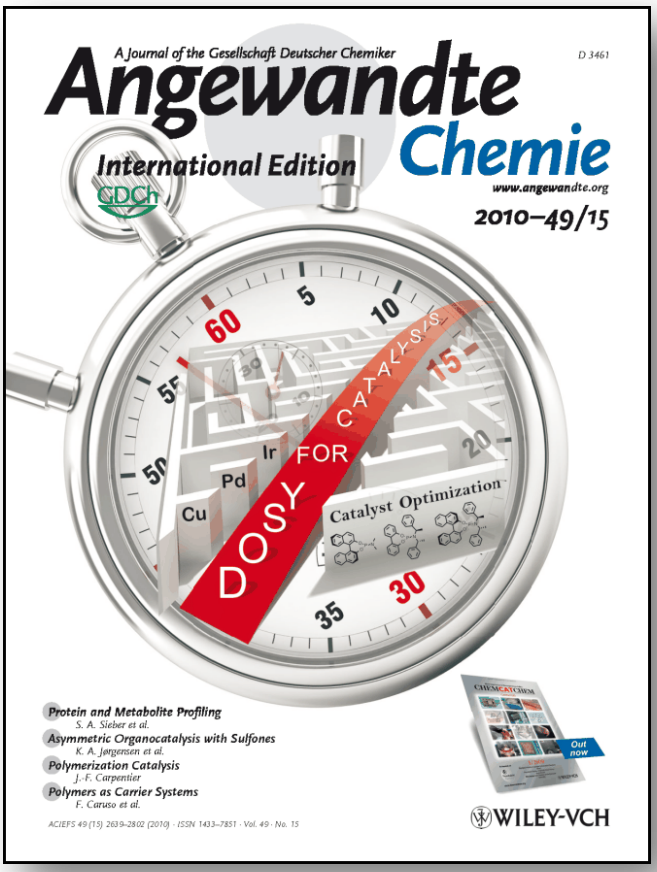

Katrin Schober, Evelyn Hartmann, Hongxia Zhang, and Ruth M. Gschwind

^{1}H DOSY studies of Pd and Ir complexes were performed by Evelyn Hartmann, ^{1}H DOSY studies of Cu complexes were performed by Hongxia Zhang, DNMR studies were performed by Katrin Schober

Angew. Chem. Int Ed. **2010**, *49*, 2794-2797

DOI: 10.1002/anie.20090724

2.1 Abstract

The development of highly enantioselective catalysts is a time-consuming process which is sometimes hampered by temperature dependent aggregation phenomena of the catalytic complexes. Therefore, the first self-aggregation studies of phosphoramidites and their transition metal complexes are reported and insights into the aggregation mechanism are presented. For complexes with highly enantioselective ligands, the aggregation of the transition metal complexes directly follows the aggregation behavior of the corresponding free ligand. In contrast, for complexes with small and moderately enantioselective ligands also other phenomena than ligand dominated aggregation can occur. Disaggregation studies, the interpretation of the aggregation curves, and DNMR analyses of the internal dynamic of the ligands revealed that rotational processes define the starting temperature of aggregation and allow insights into the different contributions of the aromatic systems to the aggregation. These results now open up a new screening possibility for a faster temperature optimization in the development of transition metal catalysts. For sterically demanding phosphoramidite ligands, which are suited for asymmetric catalysis, an easy and fast DOSY screening of the free ligand allows a reliable prediction of the temperature dependent aggregation behavior of its transition metal complexes. Even the contribution of different transition metals, complex stoichiometries, complex geometries, and additional ligands with low aggregation tendencies do not affect the predictability of aggregation. This independence of the structural knowledge of the catalytically active species makes this screening method so valuable for catalyst optimization procedures even in the early development stage.

2.5 Supporting Information

2.5.1 Sample preparation

All reactions were carried out under argon atmosphere in heat gun dried Schlenk flasks exclusively with freshly distilled solvents. CD_2Cl_2 was distilled from CaH_2. The ligands **1** and **2** were prepared according to reported protocols.[24] Ligand **3** was bought from Strem Chemicals. Copper, palladium and iridium complexes were prepared by adding solvent to a mixture of free ligand and metal salt. The solution was stirred at ambient temperature over 1 h, 2.5 h or 10 min and transferred into a NMR tube. The samples were kept at 193 K.

2.5.2 NMR Data Collection and Processing

The NMR spectra were recorded on a Bruker Avance DRX 600 (600.13 MHz) spectrometer equipped with a 5 mm broadband triple resonance Z-gradient probe (maximum gradient strength 53.5 Gauss/cm). All chemical shifts were referenced to TMS. Temperature stability was controlled by a BVT 3000 unit. The diffusion coefficients were calculated with the Bruker software package t1/t2. Dynamic NMR Simulations were performed with SpinWorks 2.5.5.[41-42]

2.5.3 ^{1}H Diffusion Studies

The aggregation studies in this paper are based on ^{1}H-DOSY measurements applying a pulse sequence developed by A. Jerschow and N. Müller.[43] The experimentally obtained diffusion coefficients were corrected with respect to temperature and viscosity using TMS as internal standard according to the literature known procedure.[44-45]

The corrected diffusion coefficients were used in the Stokes-Einstein equation to calculate the hydrodynamic radii:

$$r_H = \frac{kT}{6\pi\eta D}$$

The aggregation levels n were obtained by normalizing the obtained hydrodynamic volumes to that of the monomers for each ligand and complex, respectively. Either the experimental volume measured at ambient temperature was applied or the theoretical volume of the monomer which was calculated from hard sphere increments was used.[46]

2.5.4 Eyring Analysis

Data corresponding to the Eyring analysis in Figure 2.5 was calculated from the Eyring equation and the resulting values are listed in the following table:

$$k = \frac{k_B T}{h} \cdot \exp\left(-\frac{\Delta G^{\#}}{RT}\right)$$

Table 2.1. Data for the Eyring analysis.

compound	T / K	$\Delta S^{\#}$ / JK^{-1}mol^{-1}	$\Delta H^{\#}$ / kJmol^{-1}
1	280 – 220	-155	1
	220 – 180	18	40
2	280 – 230	-99	16
	230 – 180	68	55
[{Cu**2**Cl}$_3$]	270 - 180	12	43

2.5.5 Low Temperature ^{1}H NMR Studies

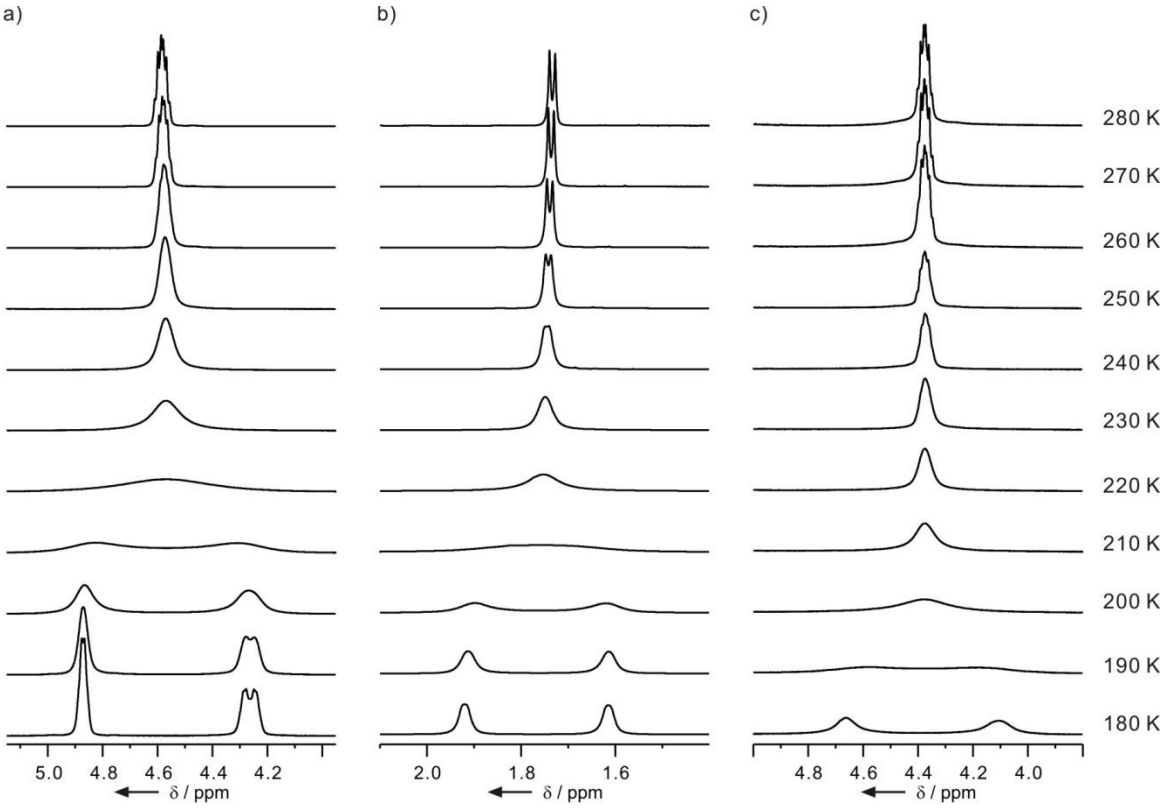

Figure 2.6: Sections from ^{1}H NMR spectra of a) CH group; b) CH_3 group of ligand **2**; c) CH group of ligand **1** in CD_2Cl_2 (0.02 M) at different temperatures.

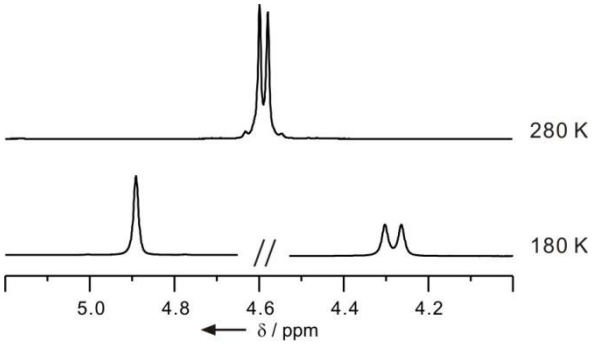

Figure 2.7: Methine sections of the $\{^1H\}^1H$ spectra of ligand **2** in CD_2Cl_2 (0.02 M) at 280 K and 180 K with homodecoupling of the adjacent CH_3 group. The spectra at 180 K revealed different $^3J_{HP}$ coupling constants of < 5 Hz and 23.5 Hz for the two methine groups.

2.5.6 Detailed Description of the Aggregation Trends in Fehler! Verweisquelle konnte nicht gefunden werden.

As expected for complexes with sterically less demanding ligands, which show only a moderate aggregation interaction, the aggregation curves of the transition metal complexes with **3** gives a more complex picture. In principle, four sets of curves can be differentiated. The first one, representing the complexes Cu**3**$_3$X (X = Cl, Br, I) and (Cu**3**Tc)$_2$, is marked orange in Figure 2.3. These coordinatively saturated complexes with a tetrahedral coordination sphere on copper show the same aggregation kink at 230 K as the free ligand. However, the absolute aggregation number is higher, most probably due to the increased number of possible interligand interactions in these complexes. The second set, representing the complexes Pd**3**$_4$Cl$_2$ and Ir(cod)**3**Cl, is marked green and grey and shows a low temperature shift of the kink to about 210 K. For Ir(cod)**3**Cl we assume that the rotational movements of the cod group counterbalance the small aggregation trend of **3** at higher temperatures. For Pd**3**$_4$Cl$_2$ we assume a saturation of the interligand interactions within the complex. The third set, representing the complexes (Cu**3**Cl)$_3$ and (Cu**3**Br)$_3$, is marked dark red and shows a slow but steadily trend to aggregation reaching higher aggregation numbers at 180 K compared to that of the free ligand. Based on this aggregation behavior and due to known crystal structures[47] we postulate a salt mediated polymerization forming ladder structures for these complexes.

2.6 References

[1] H.-U. Blaser, E. Schmidt, *Asymmetric Catalysis on Industrial Scale: Challenges, Approaches and Solutions*, Wiley-VCH, Weinheim, **2004**.

[2] V. Caprio, J. M. J. Williams, *Catalysis in Asymmetric Synthesis*, 2nd edition ed., Wiley, New York, **2009**.

[3] A. Mengel, O. Reiser, *Chem. Rev.* **1999**, *99*, 1191-1224.

[4] J. K. Whitesell, *Chem. Rev.* **1989**, *89*, 1581-1590.

[5] P. Walsh, M. Kowzlowski, *Fundamentals Of Asymmetric Catalysis*, University Science Books, **2008**.

[6] M. T. Reetz, *Angew. Chem., Int. Ed.* **2002**, *41*, 1335-1338.

[7] C. Gennari, U. Piarulli, *Chem. Rev.* **2003**, *103*, 3071-3100.

[8] K. Ding, *Chem. Commun.* **2008**, 909-921.

[9] H. Buschmann, H.-D. Scharf, N. Hoffmann, P. Esser, *Angew. Chem., Int. Ed.* **1991**, *30*, 477-515.

[10] B. Breit, *Angew. Chem., Int. Ed.* **2005**, *44*, 6816-6825.

[11] E. A. Meyer, R. K. Castellano, F. Diederich, *Angew. Chem., Int. Ed.* **2003**, *42*, 1210-1250.

[12] P. Dotta, A. Magistrato, U. Rothlisberger, P. S. Pregosin, A. Albinati, *Organometallics* **2002**, *21*, 3033-3041.

[13] A. Gillon, K. Heslop, D. J. Hyett, A. Martorell, A. G. Orpen, P. G. Pringle, C. Claver, E. Fernandez, *Chem. Commun.* **2000**, 961-962.

[14] S. Filipuzzi, P. S. Pregosin, A. Albinati, S. Rizzato, *Organometallics* **2006**, *25*, 5955-5964.

[15] K. Schober, H. Zhang, R. M. Gschwind, *J. Am. Chem. Soc.* **2008**, *130*, 12310-12317.

[16] B. L. Feringa, *Acc. Chem. Res.* **2000**, *33*, 346-353.

[17] A. Alexakis, C. Benhaim, *Eur. J. Org. Chem.* **2002**, 3221-3236.

[18] A. Alexakis, J. E. Bäckvall, N. Krause, O. Pàmies, M. Diéguez, *Chem. Rev.* **2008**, *108*, 2796-2823.

[19] S. R. Harutyunyan, T. den Hartog, K. Geurts, A. J. Minnaard, B. L. Feringa, *Chem. Rev.* **2008**, *108*, 2824-2852.

[20] A. J. Minnaard, B. L. Feringa, L. Lefort, J. G. de Vries, *Acc. Chem. Res.* **2007**, *40*, 1267-1277.

[21] Z. Hua, V. C. Vassar, H. Choi, I. Ojima, *Proc. Natl. Acad. Sci. U. S. A.* **2004**, *101*, 5411-5416.

[22] R. K. Thalji, J. A. Ellman, R. G. Bergman, *J. Am. Chem. Soc.* **2004**, *126*, 7192-7193.

[23] I. S. Mikhel, G. Bernardinelli, A. Alexakis, *Inorg. Chim. Acta* **2006**, *359*, 1826-1836.

[24] A. Alexakis, S. Rosset, J. Allamand, S. March, F. Guillen, C. Benhaim, *Synlett* **2001**, 1375-1378.

[25] L. A. Arnold, R. Imbos, A. Mandoli, A. H. M. de Vries, R. Naasz, B. L. Feringa, *Tetrahedron* **2000**, *56*, 2865-2878.

[26] Use of aggregated complex leads to lower conversion than the monomer in the copper-catalyzed conjugate addition with [Cu**3**Tc]$_2$.

[27] A. H. M. de Vries, A. Meetsma, B. L. Feringa, *Angew. Chem., Int. Ed.* **1996**, *35*, 2374-2376.

[28] H. Zhang, R. M. Gschwind, *Chem. Eur. J.* **2007**, *13*, 6691-6700.

[29] Chlorbenzene is ideal for this purpose, because it matches the dielectrict constant of the sovent CD_2Cl_2 and thus avoids compound-driven change of aggregation.

[30] G. Bellachioma, G. Ciancaleoni, C. Zuccaccia, D. Zuccaccia, A. Macchioni, *Coord. Chem. Rev.* **2008**, *252*, 2224-2238.

[31] D. Zuccaccia, G. Bellachioma, G. Cardaci, C. Zuccaccia, A. Macchioni, *Dalton Trans.* **2006**, 1963-1971.

[32] This close connection between interaction strength and reduction of dynamic processes is well known in molecular recognition processes and was also observed in NMR investigations of charge-assisted hydrogen-bond networks.

[33] G. Federwisch, R. Kleinmaier, D. Drettwan, R. M. Gschwind, *J. Am. Chem. Soc.* **2008**, *130*, 16846-16847.

[34] P. Ghosh, G. Federwisch, M. Kogej, C. A. Schalley, D. Haase, W. Saak, A. Lutzen, R. M. Gschwind, *Org. Biomol. Chem.* **2005**, *3*, 2691-2700.

[35] D. H. Williams, E. Stephens, D. P. O'Brien, M. Zhou, *Angew. Chem. Int. Ed.* **2004**, *43*, 6596-6616.

[36] M. I. Rodríguez-Franco, I. Dorronsoro, A. Castro, A. Martínez, *Tetrahedron* **2000**, *56*, 1739-1743.

[37] C. H. Bushweller, J. W. O'Neil, H. S. Bilofsky, *Tetrahedron* **1971**, *27*, 5761-5766.

[38] C. H. Bushweller, C. Y. Wang, J. Reny, M. Z. Lourandos, *J. Am. Chem. Soc.* **1977**, *99*, 3938-3941.

[39] M. J. S. Dewar, W. B. Jennings, *Tetrahedron Lett.* **1970**, *11*, 339-342.

[40] C. Monti, C. Gennari, U. Piarulli, *Chem. Eur. J.* **2007**, *13*, 1547-1558.

[41] G. Binsch, H. Kessler, *Angew. Chem. Int. Ed.* **1980**, *19*, 411-428.

[42] K. Marat, Spinworks 2.5.5 ed., **2006**.

[43] A. Jerschow, N. Muller, *J. Magn. Reson.* **1997**, *125*, 372-375.

[44] E. J. Cabrita, S. Berger, *Magn. Reson. Chem.* **2001**, *39*, 142-148.

[45] A. Macchioni, G. Ciancaleoni, C. Zuccaccia, D. Zuccaccia, *Chem. Soc. Rev.* **2008**, *37*, 479-489.

[46] D. Ben-Amotz, K. G. Willis, *J. Phys. Chem.* **1993**, *97*, 7736-7742.

[47] P. M. Graham, R. D. Pike, M. Sabat, R. D. Bailey, W. T. Pennington, *Inorg. Chem.* **2000**, *39*, 5121-5132.

3 Structures and Interligand Interaction Patterns of Phosphoramidite Palladium Complexes

NMR Insight into the Structural Features of a Privileged Class of Ligands

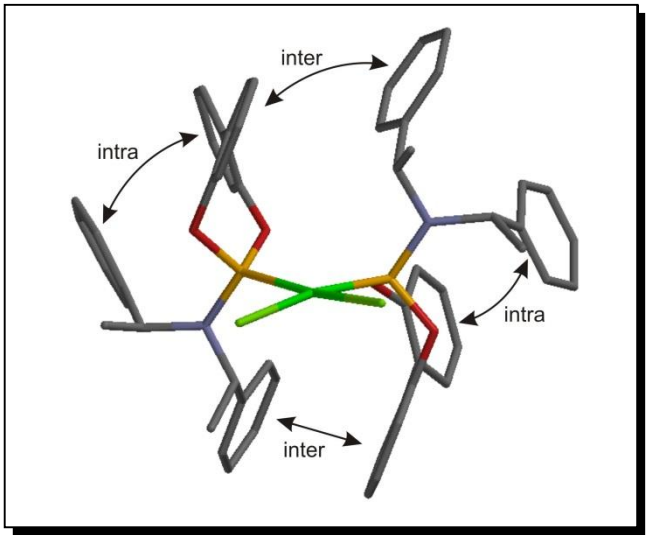

Evelyn Hartmann, and Ruth M. Gschwind

Molecular electrostatic potential surfaces were calculated by Michael Hammer.

To be submitted.

3.1 Abstract

Supramolecular interactions based on dispersive interactions between monodentate ligands are still insufficient investigated to use them for rational ligand design in transition metal catalysis. A structural screening of different homo- and hetero-phosphoramidite palladium complexes by ^{1}H chemical shift analysis and $^{1}H^{1}H$ NOESY experiments proved the formation of altogether four interaction sites in each complex – two inter- and two intraligand interaction sites. Moreover the additivity of these interaction sites mainly based on CH-π and π-π interactions and the retention of the general complex structure for all ligand combinations is experimentally shown. In addition the formation of a planar interaction surface of the chiral amine side chains of the investigated phosphoramidte ligands is proposed and a new concept of interaction modes of these surfaces as an explanation for the high stereoselectivity of these ligands in asymmetric catalysis is discussed. Furthermore the coexistence of inter- and intraligand interactions and rotational processes within the ligands is described.

3.2 Introduction

For a long time bidentate ligands have been the ligands of choice in asymmetric catalysis since in 1972 Kagan achieved best enantioselectivity in a Rh catalyzed hydrogenation reaction using a chiral diphosphine ligand.[1] In the following years the development of C_2-symmetric bidentate phosphorus ligands such as DIOP- and BINAP-derivatives dominated the field of asymmetric catalysis. The superiority of bidentate ligands was explained by the higher conformational rigidity of the ligands and a stronger coordination to the metal. However, for some transition-metal catalyzed reactions chelating bidentate ligands turned out to be unsuitable. Therefore, it was merely a matter of time when monodentate ligands would have their revival.[2-6] One important landmark of this development was in 1997 when Feringa and co-workers introduced a new class of phosphoramidite ligands in Cu-catalyzed C-C-bond forming reactions using ligand **1** (see Scheme 3.1).[7-8]

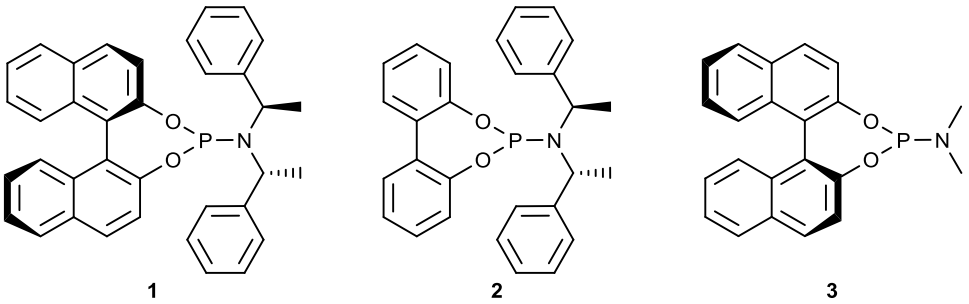

Scheme 3.1. Phosphoramidite ligands developed by Feringa and Alexakis.[7-9]

The replacement of the achiral amine group of the initially used ligand **3**[7] by the chiral and sterically more demanding (R,R)-bis-(phenylethyl)-amine led to a drastical improvement of the enantioselectivity in 1,4-additions of R_2Zn to cyclic enones with *ee*-values up to 98%.[9-10] While the matched diastereomer (S_a,R_c,R_c)-**1** provides high enantioselectivities, the mismachted diastereomer (S_a,S_c,S_c)-**1** gives only moderate results.[8] Upon these findings, Alexakis developed tropos phosphoramidite ligand **2** (see Scheme 3.1) based on the principle of induced atropisomerism:[11-12] The smaller biphenol group is able to rotate around the C-C-bond and therefore can switch between both conformers.[13] The amine group is supposed to induce atropisomerism on this flexible biphenol unit which therefore adopts the matched conformation leading to also excellent enantioselectivities in Cu-catalyzed conjugate additions.[14] After these developments monodentate phosphoramidite ligands became more and more popular in asymmetric synthesis due to their easy synthetic availability, low costs and air-stability.[6] Today, they find broad application in various transition metal catalyses[6] e.g. they are used in Cu-catalyzed conjugated additions of dialkyl zinc reagents to enones mentioned above,[7-10, 13-14] in Rh(I) catalyzed asymmetric hydrogenation and hydroformylation,[15-17] in Ir-catalyzed allylic substitutions[18-21] and in Pd-catalyzed allylic alkylation or Heck reactions.[22-24] An essential advantage of monodentate ligands in general lies in the possibility of combining two structurally simple monodentate ligands (chiral/chiral or chiral/achiral), which avoids the laborious and also time-consuming synthesis of structurally more complex bidentate ligands and therefore opens up a new period of metal catalysis. With the use of combinatorial chemistry, libraries of new catalysts can be generated and tested in a fast and easy manner.[25-27] First successful results have been reported independently by Feringa et al.[28] and Reetz et al.[29] in 2003: Heterocombinations ML_aL_b of different BINOL-based monophosphonites, monophosphites and monosphosphoramidites achieved respectable selectivity in Rh catalyzed hydrogenation and in several cases even excelled the corresponding homocomplexes. An often observed excess formation of heterocomplex

compared to the corresponding homocomplexes when using a mixture of ligands and the preferred formation of sterically less favored *cis*-Pd and *cis*-Pt complexes using monodentate ligands soon indicated the formation of weak interligand interactions.[30-32] In the last few years a growing interest in rational ligand design could be observed. Monodentate ligands have been developed which are able to self-assemble in the coordination sphere of the metal center through the formation of weak ligand-ligand interactions, such as hydrogen bonding[33-38] or metal bridged coordinative bonding.[25, 39-41] However, to the best of our knowledge, CH-π interactions or π-π stacking have not been applied for rational ligand design so far. Therefore, despite the vast progress on the field of rational ligand design in the last few years there is still a high demand for detailed structural investigations in order to gain a better understanding of the variety of ligand-ligand interactions so that the whole range of interactions – also including CH-π interactions and/or π-π stacking - can be exploited for rational ligand design.

Recent studies in our working group on the aggregation behavior of phosphoramidite ligands **1**-**3** as well as of their transition metal complexes (M = Cu, Ir and Pd) as a function of temperature by ^{1}H DOSY NMR measurements proved the general ability, or rather the tendency, of these ligands to form intermolecular interactions.[42] In case of highly enantioselective ligands **1** and **2** the aggregation trends of the complexes are predominantly determined by the ligands and almost independent of the metal or even the complex structure. However, in case of less enantioselective ligand **3** aggregation of the complexes was not ligand dominated. Structural investigations showed that the reduced bulkiness of the amine moiety in ligand **3** enables the formation of higher coordinated metal complexes [43-44] which in turn leads to oligomerization at low temperatures. Furthermore, mechanistic studies revealed that in case of ligand **1** and **2** π-π as well as CH-π interactions may play a decisive role for aggregation. Although rotation of the phenyl groups within the amine moiety also has influence on aggregation, these rotational processes are hardly affected by complexation so that aggregation trends of the complexes are similar to those of the free ligands.

Based on these studies, herein, we present structural investigations on different phosphoramidite Pd complexes and their affinity to form attractive interligand CH-π and π-π interactions. Characteristic interaction patterns have been investigated on isomeric ligand combinations by NMR studies and in addition rotational processes within the ligands and their influence on inter- and intraligand interactions are addressed.

3.3 Results and Discussion

Model systems. For the investigation of interligand interactions homo- and hetero-Pd complexes have been selected using different isomeric forms of phosporamidite ligands **1** and **2** (see Scheme 3.2b).

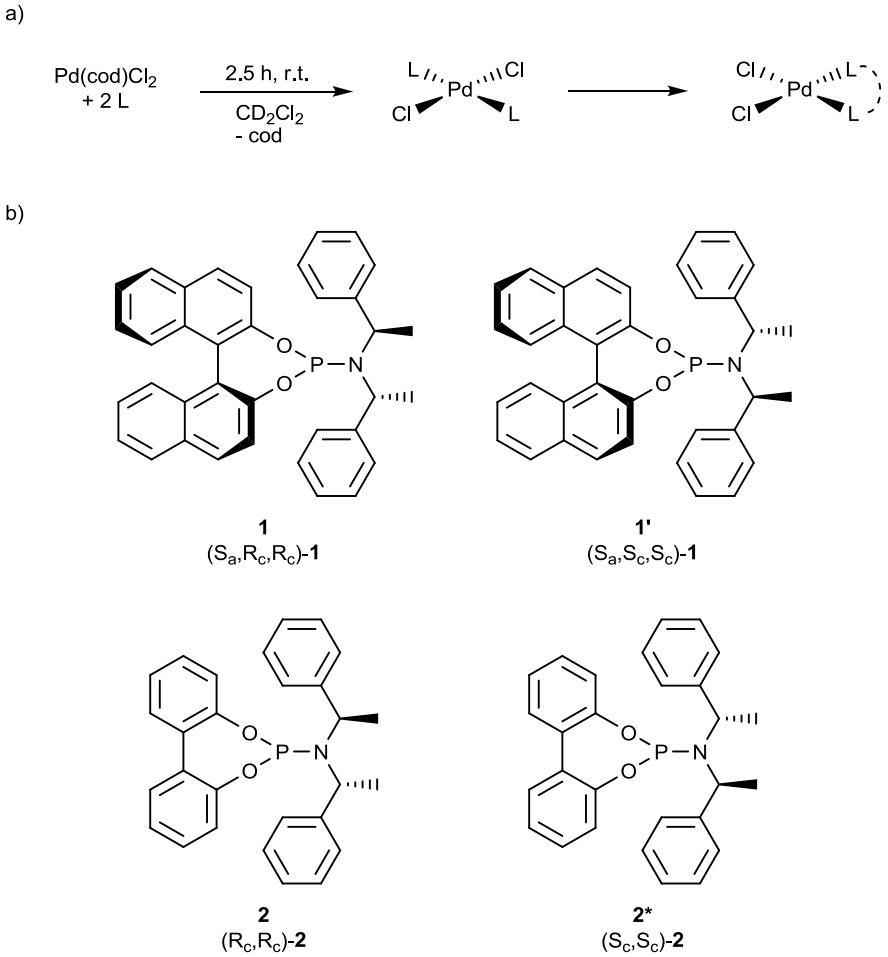

Scheme 3.2. a) Synthesis of phosphoramidite palladium complexes *trans*-PdL_2Cl_2 followed by the isomerization to *cis*-PdL_2Cl_2 and the formation of ligand-ligand interactions. b) Phosphoramidites used in this study.

Despite the vast structural knowledge about phosphoramidite Cu complexes in our working group[43-45] copper did not become the metal of choice for the investigation of ligand-ligand interactions because ligand exchange processes within Cu complexes is too fast on the NMR time scale for detailed structural investigations. Furthermore, basic structural knowledge about the Pd complexes was already available from aggregation studies: Phosphoramidite ligands **1** and **2** form palladium complexes with a composition of PdL_2Cl_2 (L = **1**, **2**). The ligand-to-metal ratio of 2:1 was proven by ^{31}P, ^{1}H, ^{13}C and ^{1}H DOSY NMR measurements.[46] However, phosphoramidite **3** forms a palladium complex containing four ligands, which also was verified by NMR.[47] Therefore, only ligands **1** and **2** were

selected for this study. Moreover, X-ray diffraction analysis by Alexakis and co-workers of the phosphoramidite palladium complex Pd**2***$_2$Cl$_2$ showed that exclusively the *cis*-isomer is formed in the crystal structure[48] which additionally made phosphoramidite palladium complexes become an attractive and also very promising model complex for the investigation of ligand-ligand interactions.

For the identification of the complex configuration – *cis*- or *trans*-PdLL'Cl$_2$ – and for the discrimination between inter- vs. intraligand interactions heterocomplexes were investigated. For that purpose altogether four different ligand combinations were selected: Pd(**1**)(**2**)Cl$_2$, Pd(**1**)(**2***)Cl$_2$, Pd(**1'**)(**2**)Cl$_2$ and Pd(**1**)(**1'**)Cl$_2$. The first two of these complexes were chosen to test if a combination of structurally almost identical ligands **1** and **2** or the quasi enantiomeric ligand combination **1** and **2*** fits better in shape and to investigate the resulting changes in interaction pattern. For a comparison between the diastereomeric ligands **1** and **1'** heterocomplex Pd(**1'**)(**2**)Cl$_2$ was also investigated. Complex Pd(**1**)(**1'**)Cl$_2$ was selected because of the reduced flexibility of the binaphthol groups within both ligands **1** and **1'** and its influence on heterocomplex formation. For reason of simplification of NMR signal assignment homocomplexes PdL$_2$Cl$_2$ (L = **1**, **1'**, **2** and **2***) have also been investigated. Because of the high structural symmetry within PdL$_2$Cl$_2$ both ligands are chemically equivalent and therefore show only one ^{31}P complex signal and only one set of ^{13}C/^{1}H signals. In addition homocomplexes Pd**2**$_2$Cl$_2$ and Pd**2***$_2$Cl$_2$ using enantiomeric ligands **2** and **2*** showed identical ^{31}P, ^{13}C and ^{1}H signals. For all investigations a ligand-to-Pd ratio of 2 : 1 have been used, which is also usually applied in asymmetric synthesis. The end of complex formation could be determined by NMR by a complete release of cod and a complete conversion of free ligand (see Scheme 3.2a).

Complex formation and *trans-cis* isomerization. For all investigated systems the formation of exclusively *trans*-complexes were observed, which subsequently completely isomerized into the corresponding *cis*-complexes. This *trans-cis* isomerization will exemplarily be described on ligand combination **1/2**. When using a mixture of ligands **1** and **2** altogether three complex species are formed, one heterocomplex Pd(**1**)(**2**)Cl$_2$ and the corresponding two homocomplexes PdL$_2$Cl$_2$ (L = **1**, **2**). After complex synthesis both homocomplexes show one singlet each, whereas the heterocomplex shows two doublet signals in the ^{31}P spectrum (see Figure 3.1a, and c for spectra simulations). The coupling pattern of the heterocomplex can hardly be realized at the first glance due to a very pronounced roof effect of both ^{31}P signals. However, spectra simulation confirmed that the very small signals at the edges of the spectrum also belong to the coupling pattern of

Pd(**1**)(**2**)Cl_2 (Figure 3.1c). The large coupling constant $^2J_{PP}$ of 1168 Hz lies at the upper limit of coupling constants typical for a *trans*-orientation of both phosphoramidite ligands within the complexes.[49-50]

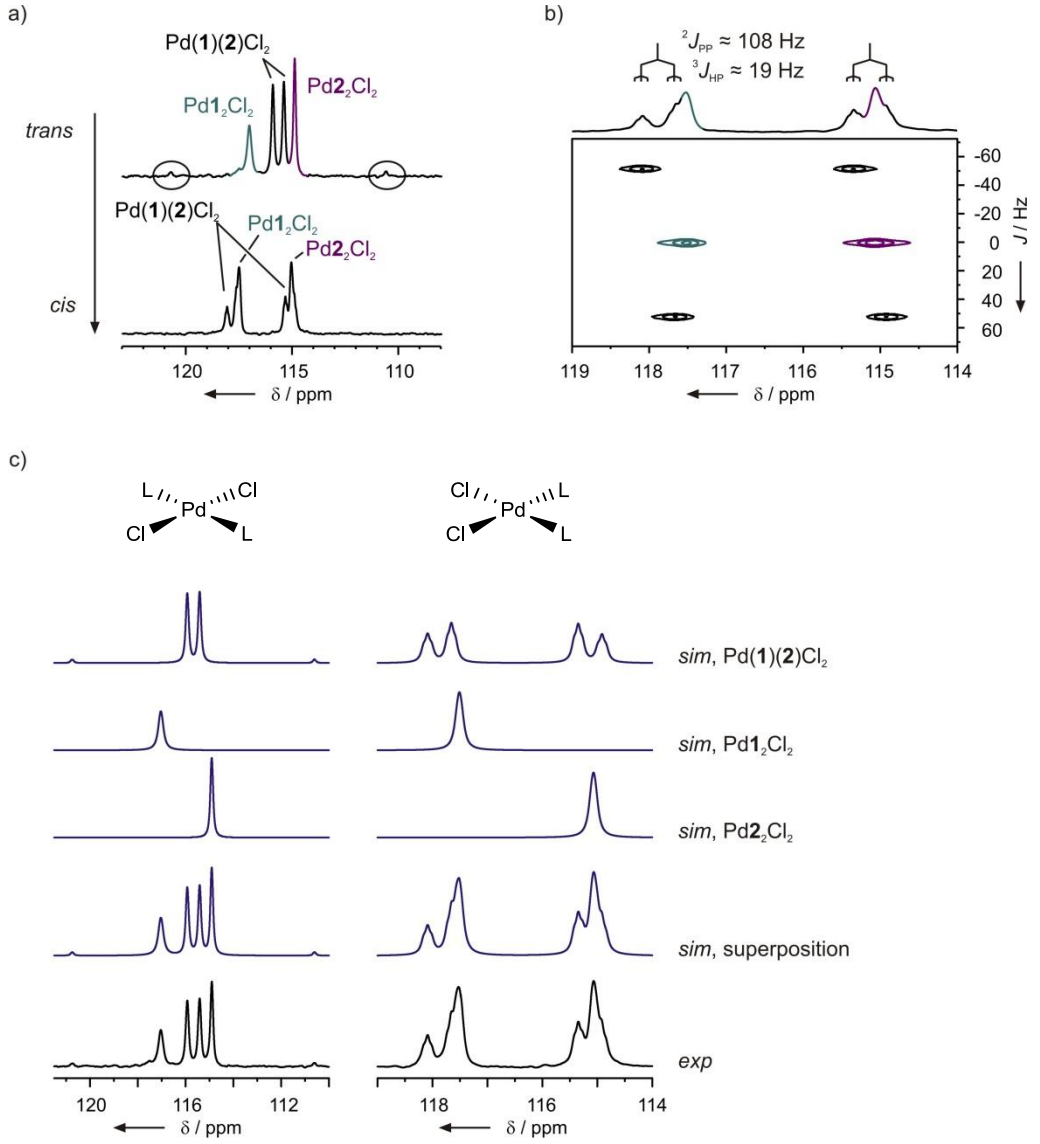

Figure 3.1. a) ^{31}P spectra of Pd(**1**)(**2**)Cl_2 and corresponding homocomplexes PdL_2Cl_2 (L = **1**, **2**) showing the *trans*-*cis*-isomerization and b) a *J*-resolved ^{31}P spectrum of the same sample after the complete conversion into *cis*-complexes. ^{31}P signals of homocomplexes are coloured. c) ^{31}P spectra of *trans*- and *cis*-complexes (black) and spectra simulations (blue).

Low temperature NMR measurements revealed that the ^{31}P signals of *trans*-Pd(**1**)(**2**)Cl_2 and those of the corresponding homocomplexes become broader with decreasing temperature and finally split up into several different complex signals (see Figure 3.2). The ^{31}P and also ^{1}H signals of these different complex species overlap for the most part and in addition aggregation phenomena at low temperature, rotational processes and conformational exchange causes a significant broadening of the ^{1}H signals, which

additionally impairs signal resolution.[42] Nevertheless some important structural information about these complex species could be gained: As no release of ligand was observed with decreasing temperature a temperature-dependent interconversion into other complex species as observed for phosphoramidite copper complexes in our working group[45] could be excluded. Moreover no $^2J_{PP}$ coupling pattern typical for a *cis*-configuration of both ligands could be detected at 180 K. Therefore a possible isomerization into *cis*-complexes at low temperatures was also excluded. In addition the large coupling constant $^2J_{PP}$ of 1168 Hz measured at 300 K lies at the upper limit of $^2J_{PP}$ constants typical for a *trans*-orientation of two phosphorus ligands in a Pd(II) complex.[49-50] That confirms that at the beginning exclusively *trans*-complexes are formed and excludes a possible partial formation of *cis*-complexes. All these data indicate that the different complex species are most probably just conformational isomers which means that in *trans*-Pd(**1**)(**2**)Cl_2 no strict conformation is preferred but several conformations are populated.

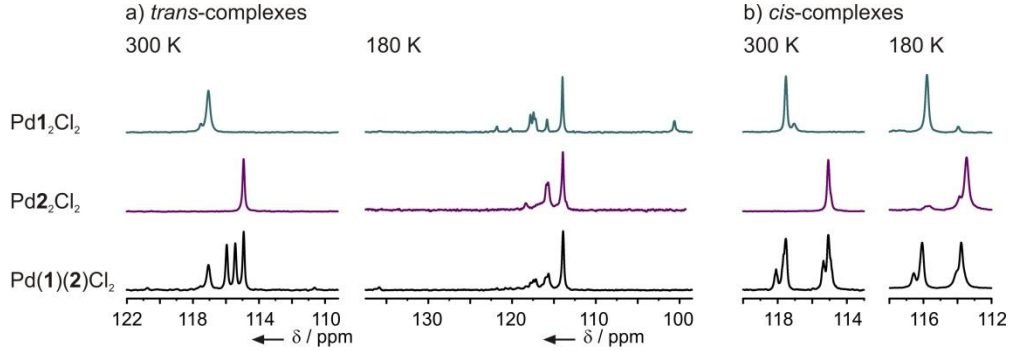

Figure 3.2. ^{31}P NMR spectra of a) *trans*- and b) *cis*-Pd(**1**)(**2**)Cl_2 (black spectra, also including homocomplexes) and ^{31}P spectra of homocomplexes Pd**1**$_2Cl_2$ (green) and Pd**2**$_2Cl_2$ (purple) at 300 K and at 180 K.

Gradually all *trans*-complexes irreversibly and completely convert into corresponding *cis*-complexes (see Figure 3.1a) which is connected with a slight decrease in size. That can be shown on the example of Pd**2**$_2Cl_2$ with a reduction of the hydrodynamic volume from 1020 Å^3 to 941 Å^3 determined by ^{1}H DOSY measurements. The ^{31}P signals of both homocomplexes are shifted a little bit downfield but remain singlets. The two doublets of *trans*-Pd(**1**)(**2**)Cl_2 completely convert into two doublets of triplets partially overlapped by the ^{31}P signals of the corresponding homocomplexes (Figure 3.1a). A *J*-resolved ^{31}P spectrum and spectra simulation confirmed these coupling patterns (Figure 3.1b and c). The coupling constant of Pd(**1**)(**2**)Cl_2 ($^2J_{PP}$ = 118 Hz) lies within the range typical for a *cis*-orientation of two phosphorus ligands in Pd(II) complexes.[49-50] The triplet splitting of 19 Hz derives from the $^3J_{HP}$ coupling of phosphor with both CH groups within one phosphoramidite ligand. This unusually quite large $^3J_{HP}$ value alludes to oriented dihedral

angles PNCH near 0° or 180°, which indicates a preferred conformational arrangement of both ligands in the *cis*-complex. In addition, low temperature investigations revealed that the ^{31}P complex signals of the *cis*-complexes do not split up upon cooling down but remain sharp signals even at 180 K (Figure 3.2). Thus - in contrast to the *trans*-complexes - there exists only one specific conformation for each *cis*-homo- and *cis*-heterocomplex with a clear defined minimum of free energy. In case of a *trans*-coordination several different ligand arrangements and interactions within the complex are possible, which differ only little in energy. Therefore a greater variety of conformational isomers can be observed for the *trans*-complexes. In contrast, the spatial proximity of the ligands in the *cis*-complexes seems to limit the ligand arrangement to such an extent that only one conformation is preferred and consequently only one complex species is detected.

The observed *trans*-*cis* isomerization is extremely slow at room temperature and takes several days, which is in accordance with reports for isolated Pd complexes in non-coordinating solvents.[51] However, under reaction conditions the presence of neutral ligands or other additives (e.g. iodides RI) accelerates isomerization processes. In agreement with these studies, further investigations confirmed that the conversion of *trans*-PdL_2Cl_2 into *cis*-PdL_2Cl_2 (L = **1** or **1'**) is much faster under reaction conditions: The addition of a small amount of Et_2Zn in toluene showed a strong acceleration of the conversion of *trans*-PdL_2Cl_2 into *cis*-PdL_2Cl_2 (data not shown, see chapter 5).

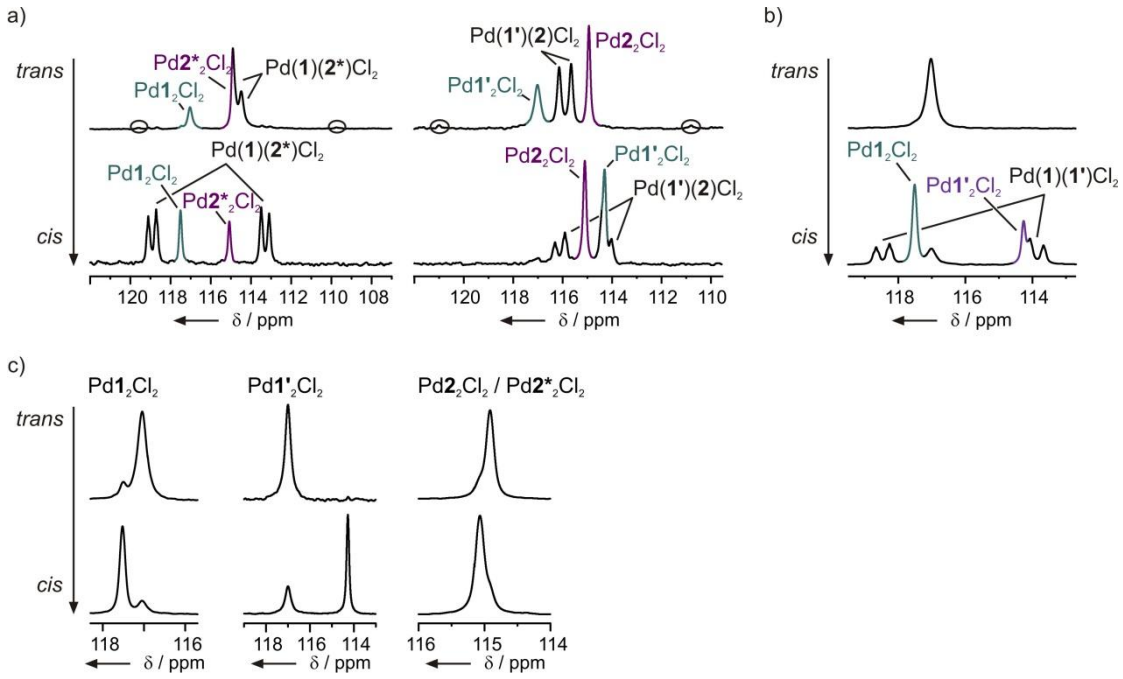

Figure 3.3. ^{31}P spectra of *trans*- and *cis*-complexes using a mixture of ligands a) **1/2*** and **1'/2** and b) **1/1'** (signals of homocomplexes are colored) and c) of homocomplexes using ligand **1**, **1'** and **2** or **2*** (left to right, spectra of enantiomeric complexes $Pd\mathbf{2}_2Cl_2$ and $Pd\mathbf{2*}_2Cl_2$ are identical).

Identical observations have been made using ligand combinations **1**/**2***, **1'**/**2** and **1**/**1'**. After complex synthesis exclusively *trans*-complexes are formed which subsequently and completely convert into the corresponding *cis*-complexes (Figure 3.3). Again, complex configurations were proven by appropriate $^2J_{PP}$ coupling constants of the heterocomplexes (see Table 3.1). Low temperature NMR measurements showed that for all *trans*-complexes again several conformational isomers exist in solution (data not shown). In contrast, for the *cis*-complexes only one conformation is preferred which is also in accordance with the larger $^3J_{HP}$ coupling constants for the *cis*-complexes (see NMR data in SI). Although ^{31}P signals of *trans*-complexes using a combination of ligand **1** and **1'** overlap completely (Figure 3.3b), the formation of both homo- and heterocomplexes could be proven by 2D NMR spectroscopy: In both COSY and NOESY spectra in total four cross signals between the CH and respective CH_3 groups have been observed, one for each homocomplex and two for the heterocomplex (one for each ligand) (see Figure 3.18 in SI).

Table 3.1. Homo-to-heterocomplex ratios and $^2J_{PP}$ coupling constants for all investigated ligand combinations in *cis*- and *trans*-configuration.

	PdL_2Cl_2 : PdL'_2Cl_2 : $Pd(L)(L')Cl_2$		$^2J_{PP}$ [Hz]	
	trans	*cis*	*trans*	*cis*
Pd(**1**)(**2**)Cl_2	1 : 1.2 : 2.2	1 : 1.1 : 2.1	1168	118
Pd(**1**)(**2***)Cl_2	1 : 1.2 : 3.5	1 : 0.9 : 4.5	1151	96
Pd(**1'**)(**2**)Cl_2	1 : 1 : 1.8	1 : 1 : 1.4	1180	97
Pd(**1**)(**1'**)Cl_2	n.d.	n.d.	n.d.	97

For all complexes investigated so far – homo- and heterocomplexes - ^{31}P signals of the ligands are shifted either upfield or downfield by the isomerization from *trans*- to *cis*-Pd complexes. In case of homocomplexes PdL_2Cl_2 using ligand **1** or tropos ligand **2** or **2*** the complex signals are shifted only a little bit downfield by about 0.1 to 0.5 ppm, whereas the complex signal using ligand **1'** is shifted into the other direction and to a larger extent by more than 2.7 ppm (Figure 3.3c). For ligand **1** and **1'** the same trends can be observed in the heterocomplexes. Thus, the greatest chemical shift difference of ^{31}P complex signals is observed for Pd(**1**)(**1'**)Cl_2 (Figure 3.3b). However, the direction into which the ^{31}P signal of ligand **2** or **2*** is shifted seems to be dependent on the ligand combination. In combination with ligand **1** the ^{31}P signal of ligand **2** and **2*** is hardly shifted by $\Delta\delta$ = 0.6 ppm downfield in Pd(**1**)(**2**)Cl_2 and by $\Delta\delta$ = 0.4 ppm upfield in Pd(**1**)(**2***)Cl_2 (see Figure 3.1 and Figure 3.3a). However, in Pd(**1'**)(**2**)Cl_2 the ^{31}P signal of **2** experiences a downfield-shift by $\Delta\delta$ = 1.3 ppm by the isomerization from *trans* to *cis* (Figure 3.3a). Thus, if the ^{31}P signal is shifted upfield or downfield by the *trans*-*cis* isomerization depends on the ligand itself and on the ligand

combination. As a result, this detailed NMR investigation of a series of phosphoramidite Pd complexes showed that a larger downfield or upfield ^{31}P chemical shift cannot generally be correlated to an either *trans*- or *cis*-configuration as previously proposed in literature.[52]

Structural properties of *trans*- and *cis*-complexes and interligand interactions. In the crystal structure of Pd**2***$_2Cl_2$ (Figure 3.4), published by Alexakis[48] and co-workers, the biphenol groups of all phosphoramidite ligands adapt the matched R_a conformation and, moreover, exclusively *cis*-isomers are detected.

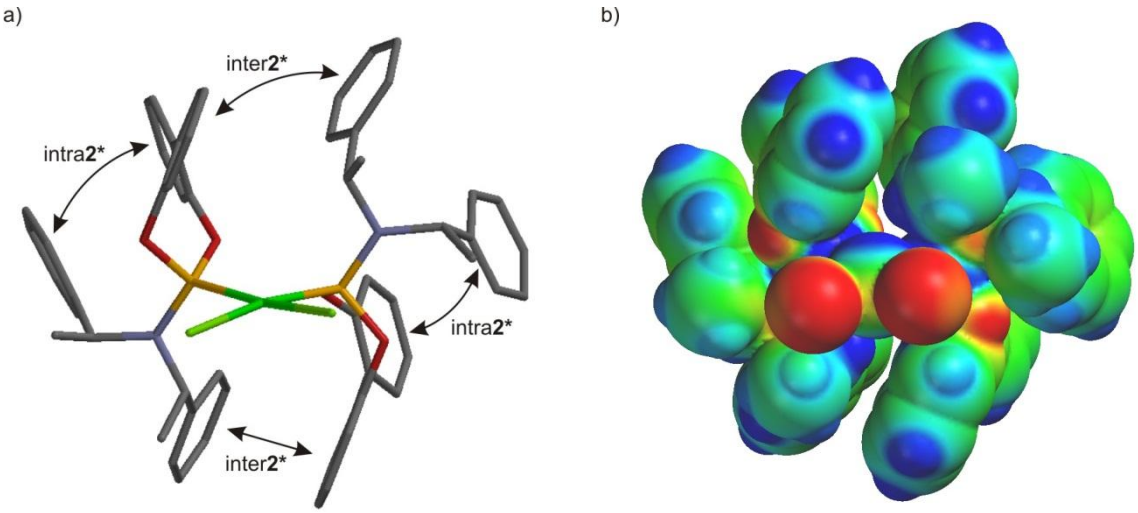

Figure 3.4. a) Crystal structure of *cis*-Pd**2***$_2Cl_2$ published by Alexakis.[48] Arrows mark inter- and intraligand interactions. b) Molecular electrostatic potential surfaces plotted on the van der Waals' surface of *cis*-Pd**2***$_2Cl_2$ (IsoVal value -0.3) calculated at an AM1 level of theory. Positive regions are shown in blue (140 kJ mol^{-1}), negative regions are shown in red (-230 kJ mol^{-1}).

A closer analysis of the crystal structure reveals that one amine side chain is in spatial proximity to the biphenol unit of the other ligand suggesting interligand CH-π interactions and π-π stacking (see inter**2*** in Figure 3.4a). At the same time, the second amine side chain is directed towards the biphenol group of the own ligand indicating intraligand π-π stacking (see intra**2*** in Figure 3.4a). Similar interaction patterns have also been reported by Pregosin[53] using ligand **1**: In the crystal structure of the allyl Pd cation $[PdCl(CH_2H(CH_3)CH_2)\mathbf{1}_2]BF_4$ one amine side chain of both ligands is involved into interligand interaction with the binaphthol group of the other ligand. In addition, within one of these ligands intraligand interactions between the second amine side chain and the own binaphthol group are formed. These observations suggest that inter- and intraligand interaction patterns are basically identical in different complex species using either ligand **1** or **2**. This raised the question if these interaction patterns can be observed exclusively in the crystal structures or if similar structural motifs and ligand arrangements can also be

observed in solution. For that purpose, the crystal structure of *cis*-Pd**2***$_2$Cl$_2$ was compared with NMR data of the same complex in solution.

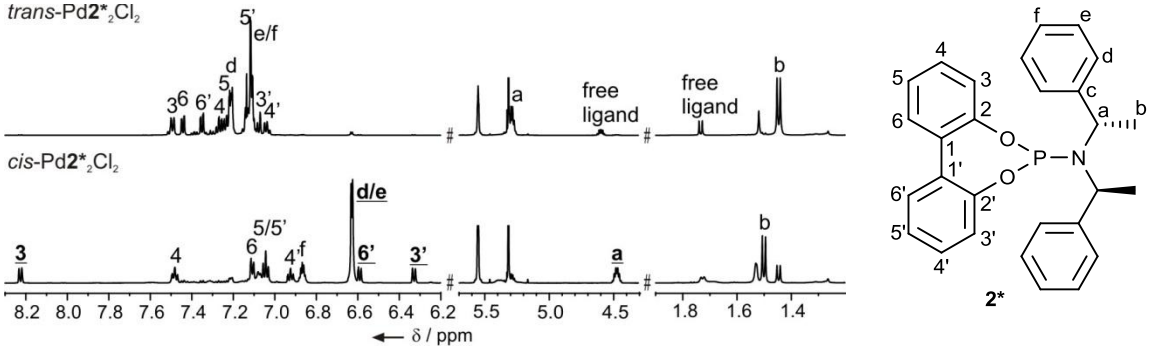

Figure 3.5. Comparison of ^{1}H spectra of *trans*- and *cis*-Pd**2***$_2$Cl$_2$ with full signal assignment to ligand **2***. Significant changes in chemical shifts (bold and underlined) provide information about the involvement into CH-π interactions or π-π stacking.

A comparison of the ^{1}H spectra of the *trans*- and *cis*-isomer provides first rough information about the structure and interactions within *cis*-Pd**2***$_2$Cl$_2$ (Figure 3.5): The aromatic signals of the biphenol group split up over a significantly larger chemical shift dispersion for the *cis*-isomer than for the *trans*-isomer indicating a stronger involvement into inter- and intraligand interactions (see for example 3 and 3' in Figure 3.5). In addition, the ^{1}H signals of the phenyl group (d-f) and of the methine group (a) experience a significant upfield-shift by the *trans*-*cis* isomerization. The crystal structure of Pd**2***$_2$Cl$_2$ suggests interligand interactions between the amine side chain of one ligand and the biphenol group of the other ligand (see inter**2*** in Figure 3.4a). This corroborates with the observed upfield-shift of the methine signal (a) and the strong downfield-shift of 3 and, to a less extent, of 4 of the biphenol group caused by the formation of interligand CH-π interactions. Moreover, the strong upfield-shift of the phenyl group (d-f) and signals of the other group of the biphenol unit (3' and 6') indicate π-π stacking within one ligand. This is also in absolute agreement with the crystal structure of Pd**2***$_2$Cl$_2$, in which the phenyl group of the second amine side chain of each ligand is involved into intraligand π-π stacking with the own biphenol group (see intra**2*** in Figure 3.4a). As there is only one set of ^{1}H signals for the amine moiety, the rotation around the P-N bond must still be fast on the NMR time scale despite the involvement into different interactions. Thus ^{1}H chemical shifts of the amine group are averaged values for both amine side chains reflecting both intra- and interligand interactions.

Interaction pattern within *cis*-heterocomplexes. To distinguish between inter- and intraligand interactions and to gain more insight into complex structures different ligand combinations have been investigated. As each ligand in one heterocomplex shows one set of ^{1}H signals, interligand NOE contacts could also be used to analyze the complex structure and the interaction pattern for different ligand combinations. It turned out that for all *cis*-complexes the general complex structure is identic with very similar interaction patterns which highly resemble the crystal structure of Pd**2***$_2$Cl$_2$ (compare Figure 3.4a): In each complex there are two intra- and two interligand interaction sites. Interligand interactions are always located between one amine side chain of one ligand (a-f) and a part of the biaryl group of the other ligand (labelled 1, 2, etc.), while the second amine side chain is involved into intraligand interactions with a part of the own biaryl group (labelled 1', 2', etc.). In addition, for all homo- and heterocomplexes a not negligible upfield-shift of the methine signal by about $\Delta\delta(^1H) = 0.8$ to 1.2 ppm can be observed by the *trans*-*cis* isomerization. This suggests that within each complex the methine group is involved into interligand CH-π interactions with the biaryl group of the other ligand (labelled 1, 2, etc.) causing a shielding ring current effect on the methine signal. This close orientation of the methine group towards the interligand interface is the sterically most favored orientation for all ligand combinations and allows optimized contact areas and interactions between both ligands (see Figure 3.4b).

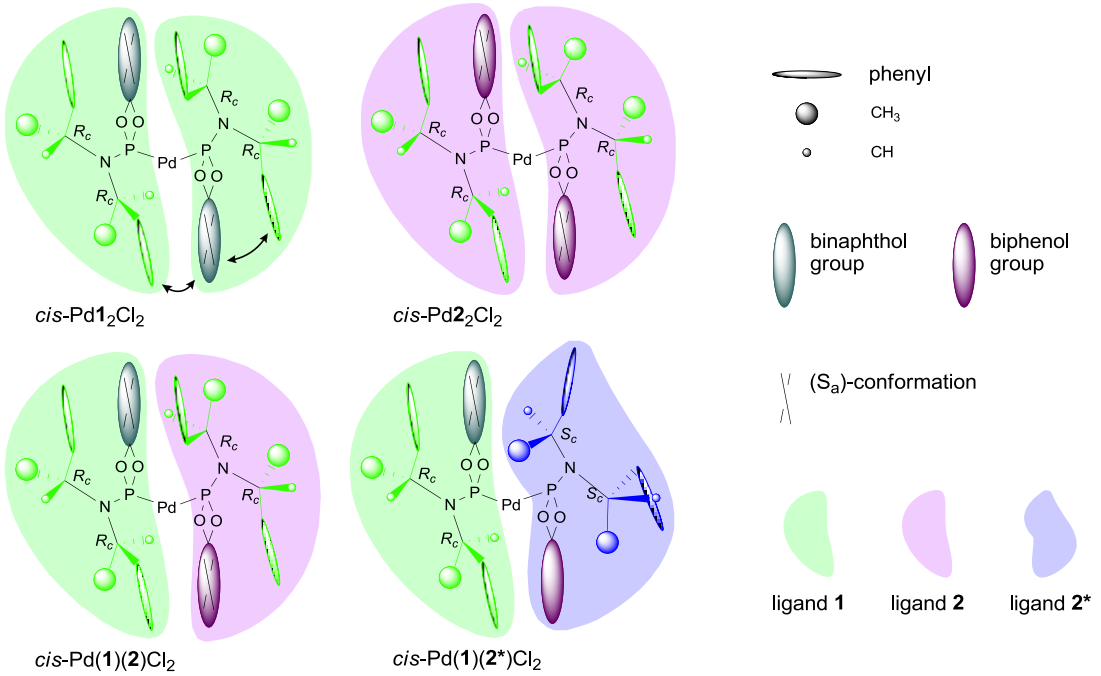

Figure 3.6. Schematic illustration of heterocomplexes *cis*-Pd(**1**)(**2**)Cl_2 and *cis*-Pd(**1**)(**2***)Cl_2 and homocomplexes *cis*-Pd**1**$_2Cl_2$ and *cis*-Pd**2**$_2Cl_2$ for comparison of inter- and intraligand interactions sites.

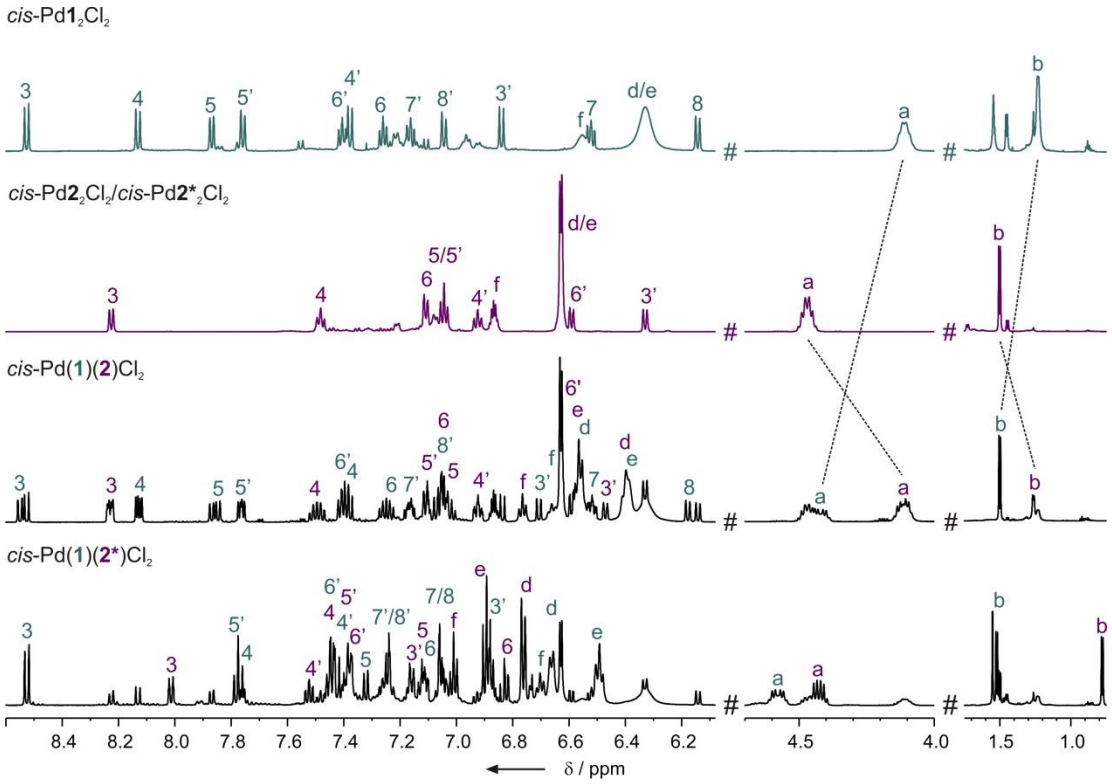

Figure 3.7. Comparison of ^{1}H spectra of heterocomplexes *cis*-Pd(**1**)(**2**)Cl_2 and *cis*-Pd(**1**)(**2***)Cl_2 (black spectra, also including the corresponding homocomplexes) with a ^{1}H signal assignment to the heterocomplexes (green: ligand **1**, purple: ligand **2** or **2***) with the ^{1}H spectra of the homocomplexes *cis*-PdL_2Cl_2 (green: L = **1**, purple: L = **2** or **2***, ^{1}H spectra are identic for both enantiomers) for chemical shift analysis.

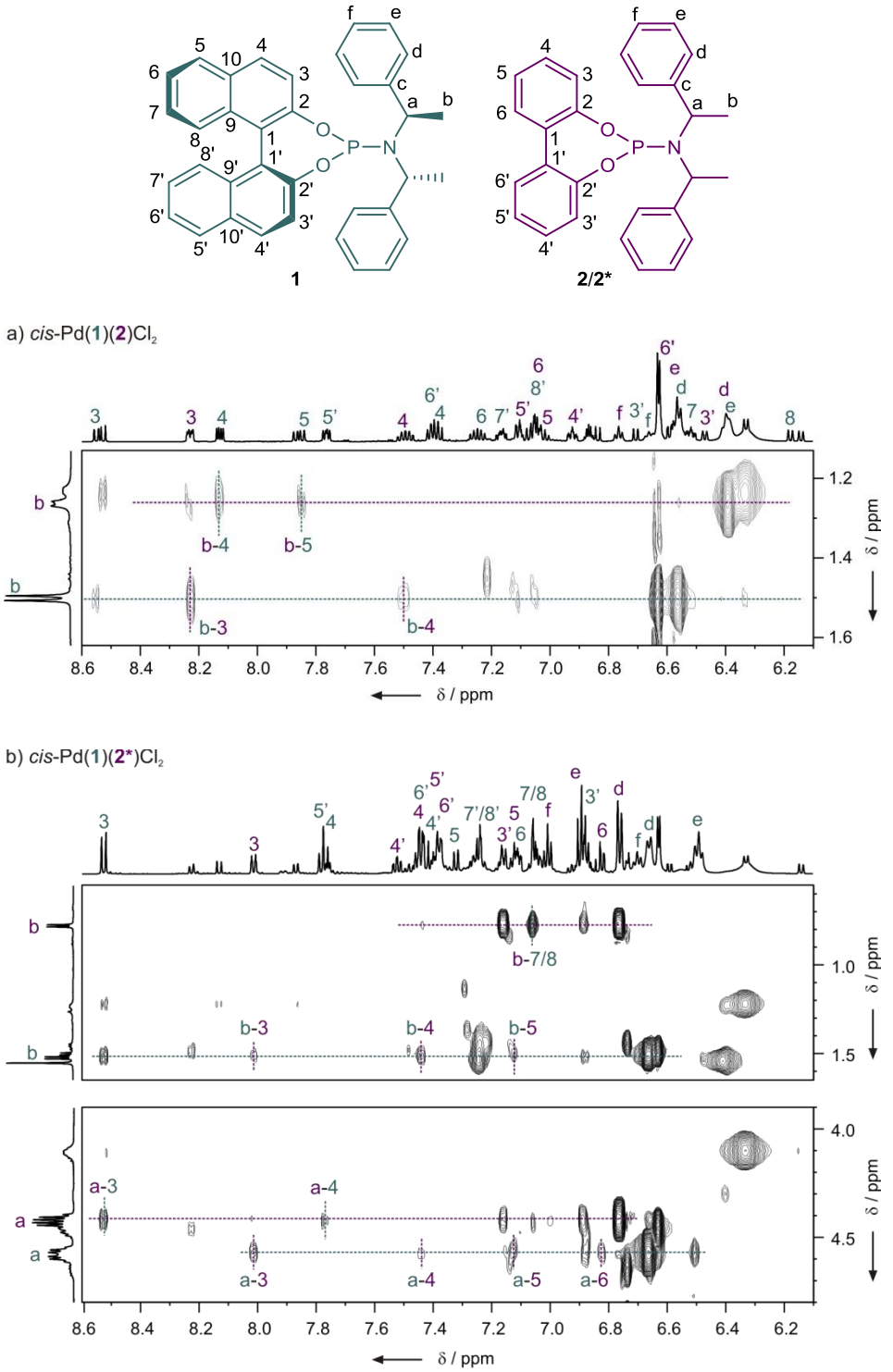

Figure 3.8. $^{1}H^{1}H$ NOESY spectra of a) *cis*-Pd(**1**)(**2**)Cl_2 and b) *cis*-Pd(**1**)(**2***)Cl_2 with a ^{1}H signal assignment to the heterocomplexes (green: ligand **1**, purple: ligand **2** or **2***). Interligand NOE contacts within the *cis*-heterocomplexes are highlighted with dotted lines.

First, ligand combinations of matched ligand **1** with the two enantiomers **2** and **2*** will be analyzed and compared. In *cis*- Pd(**1**)(**2**)Cl_2 both ligands are structurally almost identical, possess an identical amine group but differ only in the size of their biaryl groups. According to induced atropisomerism both biaryl compounds also possess the same

conformation. In contrast, the amine groups of ligand **1** and **2*** in *cis*-Pd(**1**)(**2***)Cl_2 are enantiomeric. Concerning heterocomplex *cis*-Pd(**1**)(**2**)Cl_2 strong upfield-shifts of the methine groups of both ligands already indicate the involvement of these groups into CH-π interactions. Distinctive interligand NOEs between the methyl group (b) of ligand **2** and a part of the binaphthol group (4/5) of ligand **1** and also strong NOEs between the methyl group of ligand **1** (b) and a part of the biphenol group (3/4) of ligand **2** (see Figure 3.8a) confirm the close proximity of one amine side chain of each ligand to the biaryl backbone of the other ligand in *cis*-Pd(**1**)(**2**)Cl_2. In addition the upfield-shifts of the phenyl signals (d, e, f) of both ligands also suggest the involvement of the phenyl groups in inter- and intraligand π-π stacking with parts of the different biaryl groups (see upfield-shift of 7/8 of ligand **1** and 3' of ligand **2** in Figure 3.7). Chemical shift analyses $\Delta\delta(^1H)$ reveals that interactions in *cis*-Pd(**1**)(**2**)Cl_2 are very similar to the corresponding *cis*-homocomplexes PdL_2Cl_2 (L = **1**, **2**) (for illustration see Figure 3.6). For both ligands the ^1H signals of the biaryl groups are nearly identical for homo- and heterocomplexes, whereas the methine and methyl signals of ligand **1** and **2** in *cis*-Pd(**1**)(**2**)Cl_2 are quasi exchanged compared to the spectra of the corresponding homocomplexes (dotted lines in Figure 3.7c): Since the amine moiety is identical in both ligands the chemical shifts of their methine and methyl signals are mainly determined by the groups they are interacting with. Based on the interaction pattern observed in the crystal structure, one amine side chain is involved into intraligand interaction with the own biaryl group. However, this intraligand interaction mainly encompasses π-π stacking between one phenyl group of the amine moiety and a part of the biaryl backbone so that the CH and CH_3 groups are hardly involved into intraligand interactions. However, the second amine side chain interacts with the biaryl group of the other ligand including CH-π interactions of the methine and methyl groups. Thus, predominantly interligand interactions have to be taken into account for the averaged absolute ^1H chemical shift of the CH and CH_3 groups. In the heterocomplex *cis*-Pd(**1**)(**2**)Cl_2 the interligand interacting biaryl group has changed compared to the corresponding *cis*-homocomplexes so that one amine side chain of ligand **1** interacts with the biphenol group of ligand **2**, while one amine side chain of ligand **2** interacts with the binaphthol group of ligand **1** (see Figure 3.6). This exchange of interligand interacting partner causes the observed exchange of ^1H signals. In contrast, the interacting partner of the biaryl backbone, the amine group, is identical for both ligands in the hetero- and homocomplexes. Therefore the ^1H signals of the biaryl groups of both ligands in *cis*-Pd(**1**)(**2**)Cl_2 are nearly identical with those of the corresponding *cis*-homocomplexes.

Concerning heterocomplex *cis*-Pd(**1**)(**2***)Cl_2 chemical shift analysis reveals that there is hardly any inter- or intraligand π-π stacking between the phenyl group of ligand **2*** and a part of the binaphthol group of ligand **1** or the biphenol group of the own ligand **2** as it was observed for *cis*-Pd(**1**)(**2**)Cl_2 (Figure 3.7). Instead the methyl group of ligand **2** experiences a strong upfield-shift by the *trans-cis* isomerization, which indicates the formation of strong CH_3-π interactions. Thus, a change from *cis*-Pd(**1**)(**2**)Cl_2 to *cis*-Pd(**1**)(**2***)Cl_2 causes the replacement of both inter- and intraligand π-π stacking between the phenyl group of ligand **2** and parts of the biaryl groups of ligand **1** and **2** by two CH_3-π interactions between the methyl group of ligand **2** and the biaryl groups of ligand **1** and **2**. These interaction changes are also confirmed by appropriate chemical shift changes $\Delta\delta(^1H)$ of the corresponding interacting biaryl groups, which will not be discussed in detail (for detailed description see chapter 4).

As the main difference between **2** and **2*** is the configurational change of the amine group, the observed changes in interaction patterns between *cis*-Pd(**1**)(**2**)Cl_2 and *cis*-Pd(**1**)(**2***)Cl_2 are restricted to interactions which involve the amine moiety of ligand **2** and **2***. The change from **2** to **2*** can be described by a mutual exchange of the phenyl and the methyl group which causes the observed substitution of π-π stacking by CH_3-π interactions (see Figure 3.6). In contrast, the methine group is directed towards the interligand interface in both heterocomplexes causing the observed upfield-shift by the *trans-cis* isomerization. As already explained by reference to the crystal structure this orientation allows for maximum interligand contact (Figure 3.4b).

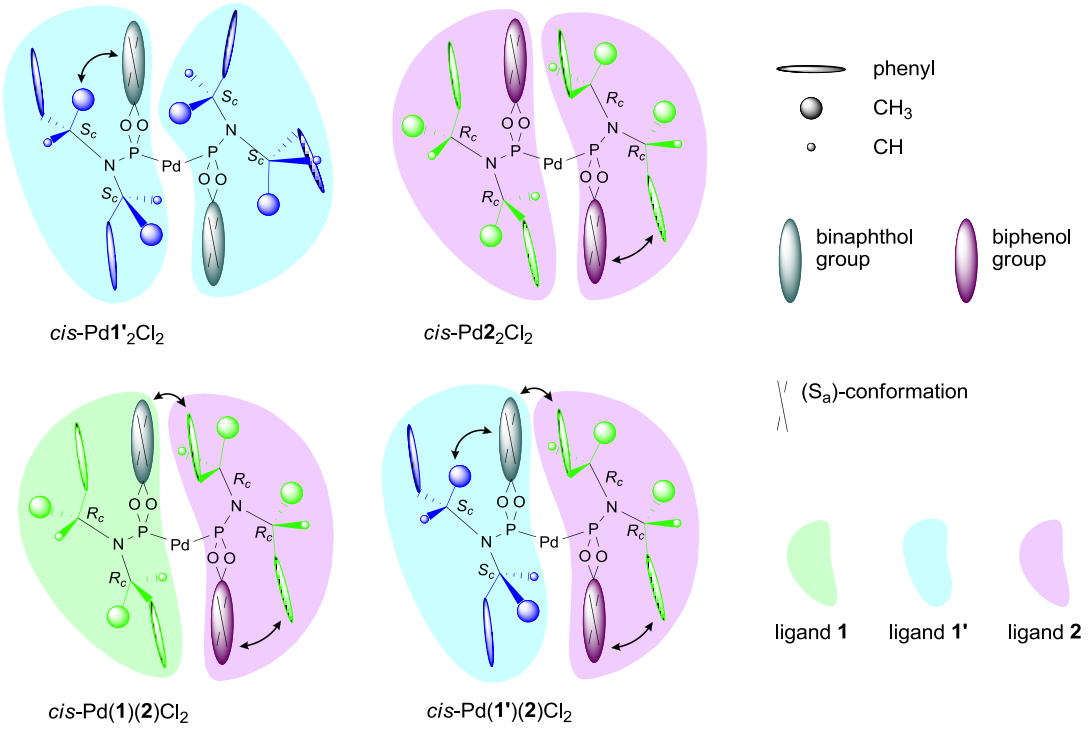

Figure 3.9. Schematic illustration of heterocomplexes *cis*-Pd(**1'**)(**2**)Cl_2 and *cis*-Pd(**1**)(**2**)Cl_2 and homocomplexes *cis*-Pd**1'**$_2Cl_2$ and *cis*-Pd**2**$_2Cl_2$ for comparison of inter- and intraligand interactions sites.

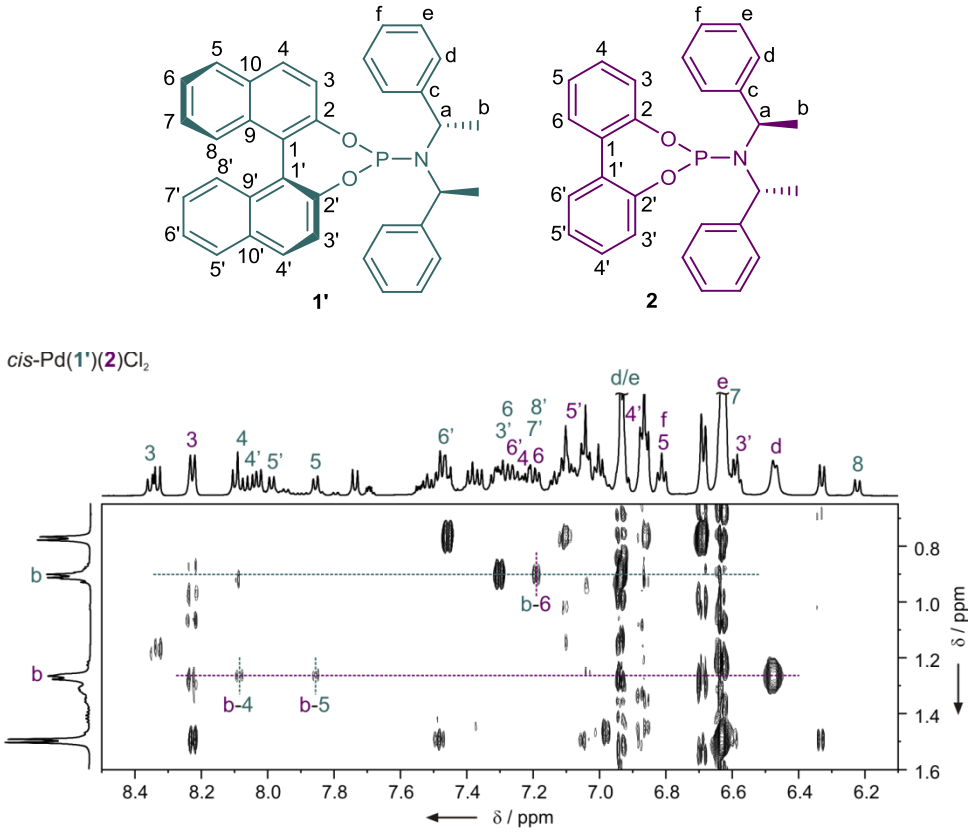

Figure 3.10. Section of a $^1H^1H$ NOESY spectrum of *cis*-Pd(**1'**)(**2**)Cl_2 and corresponding *cis*-homocomplexes with a signal assignment to the heterocomplex (green: ligand **1'**, purple: ligand **2**). Interligand NOE contacts within the *cis*-heterocomplex are highlighted with dotted lines.

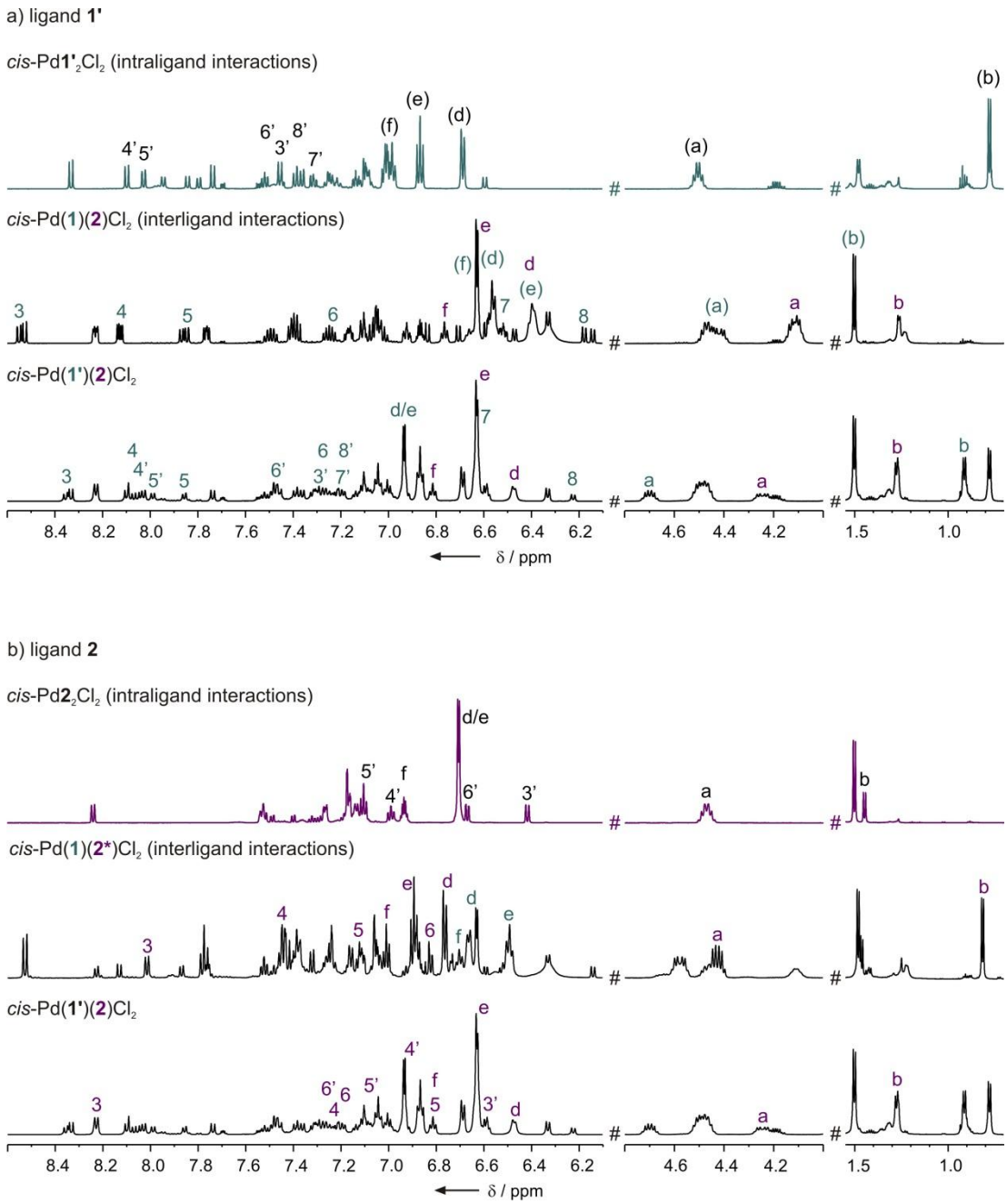

Figure 3.11. Chemical shift analysis for a) ligand **1'** and b) ligand **2** by a comparison of the ^{1}H spectrum of *cis*-Pd(**1'**)(**2**)Cl_2 with those of *cis*-Pd(**1**)(**2**)Cl_2 and *cis*-Pd**1'**$_2Cl_2$ for ligand **1'** and with *cis*-Pd(**1**)(**2***)Cl_2 and *cis*-Pd**2**$_2Cl_2$ for ligand **2**. Similar chemical shifts for the biaryl and amine groups of different complexes prove the retention of the general complex structure and distinct interaction pattern between identical functional groups (^{1}H signal assignment to the *cis*-heterocomplexes green: ligand **1** and **1'**, purple: ligand **2**).

Next, the combination of ligands **1'** and **2** will be discussed. Concerning ligand **1'** - under retention of the general complex structure - interligand interactions between the (S_a)-binaphthol group of **1'** and the (R_c,R_c)-amine group of ligand **2** in *cis*-Pd(**1'**)(**2**)Cl_2 should be similar to the corresponding interligand interaction in *cis*-Pd(**1**)(**2**)Cl_2 (see Figure 3.9) because of identical configurations and conformations of the interacting groups. Indeed, identical interligand NOE contacts within both heterocomplexes (compare b-4/5 in Figure

3.8a and Figure 3.10) confirm an extremely similar ligand arrangement. In addition, ^{1}H chemical shifts of the naphthol group (3, 4, 5, etc.), which is involved into interligand interactions with the amine group of ligand **2**, are very similar to those of ligand **1** in *cis*-Pd(**1**)(**2**)Cl_2 (see Figure 3.11a), which again confirms the retention of the general complex structure and interaction pattern. In addition, ^{1}H chemical shifts of the interacting amine group of ligand **2** (a-f) are also almost identical (see purple signal assignments a-f in Figure 3.11a): Within both complexes *cis*-Pd(**1'**)(**2**)Cl_2 and *cis*-Pd(**1**)(**2**)Cl_2 the inter- and intraligand interactions are identical (see Figure 3.9), thus the averaged ^{1}H signals of both amine side chains show very similar chemical shifts. The second naphthol group of **1'** (3', 4', 5', etc.) is expected to be involved into intraligand interactions, which should be identical to intraligand interactions within the corresponding homocomplex *cis*-Pd**1'**$_2Cl_2$. A comparison of ^{1}H spectra confirms, that ^{1}H chemical shifts of that naphthol group are indeed almost identical for *cis*-Pd(**1'**)(**2**)Cl_2 and *cis*-Pd**1'**$_2Cl_2$ (see Figure 3.11a). As to the amine group some deviations can be observed. Since only intraligand interactions are identical within both complexes, but interligand interactions of the second amine side chain of **1'** in *cis*-Pd(**1'**)(**2**)Cl_2 and *cis*-Pd**1'**$_2Cl_2$ are different, averaged ^{1}H signals of the amine groups show some differences.

Concerning ligand **2,** with exception of proton 3, the split-up of its aromatic signals is less distinct, which suggests the formation of weaker interactions in general (Figure 3.11b). The ^{1}H signals of its biphenol part (1-6), which is involved into interligand interactions with the amine side chain of ligand **1'**, are expected to be similar to those in complex *cis*-Pd(**1**)(**2***)Cl_2. In that complex the discussed interaction site has the exact enantiomeric structure and involves π-π interactions for the most part. However, a less pronounced upfield-shift of 6 of ligand **2** and of the phenyl group of ligand **1'** (d-f) indicates a reduction in π-π stacking in *cis*-Pd(**1'**)(**2**)Cl_2 (see Figure 3.11b). This change in interaction pattern can also be observed by the interligand NOE contact between the methyl group (b) of ligand **1'** and 6 of ligand **2** (Figure 3.10). Compared to *cis*-Pd(**1**)(**2***)Cl_2 (b-3/4/5 in Figure 3.8b) the relative orientation of both ligands has changed. According to intraligand interactions the involved ^{1}H signals (3'-6') exhibit lower chemical shift dispersion compared to homocomplex *cis*-Pd**2**$_2Cl_2$. Most striking is the missing upfield-shift of 6', which indicates reduced intraligand interactions in *cis*-Pd(**1'**)(**2**)Cl_2.

In summary when using ligand combination **1'** and **2** interaction patterns are maintained to a certain extent, especially for ligand **1'**. However concerning ligand **2** the biphenol group is probably forced to adapt a certain conformation in *cis*-Pd(**1'**)(**2**)Cl_2 which

interferes the formation of interactions. Thus the combination of ligand **1'** with ligand **2** is rather unfavorable, which is also reflected in the sub-statistically formation of the *cis*-heterocomplex (1:1:1.4, Table 3.1).

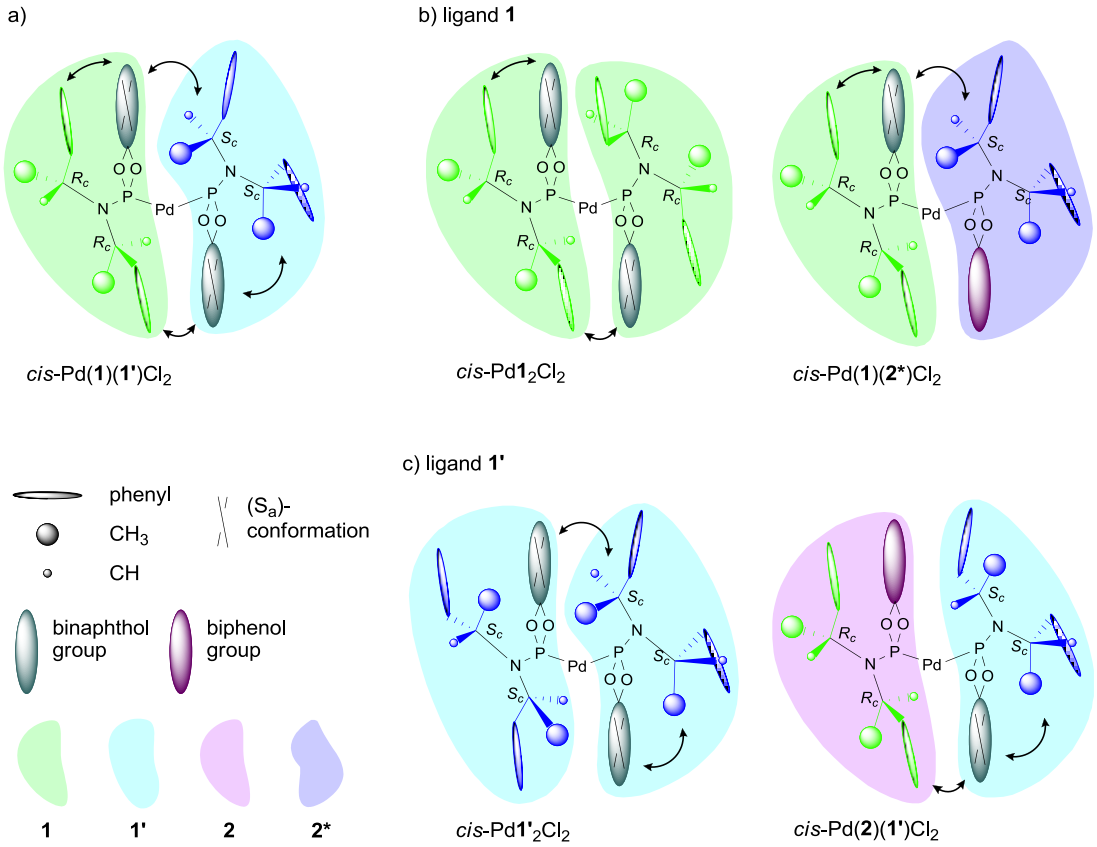

Figure 3.12. Schematic illustration of a) *cis*-Pd(**1**)(**1'**)Cl_2 and for a comparison of inter- and intraligand interactions sites b) concerning ligand **1**: *cis*-Pd**1**$_2Cl_2$ and *cis*-Pd(**1**)(**2***)Cl_2 and c) concerning ligand **1'**: *cis*-Pd**1'**$_2Cl_2$ and *cis*-Pd(**1'**)(**2**)Cl_2.

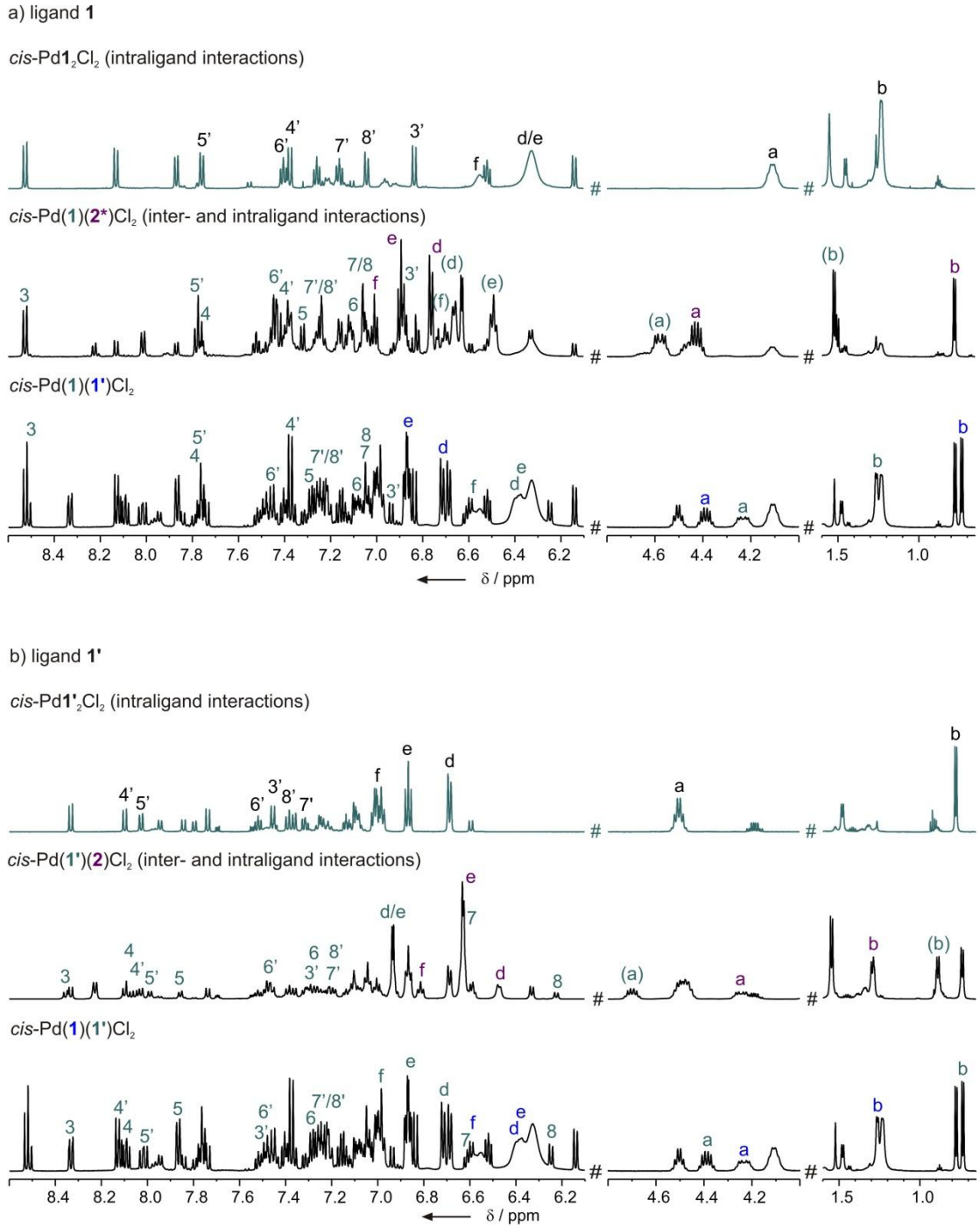

Figure 3.13. Chemical shift analysis for a) ligand **1** and b) ligand **1'** by a comparison of the ^{1}H spectrum of *cis*-Pd(**1**)(**1'**)Cl_2 with those of *cis*-Pd(**1**)(**2***)Cl_2 and *cis*-Pd**1**$_2Cl_2$ for ligand **1** and with *cis*-Pd(**1'**)(**2**)Cl_2 and *cis*-Pd**1'**$_2Cl_2$ for ligand **1'**. Similar chemical shifts for the naphthol and amine groups of different complexes prove the retention of the general complex structure and interaction pattern between identical functional groups.

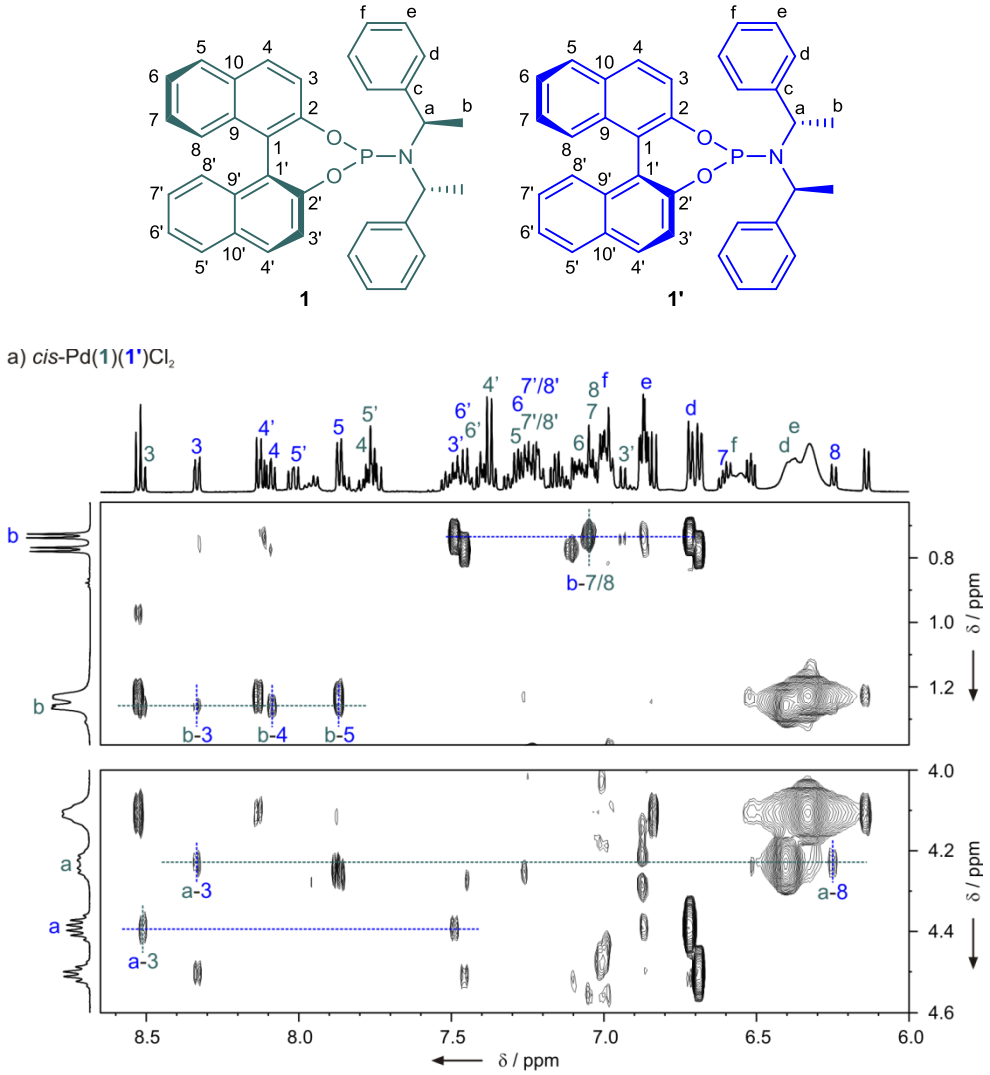

Figure 3.14. Section of a $^{1}H^{1}H$ NOESY spectrum of *cis*-Pd(**1**)(**1'**)Cl_2 also including corresponding *cis*-homocomplexes with a signal assignment to the *cis*-heterocomplex (green: ligand **1**, blue: ligand **1'**). Interligand NOE contacts within *cis*-Pd(**1**)(**1'**)Cl_2 are highlighted with dotted lines.

Next, a combination of ligand **1** and **1'** was investigated. As to ligand **1** - under retention of the general complex structure - interligand interactions in *cis*-Pd(**1**)(**1'**)Cl_2 between a part of its (S_a)-binaphthol group and the (S_c,S_c)-amine group of **1'** are expected to be similar to interligand interactions within *cis*-Pd(**1**)(**2***)Cl_2 (see Figure 3.12a and b). This is in good agreement with the observed interligand NOE contacts within both complexes (see b-7/8 in Figure 3.8b and Figure 3.14). Moreover ^{1}H chemical shift analysis showed, that the particular ^{1}H signals of the binaphthol unit (1, 2, 3, etc.) of ligand **1** are nearly identical with those of ligand **1** in *cis*-Pd(**1**)(**2***)Cl_2 (see green signal assignment in Figure 3.13a), while the ^{1}H signals of the interacting amine group of ligand **1'** are extremely similar to those of ligand **2*** in *cis*-Pd(**1**)(**2***)Cl_2 (see blue and purple signal assignment in Figure 3.13a). Moreover, intraligand interactions of ligand **1** in *cis*-Pd(**1**)(**1'**)Cl_2 are expected to be

similar to intraligand interactions within both *cis*-Pd(**1**)(**2***)Cl_2 and homocomplex *cis*-Pd**1**$_2Cl_2$, which is in perfect agreement with almost identical ^{1}H chemical shifts for the involved naphthol group (1', 2', 3', etc.) for all three complex spectra (see Figure 3.13a). As the ^{1}H signals of the amine groups possess averaged chemical shifts for both amine side chains reflecting intra- and interligand interactions due to a fast rotation around the P-N bond, ^{1}H signals of the amine group of ligand **1** in *cis*-Pd(**1**)(**1**')Cl_2 are not identical with those in *cis*-Pd(**1**)(**2***)Cl_2, as the contribution of the interligand interactions of one amine side chain is different within both complexes. However, within homocomplex *cis*-Pd**1**$_2$Cl2, both intra- and interligand interactions of the two amine side chains are identical. This perfectly corroborates with the observed very similar ^{1}H chemical shifts of the amine group of **1** in both complexes. Concerning ligand **1'**, interligand interactions of its (S_a)-binaphthol group with the (R_a,R_a)-amine group of ligand **1** are expected to be similar to those between ligand **1'** and **2** in *cis*-Pd(**1'**)(**2**)Cl_2 (see Figure 3.12a and c). This corroborates with similar interligand NOE contacts within both complexes (see b-4/5 in Figure 3.10 and b-3/4/5 in Figure 3.14). In addition similar ^{1}H chemical shifts of the particular naphthol group (3, 4, 5, etc.) of **1'** (see green signal assignment in Figure 3.13b) and also of the interacting amine group (a-f) of ligand **1** and **2** (see blue and purple signal assignment in Figure 3.13b) in *cis*-Pd(**1'**)(**1**)Cl_2 and *cis*-Pd(**1'**)(**2**)Cl_2 confirms a similar interaction pattern within both complexes. Intraligand interactions of ligand **1'** are similar to those in *cis*-Pd(**1'**)(**2**)Cl_2 and, moreover, to those in the corresponding homocomplex *cis*-Pd**1'**$_2Cl_2$. This is in perfect agreement with very similar ^{1}H chemical shifts of the particular naphthol group (3', 4', 5', etc.). Moreover, ^{1}H signals of the amine group of ligand **1'** are also very similar in *cis*-Pd(**1**)(**1**')Cl_2 and *cis*-Pd**1**'$_2Cl_2$, because both intra- and interligand interactions of the two amine side chains of **1'** are identical within both complexes leading to identical averaged ^{1}H signals of the amine group. Thus, for the complex *cis*-Pd(**1**)(**1'**)Cl_2 the retention of the general complex structure and distinct interaction patterns could clearly be shown by almost identical ^{1}H chemical shifts of identical interacting groups within different complexes.

This exhaustive structural NMR study shows that for all different ligand combinations investigated the general complex structure of the *cis*-phosphoramidite palladium complexes is retained. In addition, only for some structural motifs slight modifications in ^{1}H chemical shifts within different complexes were observed indicating small rearrangements of the ligands in order to reduce steric hindrance and to maximize interaction contact areas (see also Figure 3.4b). This extremely high similarity of the chemical shift pattern in the *cis*-complexes indicates that the different intra- and interligand

interactions form specific structural motifs which are additive. Interestingly, this additivity of the specific interactions is almost independent on the used ligand combination and on secondary interactions (neighbouring intra- and interligand interactions) but depend only on the interacting groups themselves.

Formation trends and relative stabilities of the *trans*- and *cis*-heterocomplexes. A closer look at the homo-to-heterocomplex ratios shows that some ligand combinations are preferred or disfavored in the *cis*-heterocomplex compared to the corresponding *cis*-homocomplexes (see Table 3.1). Recently we showed that the combinations of enantiopure ligand **1** with the enantiomeric ligands **2** or **2*** allows for a direct energetically connection of the two complex equilibria.[54] Since the homocomplex *cis*-Pd$\mathbf{1}_2Cl_2$ is identical within both complex equilibria and the respective second homocomplexes *cis*-Pd$\mathbf{2}_2Cl_2$ and *cis*-Pd$\mathbf{2*}_2Cl_2$ are enantiomeric, the free energies of the homocomplexes are identical for both complex equilibria. Therefore, the excess complex formation *cis*-Pd(**1**)(**2***)Cl_2 directly provides the energetically stabilization of *cis*-Pd(**1**)(**2***)Cl_2 compared to *cis*-Pd(**1**)(**2**)Cl_2. Due to the retention of the general complex structure a separation of supramolecular interactions from stereoelectronic properties was possible and for the first time the stabilization of one heterocomplex compared to another by pure supramolecular interactions was quantified.[54] The mutual exchange of a phenyl group versus a methyl group in *cis*-Pd(**1**)(**2**)Cl_2 compared to *cis*-Pd(**1**)(**2***)Cl_2 under the retention of the residual complex structure caused a replacement of π-π stacking by CH-π interactions. This enhancement in stabilizing interactions leads to a significant excess formation of the heterocomplex *cis*-Pd(**1**)(**2***)Cl_2 (1:0.9:4.5) compared to the nearly statistical distribution of *cis*-Pd(**1**)(**2**)Cl_2 (1:1.1:2.1, see also Table 3.1).

Under the assumption that the σ-donor/π-acceptor properties are identical for all phosphoramidite ligands used in this study the correlation of the relative complex ratios to the relative complex stabilities can also be extended to ligand **1'**. According to the complex ratios shown in Table 3.1 the heterocomplex stability for the ligand combination **1'** and **2** is reduced compared to *cis*-Pd(**1**)(**2***)Cl_2 and *cis*-Pd(**1**)(**2**)Cl_2. The observed destabilization of the heterocomplex using this ligand combination was ascribed to unfavorable interligand interactions between the amine group of ligand **1'** and the biphenol group of ligand **2**. In addition intraligand interactions within ligand **2** were also diminished.

Interestingly, for each ligand combination similar complex formation trends as observed for the *cis*-complexes are also found in the *trans*-complexes (see Table 3.1). For example an excess of heterocomplex *trans*-Pd(**1**)(**2***)Cl_2 was formed leading to a ratio of

1:1.2:3.5 for the two homocomplexes to the heterocomplex. In contrast heterocomplex *trans*-Pd(**1**)(**2**)Cl_2 was formed in statistical distribution and the formation of heterocomplex *cis*-Pd(**1'**)(**2**)Cl_2 is disfavored. Since ligand **2** and **2*** are enantiomers and therefore possess by definition identical σ-donor/π-acceptor characters, it can be excluded that the observed excess formation of heterocomplex *trans*-Pd(**1**)(**2***)Cl_2 was caused by favorable stereoelectronic properties of the metal-ligand bond, but by the formation of attractive supramolecular interactions such as CH-π interactions or π-stacking between ligand **1** and **2***. This finding was a little bit surprising because interligand interactions are usually expected to be formed in *cis*-complexes and additionally the *trans*-complexes are a mixture of different conformational isomers. ^{1}H DOSY aggregation studies of the free ligand combinations (**1**/**2**) and (**1**/**2***) revealed that both ligand combinations show the same aggregation trend with identical aggregation numbers at low temperature (see Figure 5 SI). Thus a preassemble between ligand **1** and **2*** in solution leading to this excess formation of *trans*-Pd(**1**)(**2***)Cl_2 can be excluded. Instead, ligand **1** and **2*** have to come in close proximity through complexation first before they can form attractive supramolecular interactions.

Based on these structural investigations we proclaim that - aside from the biaryl groups - each amine side chain forms a kind of plane surface capable of the formation of both inter- and intraligand interactions based on a combination of π-π and CH-π interactions. The planarity of the amine side chain can also be observed in the crystal structure (see Figure 3.4b). Within this interaction surface the specific groups can randomly be exchanged without changing the residual complex structure. However, the change of the interaction surface – for example by the mutual exchange of the methyl and the phenyl group in *cis*-Pd(**1**)(**2***)Cl_2 compared to *cis*-Pd(**1**)(**2**)Cl_2 – also changes the distinct interaction patterns. This change also effects the stabilization of the whole complex by supramolecular interactions, which is directly reflected in the complex ratios (Table 3.1). The general complex formation trends are identical for *cis*- and *trans*-complexes, but are less distinct for the *trans*-complexes. Thus, this interaction surface is already formed in the *trans*-complexes. However, due to a greater spatial distance between the two ligands interactions are weaker and therefore complex stabilization by a combination of dispersion and electrostatic interactions is also less.

Rotational processes. Dynamic processes of and within the amine groups have been addressed. As one amine side chain of each ligand is involved into interligand interactions while the second amine side chain is involved into intraligand interactions, rotational processes of the amine groups are expected to be essentially restricted. However,

only one set of ^{1}H signals for the whole amine moiety could be observed for all investigated *cis*-complexes: One methine and one methyl signal each and altogether only three signals d, e and f for both phenyl groups. Therefore, rotation around the P-N bond must still be fast on the NMR time scale despite the involvement into different interactions. This is in agreement with the fact that for intermolecular interactions the enthalphy and entropy changes compensate one another in such a way that the associated free energy is almost not affected.[55] During aggregation studies[42] of different phoshoramidite transition metal complexes in our working group the analysis of thermodynamic parameters already revealed that ligand dominated aggregation of these complexes not inescapably means a complete rotational stop within the amine group although the phenyl groups are most likely involved in the aggregation process: Despite aggregation of the complexes the rotation around the N-CH bonds did not stop completely, but only slowed down with decreasing temperatures. In addition to that it turned out that rotational processes within the amine group are not affected by complexation. Pregosin already reported similar observations in case of a cationic Pd complex using ligand **1**, in which the free coordination site was filled by the amine side chain through a weak η^2-arene-Pd bonding interaction between one phenyl group and the metal center: The phenyl group, which was coordinated to Pd, could still dissociate and rotate around the C-CH bond.[53]

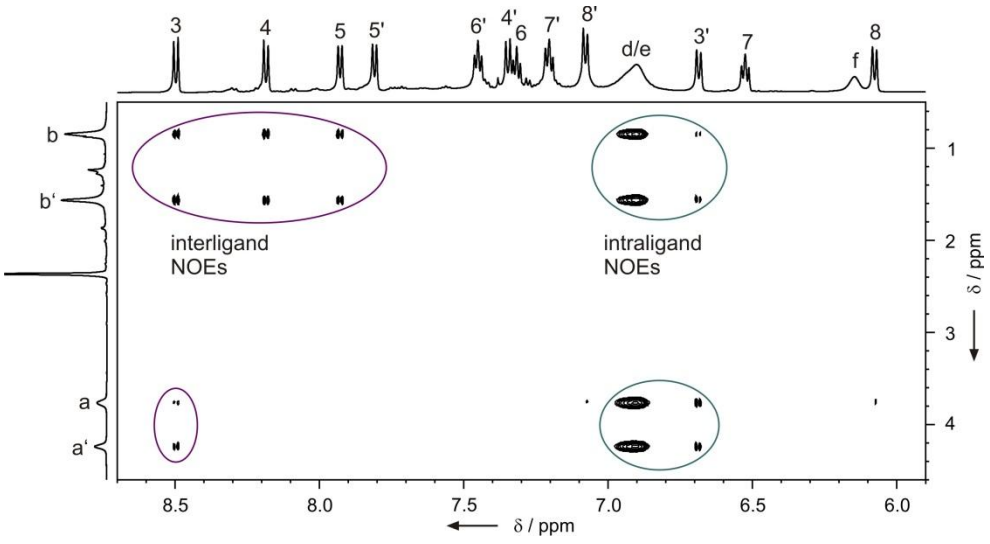

Figure 3.15. Section of a ^{1}H^{1}H NOESY spectrum of *cis*-Pd**1**$_2$Cl$_2$ measured at 220 K showing both inter- and intraligand NOE contacts.

As a monitor for rotational processes the methine and methyl signals can be used, as their ^{1}H signals split up at low temperature when rotation becomes slow enough. In a sample with a mixture of two different ligands altogether three different complexes are formed so that four (similar) set of signals are detected in one ^{1}H spectrum - one for each

homocomplex PdL_2Cl_2 and PdL'_2Cl_2 and two for heterocomplex $Pd(L)(L')Cl_2$. Therefore further investigations were done using homocomplex *cis**-Pd**1**$_2Cl_2$ for simplification. At 220 K the rotation of the amine group around the P-N bond within ligand **1** becomes slow enough so that both CH and CH_3 groups give two separated signals each in the ^1H spectrum. Since only one amine side chain interacts with the biaryl backbone of the other ligand, interligand NOEs to the biaryl group should only be detected for one of the two methyl signals and for one of the two methine signals (b or b' and a or a'). Interestingly both methyl and both methine signals show the same inter- and intraligand cross signals in the $^1H^1H$ NOESY (Figure 3.15). Thus even at 220 K and despite the involvement into intra- and interligand interactions the rotation of the amine group around the P-N bond in *cis*-Pd**1**$_2Cl_2$ is still fast enough to cause a transfer of the NOE contacts during a mixing time of 750 ms.

Discussion. It was experimentally shown that the interaction surface described above formed by the amine side chain (see also Figure 3.4) is able to form π-π and/or CH-π interactions. Since these are mainly dispersion interactions with a certain percentage of electrostatic interactions this surface will be termed dispersion surface in the following. For all heterocomplexes an identical complex formation trend was observed for the *cis*- and the respective *trans*-isomers. Therefore, general interaction motifs of the dispersion surfaces are formed which are valid in both *trans*- and *cis*-complexes. The modulation of these interaction motifs by structural changes in the dispersion surface leads to measureable energy differences which lie within the order of magnitude significant for the stereoselective catalysis (2-4 kJ/mol). Furthermore, we recently showed that the aggregation trends of different transition metal complexes using phosphoramidite ligands are predominantly determined by the ligand itself and independent of the transition metal or the complex structures. This observation indicates that similar interaction motifs of the dispersion surface and the biaryl group as experimentally shown for *cis*- and *trans*-Pd complexes are also valid for other transition metal complexes. With regard to the broad and successful application of phosphoramidite ligands in transition metal catalysis we postulate stereoselection modes of this privileged class of ligands by extensive interaction surfaces capable of a combination of π-π, CH-π and van der Waals interactions. For those stereoselection modes the interaction surfaces of the biaryl groups and those of the amine side chains have to be considered. The interaction properties of these surfaces can be modulated by changes in the electron density and charge distribution as well as by changes of the size of the interaction surface. For that purpose different substituents at the biaryl or phenyl group can be introduced or the configuration in the amine side chain can be varied. Interestingly only when a chiral amine group NR(CH)Ar was introduced - leading to a

drastically improvement of enantioselectivity - phosphoramidite ligands started their triumph. Furthermore most of the successful phosphoramidite ligands contain such a NR(CH)Ar dispersion surface.[6] Another argument for our concept of a dispersion surface as stereoselection mode is the great success of these ligands using aromatic or cyclic substrates and the failure when using acyclic substrates: When using acyclic substrates the resulting interaction energy between the dispersion surface of the ligand and the substrate is too low for a successful stereodiscrimination. However, we do not want to postulate that there is one perfect ligand but that both interaction surfaces – the biaryl group and the dispersion surface of the amine group - have to be adjusted to the used substrate. Interestingly the rotation of the amine group around the P-N bond does not hamper the detected interaction patterns. This is in agreement with the fact that for intermolecular interactions the enthalphy and entropy changes compensate one another in such a way that the associated free energy is almost not affected.[55] Therefore, variations in the amine groups such as the introduction of a cyclic amine does not show any detrimental effect on selectivity as the coexistence of rotation and interactions is not disturbed. In addition the introduction of an asymmetric amine moiety with only one dispersion surface and one small substituent such as a methyl group is still in good agreement with our concept of a dispersion surface as stereoselection mode. For example for some Rh-catalyzed hydrogenation reactions a drastic improvement in yield could be observed by the substitution of one amine side chain by a small methyl group.[16, 26, 28] Thus, for asymmetric catalysis it is crucial to guarantee the accessibility of the transition metal center on the one side and to create a dispersion surface which is adjusted to the particular substrate on the other side. In accordance with that the enlargement of the interaction surfaces of phosphoramidite ligands can lead to an improvement of enantioselectivities in Cu-catalyzed conjugated addition and allylic substitution reactions. In the precatalytic binuclear Cu-complex with a mixed trigonal/tetrahedral coordination of the ligands[43-45] an enlargement of the biphenol or amine group of the ligands does not cause a steric hindrance because of the greater distance between the ligands in the Cu-complexes, but enables the formation of stronger interactions with the substrate. For small complexes with a *cis*-orientation of the ligands substituents at the biaryl groups are detrimental due to their close proximity causing a steric hindrance. Thus methyl or allyl groups in the biphenol moiety or naphthol groups in the amine moiety are advantageous for Cu-catalysis enhancing the formation of CH-π interactions.[13, 56]

3.4 Conclusion

Homo- and hetero-phosphoramidite palladium complexes using different ligand combinations have been investigated and characterized by NMR. The slow interconversion of initially formed *trans*-complexes into the respective *cis*-isomers could be proven by characteristic $^2J_{PP}$ values of the heterocomplexes. Moreover ligand-ligand interactions could clearly be identified by ^{1}H chemical shift analysis and ^{1}H^{1}H NOESY measurements between the amine side chain of one ligand and the biaryl group of the corresponding other ligand. In addition intraligand interactions were identified between the second amine side chain and a part of the own biaryl group of the same ligand. Within these interaction sites the amine group forms planar interaction surfaces. Both CH-π and π-π interactions play an important role for inter- and intraligand interactions. The different interaction motifs turned out to be additive and therefore they are independent on ligand combination or secondary interactions. Upon changing one of the interaction sites the residual complex structure is retained and secondary interactions are hardly affected. It was experimentally shown that a change in the dispersion surface by the mutual exchange of a phenyl and a methyl group merely leads to a substitution of π-π interactions by CH-π interactions without affecting the residual interaction sites. This measureable energy differences in interaction strength is directly reflected by complex formation trends and lies in the order of magnitude significant for asymmetric catalysis. Since formation trends are generally the same for *cis*- and *trans*-isomers and since the aggregation trends of phosphoramidite transition complexes are ligand-dominated, we proclaim that the dispersion surface of the amine side chain leads to specific interaction motifs which are independent on transition metal and complex structure. In addition we proclaim that these interaction motifs are essential for the stereoselectivity in asymmetric catalysis and that the interaction sites have to be adjusted to the substrate.

Furthermore rotational processes and the effect of ligand interactions on these processes were addressed. Although both amine side chains are involved into inter- and intraligand interactions, respectively, rotational processes of the amine moiety around the P-N bond is not tremendously affected but is still quite fast on the NMR time scale even at decreased temperature. Therefore enthalphy and entropy changes compensate one another in such a way that the associated free energy is almost not affected.

3.5 Supporting Information

3.5.1 ^{31}P spectra simulations

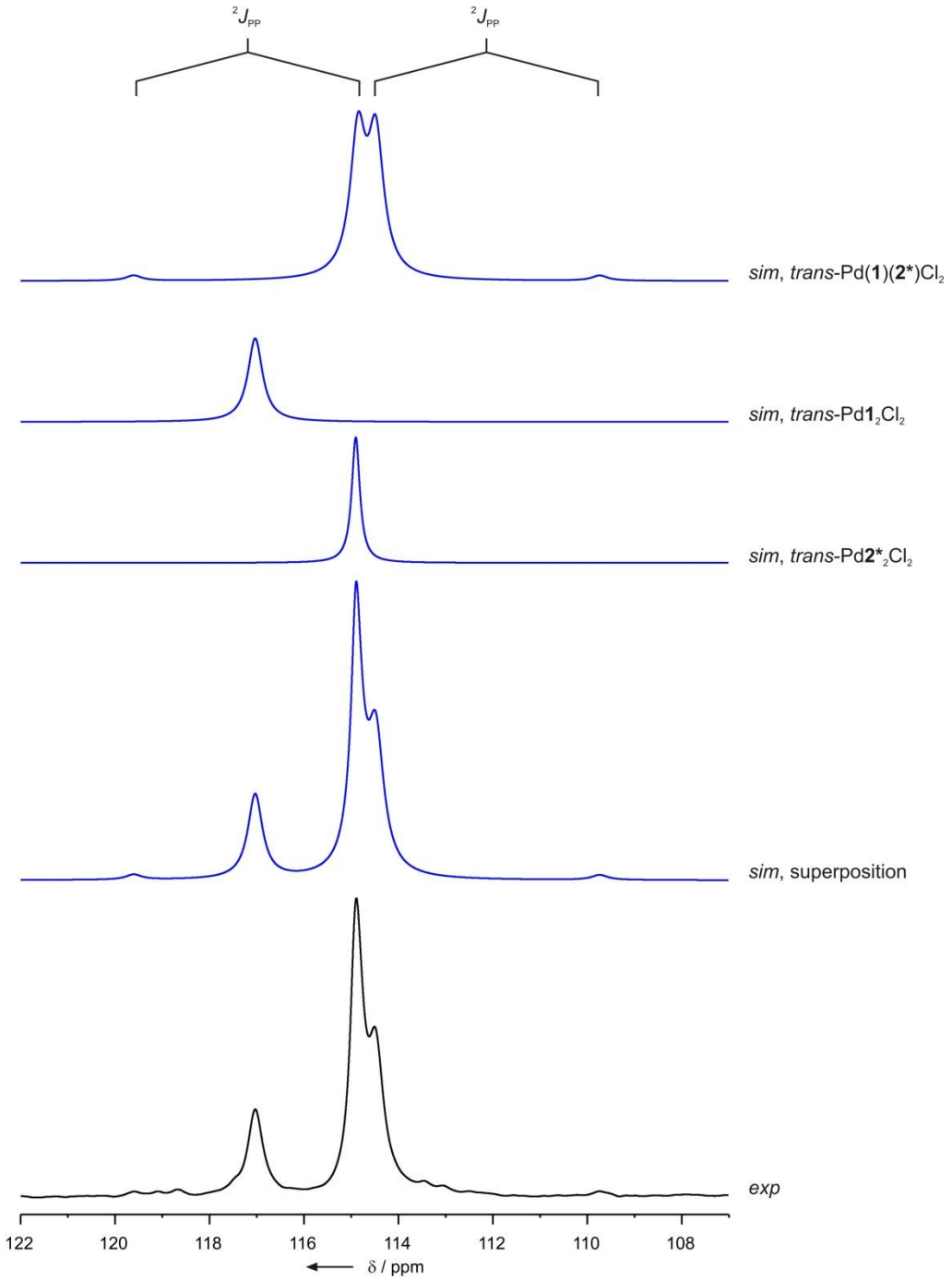

Figure 3.16. ^{31}P spectrum (black) of a sample containing *trans*-Pd(**1**)(**2***)Cl_2, homocomplexes *trans*-PdL_2Cl_2 (L = **1**, **2***) and already a small amount of the corresponding *cis*-complexes. ^{31}P spectra simulation (blue) of each *trans*-complex clarifies the superposition of complex signals signals and the $^2J_{PP}$ coupling of *trans*-Pd(**1**)(**2***)Cl_2 despite a very pronounced roof effect.

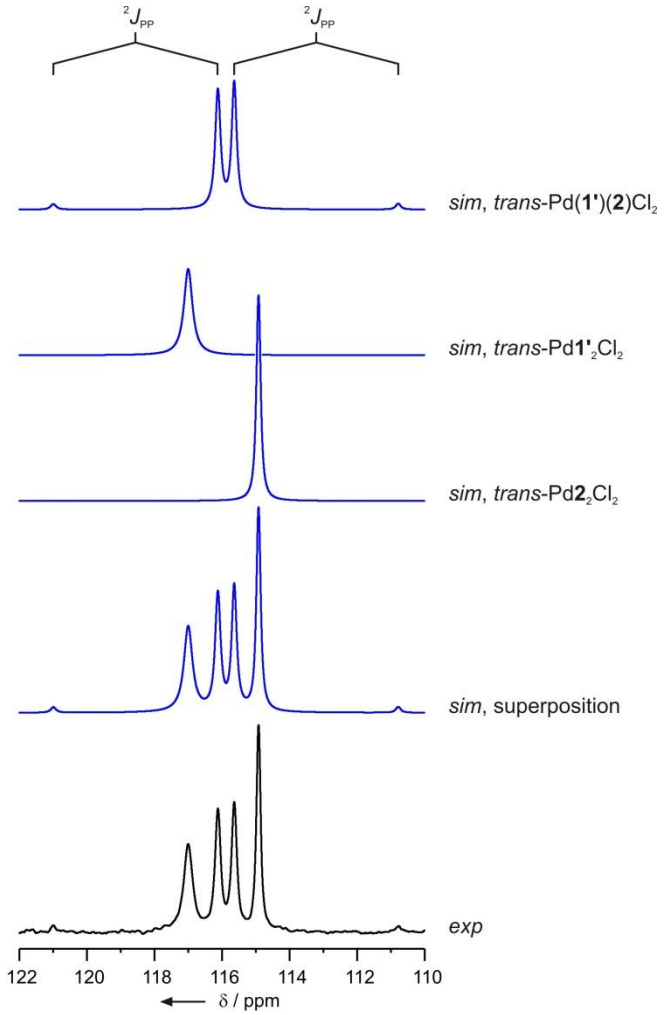

Figure 3.17. ^{31}P spectrum (black) of a sample containing *trans*-Pd(**1'**)(**2**)Cl_2 and homocomplexes *trans*-PdL_2Cl_2 (L = **1'**, **2**). ^{31}P spectra simulation of each *trans*-complex (blue) clarifies the superposition of the different complex signals and the $^2J_{PP}$ coupling of *trans*-Pd(**1'**)(**2**)Cl_2 despite a very pronounced roof effect.

3.5.2 *trans*-Pd(1)(1')Cl_2

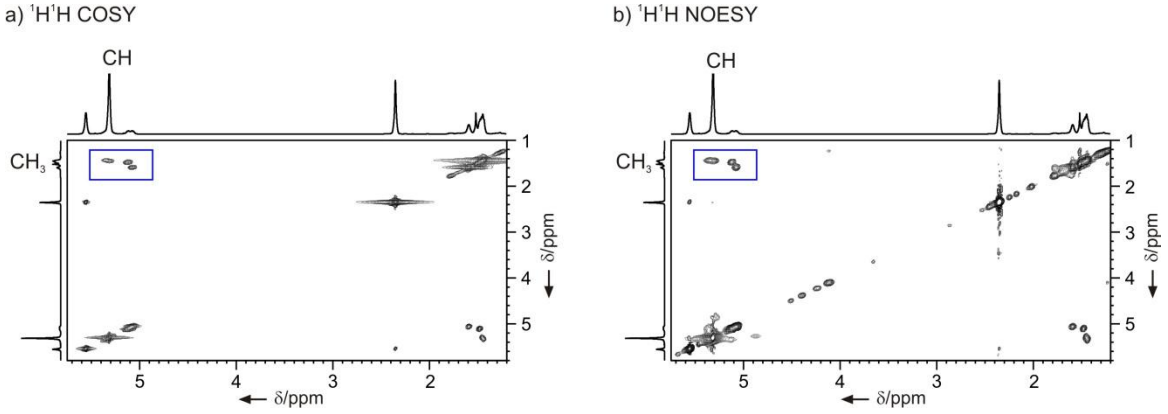

Figure 3.18. Section of a ^{1}H^{1}H COSY (left) and a ^{1}H^{1}H NOESY (right) of Pd(**1**)(**1'**)Cl_2 and corresponding homocomplexes PdL_2Cl_2 (L = **1**, **1'**). In both spectra altogether four cross signals between a methine and a methyl signal are observed proving the formation of a heterocomplex: one cross signal each for both homocomplexes and two for the heterocomplex.

3.5.3 Aggregation studies

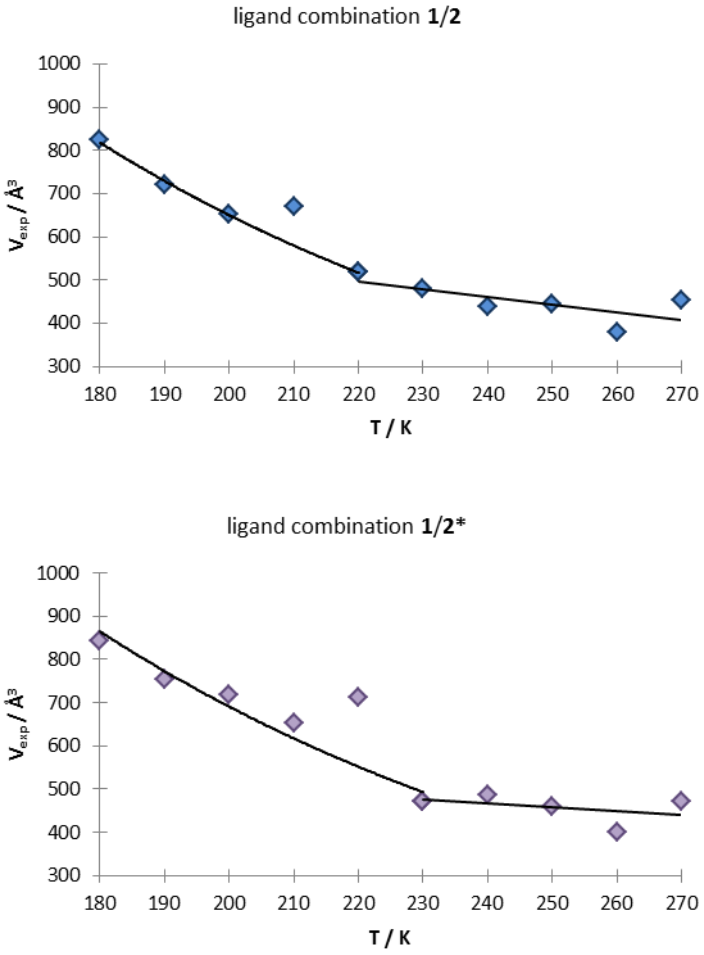

Figure 3.19. Aggregation curves of both ligand combinations (**1/2**) and (**1/2***).

3.5.4 Sample preparation

All reactions were carried out under argon atmosphere in heat gun dried Schlenk flask using freshly distilled solvents. CD_2Cl_2 was distilled from CaH_2. Ligand **1** and **2** were prepared according to reported protocolse[13] or bought from Sigma-Aldrich. Pd(cod)Cl_2 was bought from Alfa Aesar. The samples were prepared by adding solvent to a mixture of free ligand(s) and Pd(cod)Cl_2 with a total ligand-to-Pd ration of 2:1. The solution was stirred for at least 2.5 h for *trans*-PdL_2Cl_2 and stored at room temperature to obtain *cis**-PdL_2Cl_2. Sample concentrations used for NMR studies varied between 0.02 and 0.03 M.

3.5.5 NMR data collection and processing

NMR spectra were recorded on a Bruker Avance DRX 600 (600.13 MHz) spectrometer equipped with a 5 mm broadband triple resonance z-gradient probe

(maximum gradient strength 53.5 Gauss/cm) and a Bruker Avance III 600 (600.25 MHz) spectrometer, equipped with a TCI cryoprobe with z-gradient (53.5 G/cm). ^{1}H and ^{13}C chemical shifts were referenced to TMS, for ^{31}P chemical shifts the corresponding Ξ value was applied. All measurements were performed at 300 K unless stated otherwise. For the characterization of the different observed complex species detailed 2D NMR spectroscopic investigation have been performed: ^{1}H^{31}P HMBC, ^{1}H^{1}H COSY, ^{1}H^{1}H NOESY, ^{1}H^{13}C HSQC, ^{1}H^{13}C HMBC and *J*-resolved ^{31}P. For appropriate ^{1}H^{1}H NOESY measurements mixing times of 750 to 800 ms have been applied. NMR data were processed and evaluated with Bruker Topspin 2.1.

^{1}H DOSY measurements were performed in a temperature range between 180 K and 270 K for each ligand combination using a pulse sequence by A. Jerschow and N. Müller developed for suppression of convection artifacts.[57] For viscosity correction TMS was used as internal standard according to literature known procedure[58] and the hydrodynamic volume was calculated using the Stokes-Einstein equation.

$$r_h = \frac{k_B T}{6\pi\eta D_{exp}} \qquad \Rightarrow V_h = \frac{4}{3}\pi r_h^3$$

3.5.6 NMR data

Pd**2**$_2$Cl$_2$/Pd**2***$_2$Cl$_2$

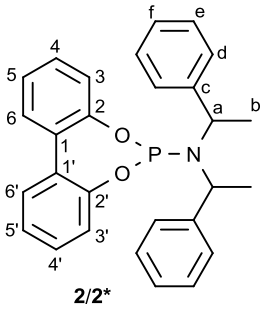

2/**2***

Table 3.2. NMR data of complexes *trans*- and *cis*-Pd**1**$_2$Cl$_2$ measured at 300 K in CD_2Cl_2.

trans-Pd**2**$_2$Cl$_2$ / *trans*-Pd**2***$_2$Cl$_2$					*cis*-Pd**2**$_2$Cl$_2$ / *cis*-Pd**2***$_2$Cl$_2$				
δ(^{31}P) = 114.9 ppm (*s*)					δ(^{31}P) = 115.1 ppm (*s*)				
	δ (^{13}C) [ppm]	δ (^{1}H) [ppm]		*J* [Hz]		δ (^{13}C) [ppm]	δ (^{1}H) [ppm]		*J* [Hz]
3	124.1	7.49	*d*	8.10	3	125.5	8.22	*d*	8.10
4	129.9	7.26	*td*	7.76 1.87	4	130.0	7.48	*td*	7.78 1.66
5	126.4	7.23	*td*	7.60 1.23	5	125.4	7.04	*t*	7.45
6	130.2	7.44	*dd*	7.57 1.81	6	129.4	7.11	*d(d)*	7.74 (1.49)
3’	122.3	7.08	*d*	7.80	3’	120.1	6.33	*d*	8.02
4’	129.8	7.03	*t + lr*	7.74	4’	130.5	6.96	*td*	7.71 1.45
5’	125.7	7.13	*d + lr*	7.35	5’	126.7	7.04	*t*	7.54
6’	130.1	7.35	*dd*	7.78 1.65	6’	130.1	6.59	*dd*	7.74 1.64
a	55.6	5.29	*m*	7.26	a	56.3	4.47	*m*	7.64
b	20.2	1.45	*d*	7.23	b	18.6	1.50	*d*	7.06
d	128.9	7.21	-	-	d	127.6	6.63	*d*	4.44
e	128.1	7.11	-	-	e	128.8			
f	-	7.11	-	-	f	127.6	6.87	*quint*	4.26
hydrodynamic volume V = 1020 Å^3 D_{corr} = 4.01·10^{-10} m^2/s					hydrodynamic volume V = 941 Å^3 D_{corr} = 3.91·10^{-10} m^2/s				

Pd**1**$_2$Cl$_2$

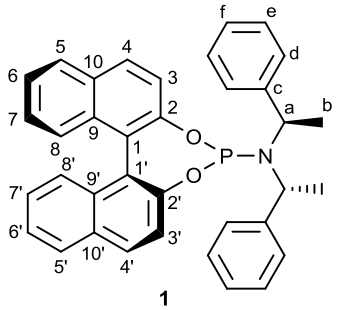

1

Table 3.3. NMR data of complexes *trans*- and *cis*-Pd**1**$_2$Cl$_2$ measured at 300 K in CD_2Cl_2.

trans-Pd**1**$_2$Cl$_2$					*cis*-Pd**1**$_2$Cl$_2$				
δ(^{31}P) = 117.0 ppm (*s*)					δ(^{31}P) = 117.5 ppm (*s*)				
	δ (^{13}C) [ppm]	δ (^{1}H) [ppm]		*J* [Hz]		δ (^{13}C) [ppm]	δ (^{1}H) [ppm]		*J* [Hz]
3	122.9	7.56	*broad s*		3	123.9	8.53	*d*	8.92
4	-	-	-	-	4	131.0	8.13	*d*	8.98
5	128.8	7.84	*d*	8.15	5	128.0	7.78	*d*	8.15
6	125.6	7.52	*broad s*	-	6	125.6	7.26	*t*	7.44
7	126.4	7.25	*broad s*	-	7	126.1	6.52	*t(d)*	7.64 (1.08)
8	-	-	-	-	8	126.7	6.14	*d*	8.58
3’	120.9	7.11	*d*	8.88	3’	119.4	6.84	*d*	8.85
4’	130.6	7.55	*d*	8.94	4’	131.5	7.38	*d*	8.86
5’	128.5	7.77	*d*	8.32	5’	128.6	7.76	*d*	8.20
6’	125.2	7.39	*t + lr*	7.46	6’	125.5	7.40	*t*	7.40
7’	126.2	7.18	*t + lr*	7.65	7’	126.5	7.16	*t*	7.65
8’	127.3	7.13	*d*	8.68	8’	127.2	7.04	*d*	8.46
a	55.4	5.30	-	-	a	55.6	4.11	*m*	7.64
b	19.6	1.45	*d*	7.19	b	18.3	1.23	*d*	5.01
d	128.4	7.22	*d*	7.31	d	127.3	6.32	*s*	-
e	127.9	6.97	*t*	7.34	e				
f	127.1	6.92	*t*	6.96	f	128.6	6.55	*s*	-

Pd**1'**$_2$Cl$_2$

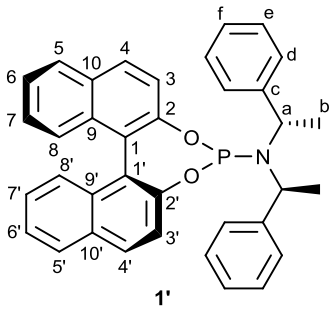

1'

Table 3.4. NMR data of complexes *trans*- and *cis*-Pd**1'**$_2$Cl$_2$ measured at 300 K in CD_2Cl_2.

trans-Pd**1'**$_2$Cl$_2$					*cis*-Pd**1'**$_2$Cl$_2$				
δ(^{31}P) = 117.0 ppm (*s*)					δ(^{31}P) = 114.3 ppm (*s*)				
	δ (^{13}C) [ppm]	δ (^{1}H) [ppm]		*J* [Hz]		δ (^{13}C) [ppm]	δ (^{1}H) [ppm]		*J* [Hz]
3	123.5	7.97	*d*	8.51	3	123.2	8.33	*d*	8.93
4	130.9	7.38	-	-	4	132.0	7.74	*d*	9.00
5	129.1	7.79	*d*	8.27	5	129.2	7.36	*d*	7.97
6	126.0	7.48	*t*	7.35	6	125.9	7.14	*t+lr*	7.15
7	126.9	7.22	-	-	7	127.5	7.09	-	-
8	127.7	7.21	*d*	8.46	8	126.5	7.10	-	-
3'					3'	121.2	7.46	*d*	8.81
4'	130.9	7.84	*d*	8.91	4'	131.2	8.10	*d*	8.78
5'	128.8	7.94	*d*	8.18	5'	128.6	8.03	*d*	8.21
6'	126.0	7.45	*t+lr*	7.32	6'	126.4	7.52	*t+lr*	7.52
7'	126.9	7.25	-	-	7'	127.4	7.31	*t+lr*	7.66
8'	127.7	7.26	*d*	7.90	8'	127.6	7.39	*d*	8.48
a	56.3	5.12	*m*	7.22	a	56.0	4.50	*m*	7.09
b	21.5	1.48	*d*	7.07	b	20.4	0.78	*d*	7.21
d	129.4	6.98	*d*	7.45	d	129.2	6.69	*d*	7.68
e	128.1	7.01	*t*	7.49	e	127.5	6.87	*t*	7.66
f	127.7	7.09	*t*	7.11	f	-	7.00	*t*	7.06

cis-Pd(**1**)(**2**)Cl_2

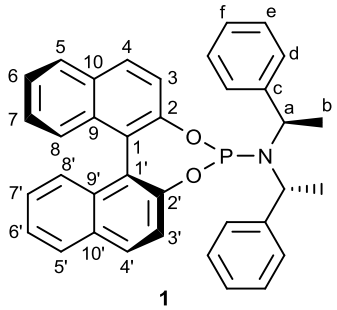

1

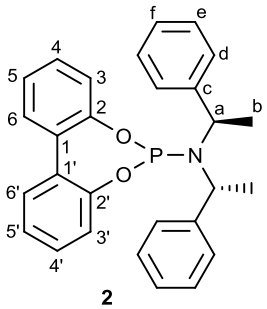

2

Table 3.5. NMR data of ligand **1** (left) and **2** (right) in *cis*-Pd(**1**)(**2**)Cl_2 (0.02 M in CD_2Cl_2, 300 K).

Ligand **1**					Ligand **2**				
δ(^{31}P) = 117.9 ppm (*dt*)					δ(^{31}P) = 115.1 ppm (*dt*)				
$^2J_{PP}$ = 103 Hz			$^3J_{HP}$ = 19 Hz		$^2J_{PP}$ = 104 Hz			$^3J_{HP}$ = 19 Hz	
	δ (^{13}C) [ppm]	δ (^{1}H) [ppm]		*J* [Hz]		δ (^{13}C) [ppm]	δ (^{1}H) [ppm]		*J* [Hz]
3	123.8	8.55	*dd*	8.95 1.00	3	125.5	8.23	*dt*	8.32 1.46
4	131.0	8.12	*d*	9.05	4	130.0	7.51	*t(d)*	7.85 (1.63)
5	128.0	7.85	*d*	8.10	5	125.4	7.02	*t*	7.54
6	125.6	7.24	*t*	7.46	6	129.4	7.06	*d*	7.74
7	126.1	6.52	*t(d)*	7.65 (1.18)					
8	126.9	6.18	*d*	8.58					
3’	119.4	6.71	*dd*	8.85 0.81	3’	120.1	6.47	*d(t)*	8.15 (1.33)
4’	131.5	7.39	*d*	8.67	4’	130.5	6.92	*td*	7.68 1.93
5’	128.6	7.77	*d*	8.32	5’	126.7	7.11	*t*	7.54
6’	125.5	7.41	*t*	6.77	6’	130.0	6.63	-	-
7’	126.5	7.17	*t*	7.60					
8’	127.2	7.07	*d*	7.87					
a	56.2	4.42	*qd*	7.10 18.32	a	55.7	4.11	*qd*	6.76 18.34
b	18.8	1.54	*d*	7.13	b	18.2	1.26	*d*	6.80
d		6.56	*(d)*	(7.5)	d	128.7	6.39	*(s)*	-
e	127.2	6.40	*t*	7.20	e	127.7	6.57	*t*	7.54
f	127.3	6.66	*t*	7.20	f	127.5	6.77	*t*	7.29

cis-Pd(**1**)(**2***)Cl_2

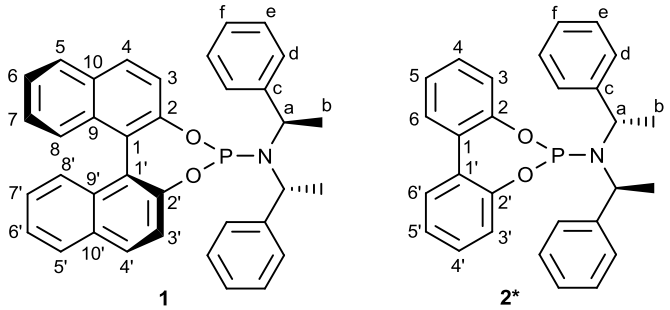

Table 3.6. NMR data of ligand ligand **1** (left) and ligand **2*** (right) in *cis*-Pd(**1**)(**2***)Cl_2 (0.02 M in CD_2Cl_2, 300 K).

Ligand **1**					Ligand **2**				
$\delta(^{31}P)$ = 118.9 ppm (*dt*)					$\delta(^{31}P)$ = 113.3 ppm (*dt*)				
$^2J_{PP}$ = 96 Hz			$^3J_{HP}$ = 17 Hz		$^2J_{PP}$ = 96 Hz			$^3J_{HP}$ = 16 Hz	
	δ (^{13}C) [ppm]	δ (^{1}H) [ppm]		*J* [Hz]		δ (^{13}C) [ppm]	δ (^{1}H) [ppm]		*J* [Hz]
3	123.4	8.52	*d*	8.96	3	125.0	8.01	*dt*	8.30 1.34
4	131.6	7.77	*d*	8.68	4	130.3	7.45	-	-
5	129.0	7.32	*d*	8.20	5	126.6	7.12	*tt*	7.47 1.25
6	125.4	7.11	-	-	6	129.8	6.82	*dd*	7.61 1.63
7/8	126.5	7.05	-	-					
3’	119.6	6.88	*dd*	8.74 1.13	3’	121.3	7.16	*dt*	8.39 1.47
4’	131.4	7.42	*d*	8.20	4’	130.0	7.52	*td*	7.71 1.68
5’	128.5	7.78	*d*	8.48	5’	126.3	7.39	*t(t)*	8.63 1.26
6’	125.5	7.45	-	-	6’	129.8	6.82	*dd*	7.61 1.63
7’	126.6	7.24	-	-					
8’	127.4	7.24	-	-					
a	56.1	4.58	*qd*	7.09 18.27	a	55.4	4.43	*qd*	7.26 15.23
b	19.0	1.52	*d*	7.13	b	20.2	0.78	*d*	7.08
d	128.5	6.66	*d*	7.18	d	128.8	6.76	*d*	7.62
e	127.4	6.49	*t*	7.51	e	127.3	6.89	*t*	7.73
f	127.1	6.70	*t*	7.18	f	127.1	7.01	*tt*	7.26 1.25

cis-Pd(**1'**)(**2**)Cl_2

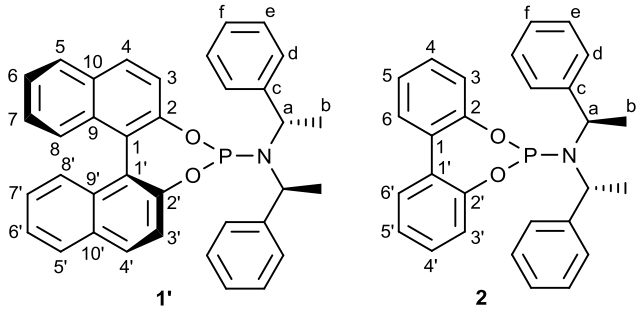

Table 3.7. NMR data of ligand **1'** (left) and ligand **2** (right) in *cis*-Pd(**1'**)(**2**)Cl_2 (0.02 M in CD_2Cl_2, 300 K).

Ligand **1'**					Ligand **2**				
δ(^{31}P) = 114.2 ppm (*dt*)					δ(^{31}P) = 116.1 ppm (*dt*)				
$^2J_{PP}$ = 97 Hz			$^3J_{HP}$ = 15 Hz		$^2J_{PP}$ = 98 Hz			$^3J_{HP}$ = 17 Hz	
	δ (^{13}C) [ppm]	δ (^{1}H) [ppm]		*J* [Hz]		δ (^{13}C) [ppm]	δ (^{1}H) [ppm]		*J* [Hz]
3	123.7	8.36	*d*	9.05	3	125.4	8.23	*d*	8.08
4	131.2	8.08	*d*	9.19	4	130.5	7.25	*t*	8.34
5	128.2	7.86	*d*	7.93	5	127.0	6.81	*t*	7.23
6	125.7	7.28	*t+lr*	9.34	6	129.6	7.19	*dd*	7.62 1.27
7	126.4	6.62	-	-					
8	126.7	6.22	*d*	8.51					
3'	121.0	7.30	*d*	8.93	3'	119.9	6.58	*d*	8.52
4'	131.1	8.05	*d*	8.87	4'	130.6	6.94	-	-
5'	128.7	7.99	*d*	8.13	5'	125.8	7.08	-	-
6'	125.7	7.47	-	-	6'	129.7	7.27	*d+lr*	8.10
7'	126.8	7.22	-	-					
8'	127.4	7.21	-	-					
a	56.0	4.70	*dq*	14.92 7.22	a	55.9	4.24	*dq*	18.31 7.13
b	20.4	0.91	*d*	7.09	b	18.5	1.27	*d*	7.16
d	129.1	6.93	-	-	d	128.4	6.47	*d*	6.93
e	127.6	6.93	-	-	e	127.4	6.63	-	-
f	-	-	-	-	f	127.0	6.81	*t*	7.23

cis-Pd(**1**)(**1'**)Cl_2

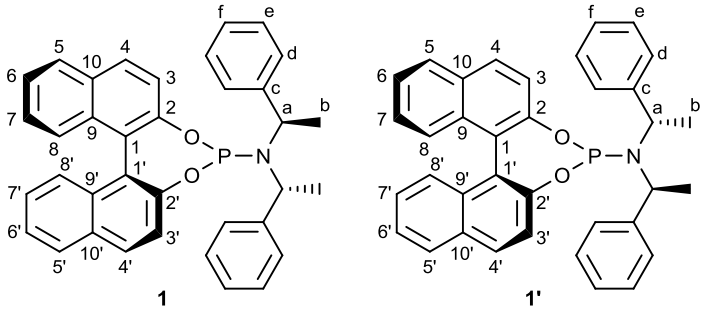

Table 3.8. NMR data of ligand ligand **1** (left) and ligand **1'** (right) in *cis*-Pd(**1**)(**1'**)Cl_2 (0.02 M in CD_2Cl_2, 300 K).

Ligand **1**					Ligand **1'**				
δ(^{31}P) = 118.5 ppm (*dt*)					δ(^{31}P) = 113.9 ppm (*dt*)				
$^2J_{PP}$ = 97 Hz			$^3J_{HP}$ = 19 Hz		$^2J_{PP}$ = 97 Hz			$^3J_{HP}$ = 15 Hz	
	δ (^{13}C) [ppm]	δ (^{1}H) [ppm]		*J* [Hz]		δ (^{13}C) [ppm]	δ (^{1}H) [ppm]		*J* [Hz]
3	123.5	8.51	*d*	8.82	3	123.6	8.33	*d*	8.92
4	130.9	7.77	*d*	8.83	4	131.2	8.08	*d*	8.93
5	128.0	7.28	*d*	7.61	5	128.1	7.87	*d*	8.07
6	125.7		-	-	6	125.7	7.29	*t*	-
7	162.5	7.05	-	-	7	126.4	6.61	*t*	7.72
8	127.3		-	-	8	126.6	6.25	*d*	8.55
3'	119.4	6.93	*d*	8.86	3'	121.0	7.49	*d*	8.66
4'	131.7	7.37	*d*	8.88	4'	131.0	8.12	*d*	8.67
5'	128.7	7.76	-	-	5'	128.8	8.01	*d*	8.30
6'	125.8	7.45	-	-	6'	126.0	7.50	-	-
7'/8'	126.7 – 127.4	7.19 – 7.28	- -	- -	7'/8'	126.7 – 127.4	7.19 – 7.28 -	- -	- -
a	55.9	4.23	*dq*	18.9 6.83	a	55.8	4.39	*dq*	15.2 6.98
b	18.6	1.26	*d*	6.51	b	20.3	0.73	*d*	7.11
d	128.6	6.40	-		d	128.9	6.72	*d*	7.72
e	127.5	6.37			e	127.4	6.87	*t*	7.78
f	127.1	6.58			f	129.2	6.98		

3.6 Additional Experimental Findings

3.6.1 Interactions within $Pd1_2Cl_2$ and $Pd1'_2Cl_2$

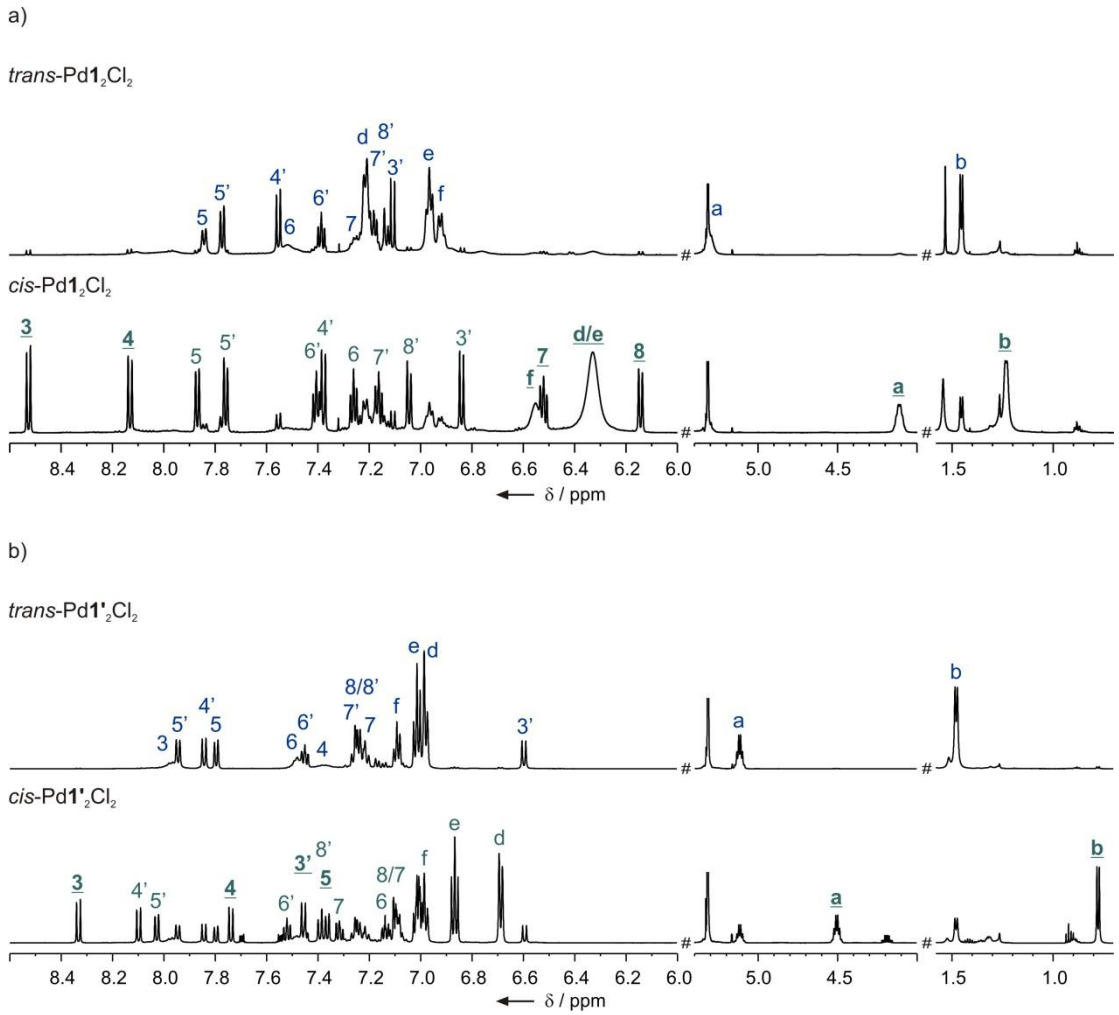

Figure 3.20. Comparison of ^{1}H spectra of *trans*- and *cis*-isomers of a) $Pd\mathbf{1}_2Cl_2$ and b) $Pd\mathbf{1'}_2Cl_2$ with full signal assignment to ligand **1** and **1'**, respectively. Significant changes in chemical shifts (bold and underlined) provide information about the involvement into CH-π interactions or π-π stacking.

Chemical analysis $\Delta\delta(^1H)$ provides information about CH-π interactions and π-π stacking within homocomplexes $Pd\mathbf{1}_2Cl_2$ and $Pd\mathbf{1'}_2Cl_2$ (for spectra see Figure 3.20). Analogue to all phosphoramidite palladium complexes discussed so far both inter- and intraligand interactions are formed between one amine side chain and different parts of the binaphthol unit (interligand interactions: 3-8, intraligand interactions: 3'-8'). Because of a fast rotation around the P-N bond, again only one set of signals is detected for the whole amine moiety for both complexes. Therefore, $\Delta\delta(^1H)$ values encompass inter- and intraligand interactions of both amine side chains. When using ligand **1** the methine (a) and to some extent also the methyl group (b) are shifted upfield due to the involvement into

interligand CH-π interactions with the naphthol group of the other ligand (see downfield-shift of 3,4 in Figure 3.20a). The phenyl group of the amine moiety (upfield-shift of d-f) and a part of the binaphthol group (upfield-shift of 7,8) perform π-π stacking. In contrast to that, in *cis*-Pd**1'**$_2$Cl$_2$ the methyl group is strongly involved into CH-π interactions (upfield-shift of b, Figure 3.20b), while the methine group (a) is involved to a less extent. Moreover, π-π stacking between the phenyl group and the naphthol group is less distinct in *cis*-Pd**1'**$_2$Cl$_2$ compared to *cis*-Pd**1**$_2$Cl$_2$. Instead, the significant downfield-shift of 3' and the strong upfield-shift of the methyl signal b indicate that the previously observed π-π stacking in the intraligand interactions have been replaced by CH-π interactions between the methyl and a naphthol group. Thus, in *cis*-Pd**1'**$_2$Cl$_2$ CH-π interactions overweigh, whereas in *cis*-Pd**1**$_2$Cl$_2$ both CH-π and π-π interactions are formed.

3.6.2 Heterocomplex Pd(1')(1'')Cl$_2$

For the sake of completeness ligand combination (S_a,S_c,S_c)-**1**/(R_a,R_c,R_c)-**1** was also investigated. Unfortunately quite much precipitation in the sample made a detailed NMR investigation difficult. Therefore the main complex species will be discussed in the following only briefly.

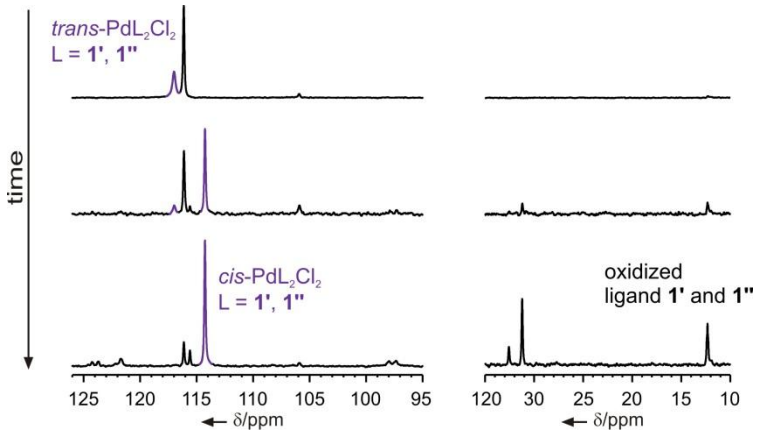

Figure 3.21. ^{31}P spectra of a sample containing Pd(**1'**)(**1''**)Cl$_2$ and corresponding homo-complexes and several by-products measured in different time-intervals after complex synthesis. ^{31}P signals of enantiomeric homocomplexes are colored.

Besides the ^{31}P signals of Pd(**1'**)(**1''**)Cl$_2$ (highlighted in Figure 3.21) and of the corresponding homocomplexes PdL$_2$Cl$_2$ (L = **1'**, **1''**) the ^{31}P signal of oxidized ligand **1** and several more – partially only small - ^{31}P signals indicate the formation of other (complex) species. Most striking are the ^{31}P signals at δ(^{31}P) = 31.2 and 32.6 ppm, which is a quite unusual chemical shift for phosphoramidite Pd complexes. Therefore these signals might also belong to decomposition products of the ligands. Surprisingly, these ^{31}P species possess

two different methine and methyl signals each alluding to heteroligand complexes. Two different methine and two methyl signals could also be assigned to another complex species at $\delta(^{31}P) = 105.9$ ppm. In addition to that a third signal at $\delta(^{1}H) = 1.37$ ppm could be assigned to this complex species by $^{1}H^{31}P$ HMBC showing NOEs to both methine signals. However, as already mentioned a precipitation in the sample substantially hampered NMR investigation, so that no further structural investigations have been made. Furthermore no complete ^{1}H signal assignment was achieved and a correct determination of the exact complex ratio in the sample could not be obtained by integration. summarizes the results obtained from $^{1}H^{31}P$ HMBC and $^{1}H^{1}H$ COSY.

Table 3.9. Summary of main NMR data of a sample (S_a,S_c,S_c)-**1'**•(R_a,R_c,R_c)-**1''**•Pd(cod)Cl_2 (0.02 M in CD_2Cl_2, 300 K)

species	$\delta(^{31}P)$ [ppm]	$\delta(^{1}H)$ / [ppm]		
		CH_{arom}	CH	CH_3
1	32.6	7.81 7.58 7.50 7.18	4.14 3.85	0.64 1.19
2	21.2	8.02 7.68 7.34 7.08 6.96 5.99	4.95 3.99	1.69 1.22
3	105.9	8.12	4.18 3.99	1.82 1.23 1.37
4	115.6	7.80 7.39 6.92	5.15	1.91
5	116.1	8.15 7.96 7.87 7.61 7.45 7.35 7.28 6.52	5.06	1.51

3.6.3 4(S_a,R_c,R_c)-1•$Pd_2(dba)_3$

As Pd(0) salts are usually used for catalysis, system 4(S_a,R_c,R_c)-**1**•$Pd_2(dba)_3$ (dba = dibenzylideneacetone) was investigated to find out if interligand interactions are also formed in Pd(0) complexes. During stirring time a temporary yellow coloration of the actual dark solution could be observed which vanished again soon and the initial dark coloration of the reaction mixture was regained. These changes of coloration indicate that Pd(0) must somehow have been oxidized to Pd(II) which was subsequently re-reduced to Pd(0). So far it is not clear which reagents in solution acted as oxidizing and reducing agent, respectively.

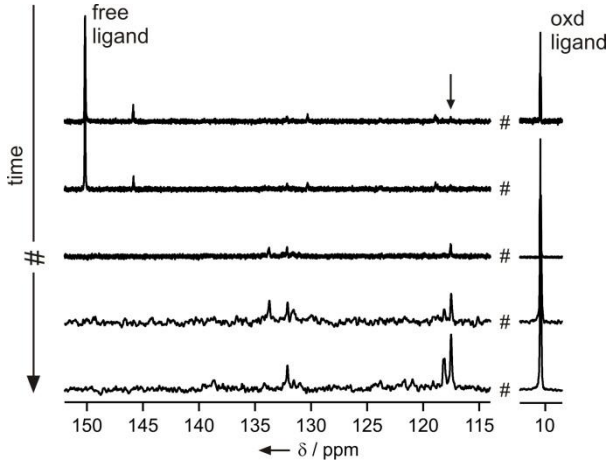

Figure 3.22. Time dependent ^{31}P NMR measurements of a sample 4(S_a,R_c,R_c)-**1**•$Pd_2(dba)_3$ (0.03 M in CD_2Cl_2).

^{31}P NMR investigations revealed that after about 2.5 h of stirring time two main species exist in solution with ^{31}P signals at $\delta(^{31}P)$ = 150.1 and 10.6 ppm. The signal at $\delta(^{31}P)$ = 150.1 ppm probably belongs to free ligand, whereas the signal at $\delta(^{31}P)$ = 10.6 ppm most likely belongs to oxidized ligand **1**.

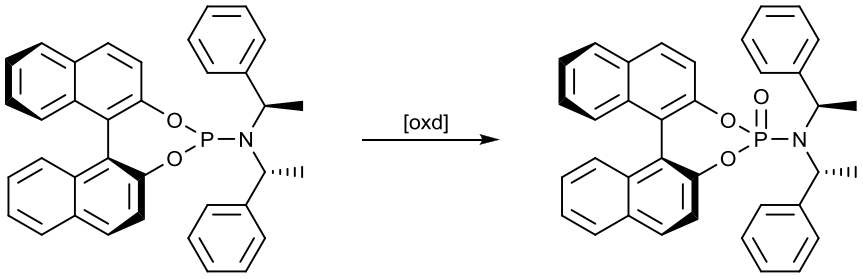

Scheme 3.3. Oxidation of phosphoramidite ligand **1**.

Besides free and oxidized ligand **1** small ^{31}P signals suggest the existence of several further complex species (see Figure 3.22). Time dependent ^{31}P NMR investigations pointed out a complete conversion of free ligand within about 10 to 12 h so that almost exclusively

oxidized ligand could be detected. However, after 5 days new ^{31}P measurements and $^{1}H^{31}P$ HMBC confirmed the formation of different complexes, but only to a small extent.

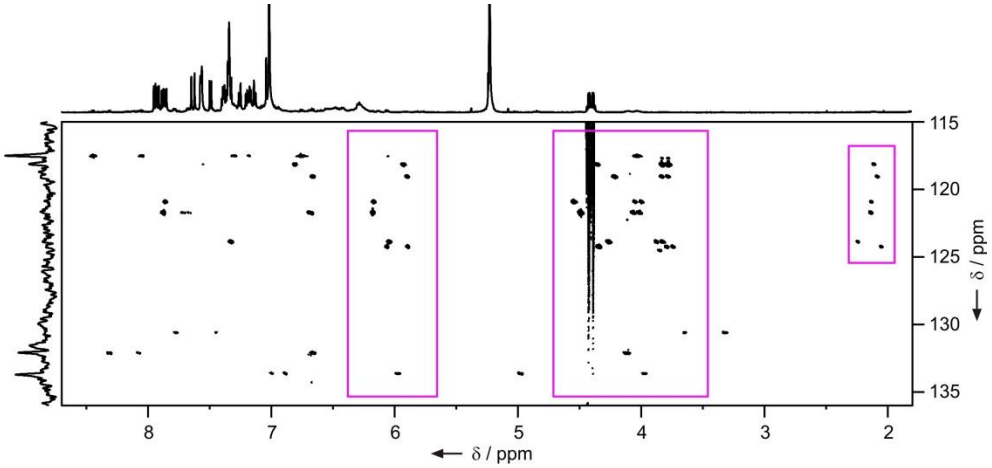

Figure 3.23. Section of a $^{1}H^{31}P$ HMBC of a sample 4(S_a,R_c,R_c)-**1**•$Pd_2(dba)_3$ measured five days after complex synthesis (0.03 M in CD_2Cl_2).

The $^{1}H^{31}P$ HMBC confirmed that more complex species than detectable in the ^{31}P spectra were formed. The cross signals in the region between δ(^{1}H) = 1.9 and 2.3, 3.6 and 4.6 and between 5.5 and 6.5 ppm (regions highlighted in Figure 3.23) intensely allude to allyl groups coordinated to Pd, most probably dba or derivatives of dba, which is also in accordance with the corresponding ^{13}C chemical shifts between δ(^{13}C) = 80 and 115 ppm for ^{1}H signals in the region at about 6 ppm in the $^{1}H^{13}C$ HSQC. However further structural investigations on these complexes have not been made.

In the latest ^{31}P spectra one striking signal at δ(^{31}P) = 117.5 ppm emerged (marked with an arrow in Figure 3.22). For that species no indication for dba or dba derivatives as described above could be found. Moreover the ^{31}P chemical shift as well as the cross signals in the $^{1}H^{31}P$ HMBC are identical with those of *cis*-Pd**1**$_2Cl_2$. Especially the significant upfield shift of the methine signal can also be observed for that species. Furthermore there are NOE signals between the methyl group and the binaphthol group. All these observations confirm that the formation of interligand interactions is also possible in Pd(0) complexes.

3.6.4 Low temperature studies

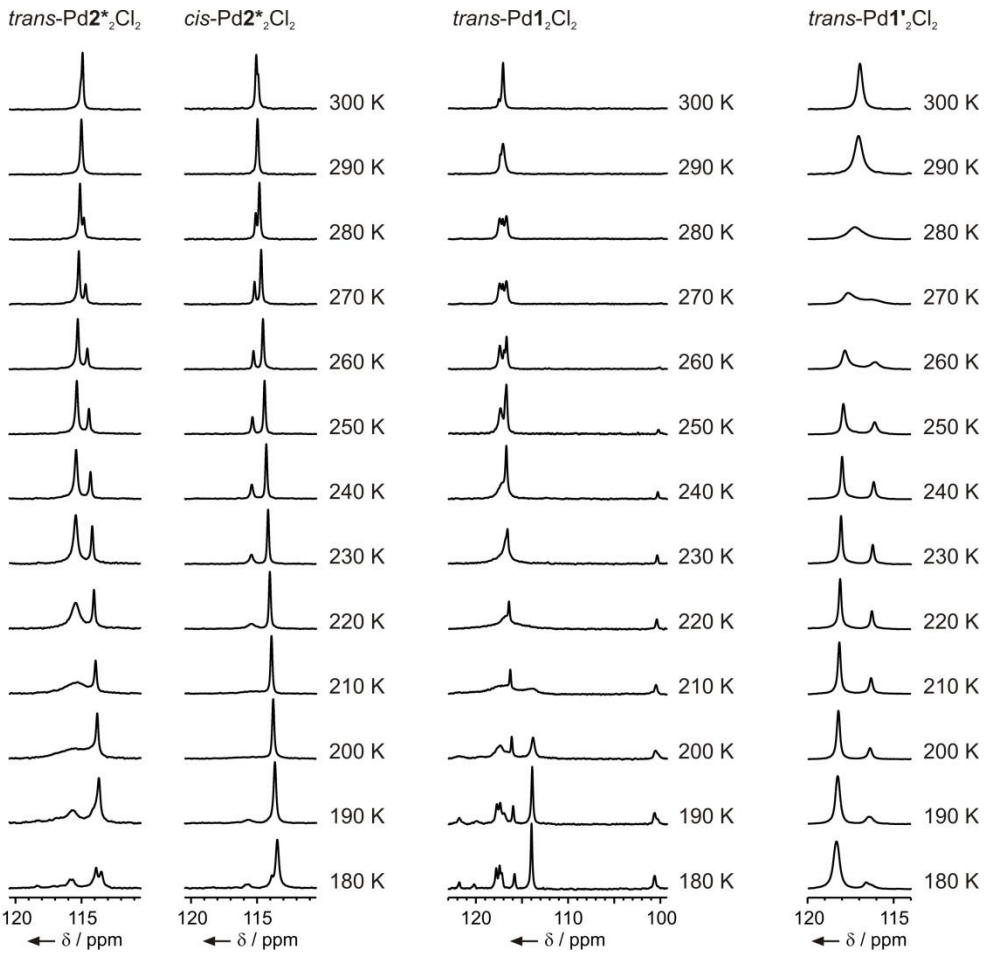

Figure 3.24. ^{31}P spectra of a sample with a majority of *trans*-Pd**2***$_2$Cl$_2$, *cis*-Pd**2***$_2$Cl$_2$, *trans*-Pd**1**$_2$Cl$_2$, *trans*-Pd**1'**$_2$Cl$_2$ (from left to right) measured at different temperatures in the range between 180 K and 300 K (0.03 M in CD_2Cl_2).

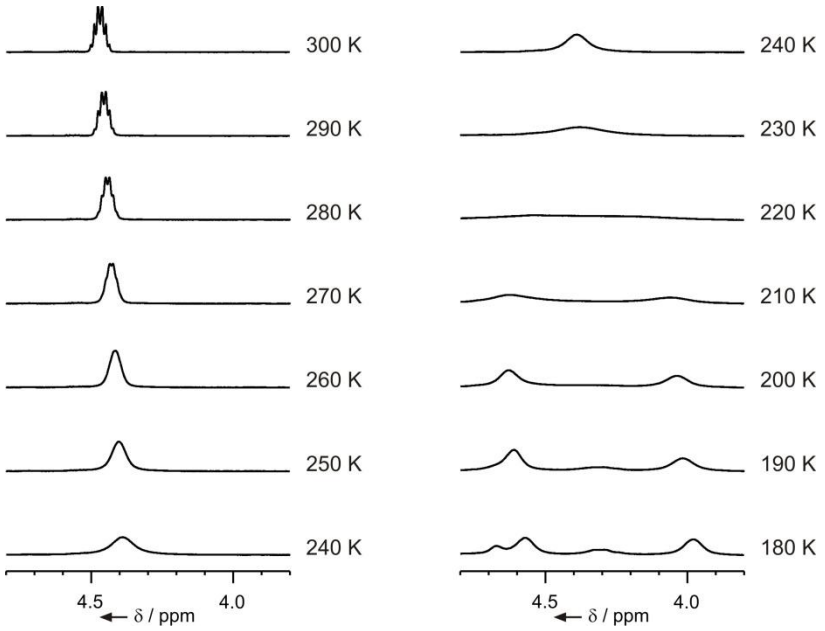

Figure 3.25. Section of ^{1}H spectra measured at different temperatures showing the methane signals of *cis*-Pd**2***$_2$Cl$_2$ (0.03 M in CD_2Cl_2).

Despite the involvement of the amine group into intra- and interligand interactions the rotation of the amine moiety around the P-N bond is still quite fast in *cis*-Pd**2***$_2$Cl$_2$. As a monitor for rotational processes the methine signal can be used. By cooling down the methine signal becomes broader until a coalescence temperature of 220 K is reached. Below 220 K the methine signal splits up into two separated signals, one for each CH group. Therefore below 220 K rotation of the amine group slows down on the NMR time scale. The coalescence temperature of 220 K is identical with that of the free ligand. However, not only the rotation around the P-N bond has to be considered, but also the rotation around the N-C bonds.

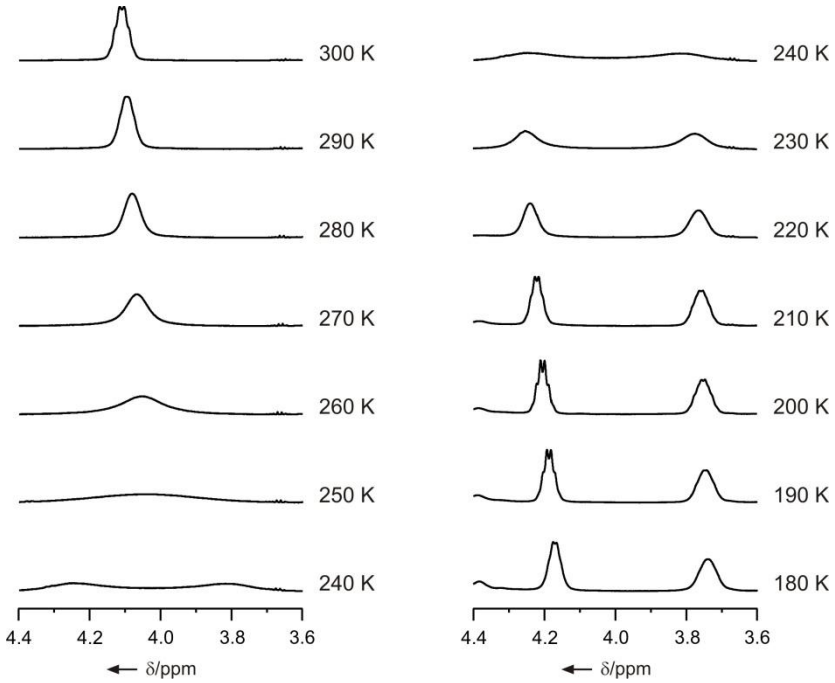

Figure 3.26. Sections of ^{1}H spectra measured at different temperatures showing the methine signals of *cis*-Pd**1**$_2$Cl$_2$ (0.03 M in CD_2Cl_2).

Within *cis*-Pd**1**$_2$Cl$_2$ the rotation of the amine group around the P-N bond slows down quite fast on the NMR time scale with decreasing temperature. The coalescence temperature of 250 K is similar to that of the free ligand. However, not only the rotation around the P-N bond has to be considered for the free ligand, but also the rotation around the N-C bonds.

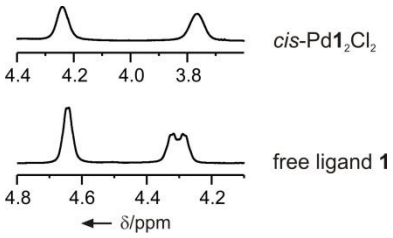

Figure 3.27. Comparison of the methine signals of *cis*-Pd**1**$_2$Cl$_2$ (above) and those of free ligand (S_a,R_c,R_c)-**1** measured at 220 K (0.02 M in CD_2Cl_2).

A comparison of the methine signals of *cis*-Pd**1**$_2$Cl$_2$ and **1** shows that in the free ligand the preferred spatial arrangement of the amine moiety leads to differently strong $^{3}J_{HP}$ couplings so that one of both signals is hardly affected by H-P coupling whereas the other methine signal experience a distinct doublet splitting (Figure 3.27). However, in *cis*-Pd**1**$_2$Cl$_2$ the $^{3}J_{HP}$ couplings between phosphor and both CH groups are fairly similar so that both methine signals experience only a (slight) broadening but no defined doublet splitting.

3.7 References

[1] H. B. Kagan, P. Dang Tuan, *J. Am. Chem. Soc.* **1972**, *94*, 6429-6433.

[2] U. Christmann, R. Vilar, *Angew. Chem. Int. Ed.* **2005**, *44*, 366-374.

[3] R. Hulst, N. K. de Vries, B. L. Feringa, *Tetrahedron: Asymmetry* **1994**, *5*, 699-708.

[4] M. T. Reetz, L. J. Goossen, A. Meiswinkel, J. Paetzold, J. F. Jensen, *Org. Lett.* **2003**, *5*, 3099-3101.

[5] D. S. Surry, S. L. Buchwald, *Angew. Chem. Int. Ed.* **2008**, *47*, 6338-6361.

[6] J. F. Teichert, B. L. Feringa, *Angew. Chem. Int. Ed.* **2010**, *49*, 2486-2528.

[7] A. H. M. de Vries, A. Meetsma, B. L. Feringa, *Angew. Chem. Int. Ed.* **1996**, *35*, 2374-2376.

[8] B. L. Feringa, M. Pineschi, L. A. Arnold, R. Imbos, A. H. M. de Vries, *Angew. Chem. Int. Ed.* **1997**, *36*, 2620-2623.

[9] L. A. Arnold, R. Imbos, A. Mandoli, A. H. M. de Vries, R. Naasz, B. L. Feringa, *Tetrahedron* **2000**, *56*, 2865-2878.

[10] B. L. Feringa, *Acc. Chem. Res.* **2000**, *33*, 346-353.

[11] C. Bolm, O. Beckmann, *Chirality* **2000**, *12*, 523-525.

[12] M. T. Reetz, T. Neugebauer, *Angew. Chem. Int. Ed.* **1999**, *38*, 179-181.

[13] A. Alexakis, S. Rosset, J. Allamand, S. March, F. Guillen, C. Benhaim, *Synlett* **2001**, *9*, 1375-1378.

[14] A. Alexakis, C. Benhaim, S. Rosset, M. Humam, *J. Am. Chem. Soc.* **2002**, *124*, 5262-5263.

[15] Z. Hua, V. C. Vassar, H. Choi, I. Ojima, *Proceedings of the National Academy of Sciences of the United States of America* **2004**, *101*, 5411-5416.

[16] D. Peña, A. J. Minnaard, J. G. de Vries, B. L. Feringa, *J. Am. Chem. Soc.* **2002**, *124*, 14552-14553.

[17] M. van den Berg, A. J. Minnaard, R. M. Haak, M. Leeman, E. P. Schudde, A. Meetsma, B. L. Feringa, A. H. M. de Vries, C. E. P. Maljaars, C. E. Willans, D. Hyett, J. A. F. Boogers, H. J. W. Henderickx, J. G. de Vries, *Adv. Synth. Catal.* **2003**, *345*, 308-323.

[18] A. Alexakis, D. Polet, *Org. Lett.* **2004**, *6*, 3529-3532.

[19] M. J. Pouy, A. Leitner, D. J. Weix, S. Ueno, J. F. Hartwig, *Org. Lett.* **2007**, *9*, 3949-3952.

[20] C. Shu, J. F. Hartwig, *Angew. Chem. Int. Ed.* **2004**, *43*, 4794-4797.

[21] M. Ueda, J. F. Hartwig, *Org. Lett.* **2009**, *12*, 92-94.

[22] M. D. K. Boele, P. C. J. Kamer, M. Lutz, A. L. Spek, J. G. de Vries, P. W. N. M. van Leeuwen, G. P. F. van Strijdonck, *Chem. Eur. J.* **2004**, *10*, 6232-6246.

[23] G. P. F. van Strijdonck, M. D. K. Boele, P. C. J. Kamer, J. G. de Vries, P. W. N. M. van Leeuwen, *Eur. J. Inorg. Chem.* **1999**, *1999*, 1073-1076.

[24] R. Imbos, A. J. Minnaard, B. L. Feringa, *Dalton Transactions* **2003**, 2017-2023.

[25] J. Meeuwissen, M. Kuil, A. M. van der Burg, A. J. Sandee, J. N. H. Reek, *Chem. Eur. J.* **2009**, *15*, 10272-10279.

[26] C. Monti, C. Gennari, U. Piarulli, *Chem. Eur. J.* **2007**, *13*, 1547-1558.

[27] M. T. Reetz, *Angew. Chem. Int. Ed.* **2008**, *47*, 2556-2588.

[28] D. Peña, A. J. Minnaard, J. A. F. Boogers, A. H. M. de Vries, J. G. de Vries, B. L. Feringa, *Org. Biomol. Chem.* **2003**, *1*, 1087-1089.

[29] M. T. Reetz, T. Sell, A. Meiswinkel, G. Mehler, *Angew. Chem. Int. Ed.* **2003**, *42*, 790-793.

[30] A. Duursma, R. Hoen, J. Schuppan, R. Hulst, A. J. Minnaard, B. L. Feringa, *Org. Lett.* **2003**, *5*, 3111-3113.

[31] C. Monti, C. Gennari, U. Piarulli, *Chem. Commun.* **2005**, 5281-5283.

[32] P.-A. R. Breuil, F. W. Patureau, J. N. H. Reek, *Angew. Chem. Int. Ed.* **2009**, *48*, 2162-2165.

[33] B. Breit, W. Seiche, *J. Am. Chem. Soc.* **2003**, *125*, 6608-6609.

[34] F. Chevallier, B. Breit, *Angew. Chem. Int. Ed.* **2006**, *45*, 1599-1602.

[35] M. de Greef, B. Breit, *Angew. Chem. Int. Ed.* **2009**, *48*, 551-554.

[36] Y. Liu, C. A. Sandoval, Y. Yamaguchi, X. Zhang, Z. Wang, K. Kato, K. Ding, *J. Am. Chem. Soc.* **2006**, *128*, 14212-14213.

[37] C. Waloch, J. Wieland, M. Keller, B. Breit, *Angew. Chem.* **2007**, *119*, 3097-3099.

[38] M. Weis, C. Waloch, W. Seiche, B. Breit, *J. Am. Chem. Soc.* **2006**, *128*, 4188-4189.

[39] S. Carboni, C. Gennari, L. Pignataro, U. Piarulli, *Dalton Transactions* **2011**, *40*, 4355-4373.

[40] G. Gasparini, M. Dal Molin, L. J. Prins, *Eur. J. Org. Chem.* **2010**, *2010*, 2429-2440.

[41] V. F. Slagt, P. W. N. M. van Leeuwen, J. N. H. Reek, *Chem. Commun.* **2003**, 2474-2475.

[42] K. Schober, E. Hartmann, H. Zhang, R. M. Gschwind, *Angew. Chem. Int. Ed.* **2010**, *49*, 2794-2797.

[43] H. Zhang, R. M. Gschwind, *Angew. Chem. Int. Ed.* **2006**, *45*, 6391-6394.

[44] H. Zhang, R. M. Gschwind, *Chem. Eur. J.* **2007**, *13*, 6691-6700.

[45] K. Schober, H. Zhang, R. M. Gschwind, *J. Am. Chem. Soc.* **2008**, *130*, 12310-12317.

[46] When using a ligand-to-metal ratio of 2 : 1 no free ligand was left after complex formation as could be seen in the ^{31}P spectrum. All of the employed $Pd(cod)Cl_2$ was converted as well because only ^{1}H and ^{13}C signals of released (cod) could be detected

in the corresponding NMR spectra after the formation of phosphoramidite Pd complexes.

[47] When using a ligand-to-metal ratio of 2 : 1 no free ligand was left. However integration of ^{1}H signals of released cod and of cod still coordinated to Pd revealed that only half of the employed $Pd(cod)Cl_2$ salt was converted. ^{1}H DOSY NMR measurements also confirmed the complexation of palladium by four phosphoramidites.

[48] I. S. Mikhel, G. Bernardinelli, A. Alexakis, *Inorg. Chim. Acta* **2006**, *359*, 1826-1836.

[49] J. Mason, *Multinuclear NMR*, Plenum Press, New York and London, **1987**.

[50] J. G. Verkade, *Coord. Chem. Rev.* **1972**, *9*, 1-106.

[51] A. L. Casado, P. Espinet, *Organometallics* **1998**, *17*, 954-959.

[52] I. Mikhel, K. Gavrilov, A. Polosukhin, A. Rebrov, *Russ. Chem. Bull.* **1998**, *47*, 1585-1588.

[53] S. Filipuzzi, P. S. Pregosin, A. Albinati, S. Rizzato, *Organometallics* **2006**, *25*, 5955-5964.

[54] E. Hartmann, R. M. Gschwind, *in preperation* **2012**.

[55] C. A. Hunter, *Angew. Chem. Int. Ed.* **2004**, *43*, 5310-5324.

[56] X. Rathgeb, S. March, A. Alexakis, *J. Org. Chem.* **2006**, *71*, 5737-5742.

[57] A. Jerschow, N. Muller, *J. Magn. Reson.* **1997**, *125*, 372-375.

[58] A. Macchioni, G. Ciancaleoni, C. Zuccaccia, D. Zuccaccia, *Chem. Soc. Rev.* **2008**, *37*, 479-489.

4 Diastereotopic Balance

The Supramolecular Balance for Transition Metal Complexes: Assessment of Noncovalent Interactions in Phosphoramidite Palladium Complexes

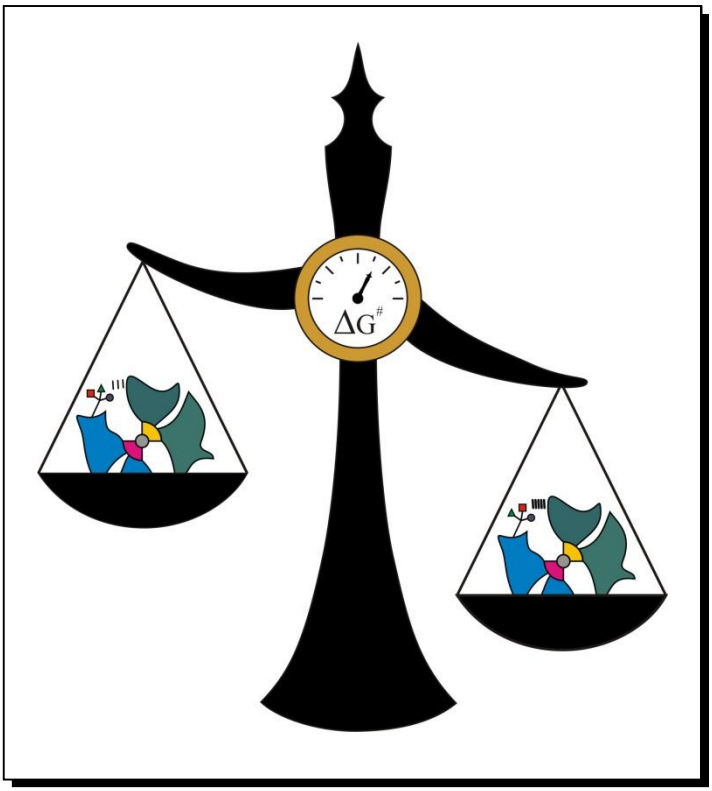

Evelyn Hartmann, and Ruth M. Gschwind

Molecular electrostatic potential surfaces were calculated by Michael Hammer.

To be submitted.

4.1 Abstract

A new and general method is presented to measure non-covalent interactions within transition metal complexes separated from electronic effects. Two equilibria between homo- and heterocomplexes are used to measure the free energy difference $\Delta\Delta G$ of the non-covalent interactions within two heterocomplexes. The selection of two enantiomeric and one enantiopure ligand allows for the energetic linkage of the two equilibria and for the separation of non-covalent interactions from electronic effects provided that the identical electronic properties of the enantiomers are retained in the heterocomplexes. The approach has been tested on phosphoramidite palladium complexes. NOESY spectra and ^{1}H chemical shift analyses prove the retention of the general complex structure and the calculated $\Delta\Delta G$ value fits to the experimentally determined interaction changes. Thus, for the first time non-covalent interactions in transition metal complexes are experimentally quantified and a pseudo-bidentate character of the privileged class of phosphoramidite ligands is shown.

4.2 Introduction

For some decades bidentate ligands prevailed in the field of transition-metal catalysis.[1-3] The superiority of bidentate ligands compared to monodentates was explained by the higher conformational rigidity of the ligands and a stronger coordination to the metal.[2] However, in the last few years monodentate ligands experienced a terrific revival and moreover, an immensely growing interest in rational ligand design could be observed:[4-13] Monodentate ligands have been developed which are able to self-assemble in the coordination sphere of the metal center through the formation of weak ligand-ligand interactions, such as hydrogen bonding[4-7] or metal bridged coordinative bonding.[8-10] However, the use of weak interligand interactions based on CH-π- or π-π interactions for rational ligand design is still very difficult.[11]

Various experimental and theoretic approaches have been made to investigate and quantify non-covalent interactions such as hydrogen bonding or π-π stacking and to explore their dependency on different solvent properties.[14-20] 'Double mutant cycles' developed by Fersht have become a powerful thermodynamic tool for the experimental quantification of non-covalent interactions in proteins or in host-guest model systems.[21-24] An essential advantage of this method is the elimination of secondary effects, such as changing H-bond strengths caused by single mutations in the system. As a result the free energy of an individual interaction of interest can be analyzed out of an array of secondary interactions.

In addition the 'molecular torsion balance' developed by Wilcox[25-26] finds application in the quantification of CH- π interactions and aromatic interactions in organic molecules.[14-15] However, no method has been presented so far to measure the contribution of non-covalent ligand-ligand interactions within transition metal complexes. For guest-host systems binding constants are typically used for the quantification of non-covalent interactions. However, in case of metal complexes the binding constant reflects not only non-covalent interactions, but primarily metal-ligand bindings based on the electronic properties such as σ-donor/π-acceptor properties of the ligands. Therefore, for the measurement of pure ligand-ligand interactions covalent and non-covalent contributions to the binding constant have to be separated, In addition possible changes in the electronic and electrostatic properties have to be regarded, i.e. changes in the stereoelectronic properties of the metal-ligand bond and of the electrostatic contributions of the dipoles due to reorientation within the ligands upon *trans-cis* isomerization has to be considered. To the best of our knowledge, until now it was not possible to separate the contributions of non-covalent interactions (e.g. van der Waals interactions, CH-π and π-π interactions) from stereoelectronic properties and electrostatic interactions in transition-metal complexes and to quantify them experimentally.

Therefore, in this study the first method is presented which allows the quantification of non-covalent ligand-ligand interactions in transition metal complexes separated from stereoelectronic and electrostatic effects. Based on the formation trends of different phosphoramidite palladium complexes the free energy difference $\Delta\Delta G$ caused by the formation of additional attractive CH-π interactions is determined. Moreover, $^{1}H^{1}H$ NOESY measurements and ^{1}H chemical shift changes Δδ were used to gain insights into the complex structures and their interaction patterns and to establish the reliability of the presented method.

4.3 Results and Discussion

General principle. The basic method presented in this study to measure non covalent interactions in transition metal complexes is not restricted to special ligands or transition metals. Therefore, first the general principle of the supramolecular balance for transition metal complexes is explained on complexes with the stoichiometry ML_2X_n (M = transition metal, L = chiral ligand, X = achiral ligand, for schematic illustration see Scheme 4.1):

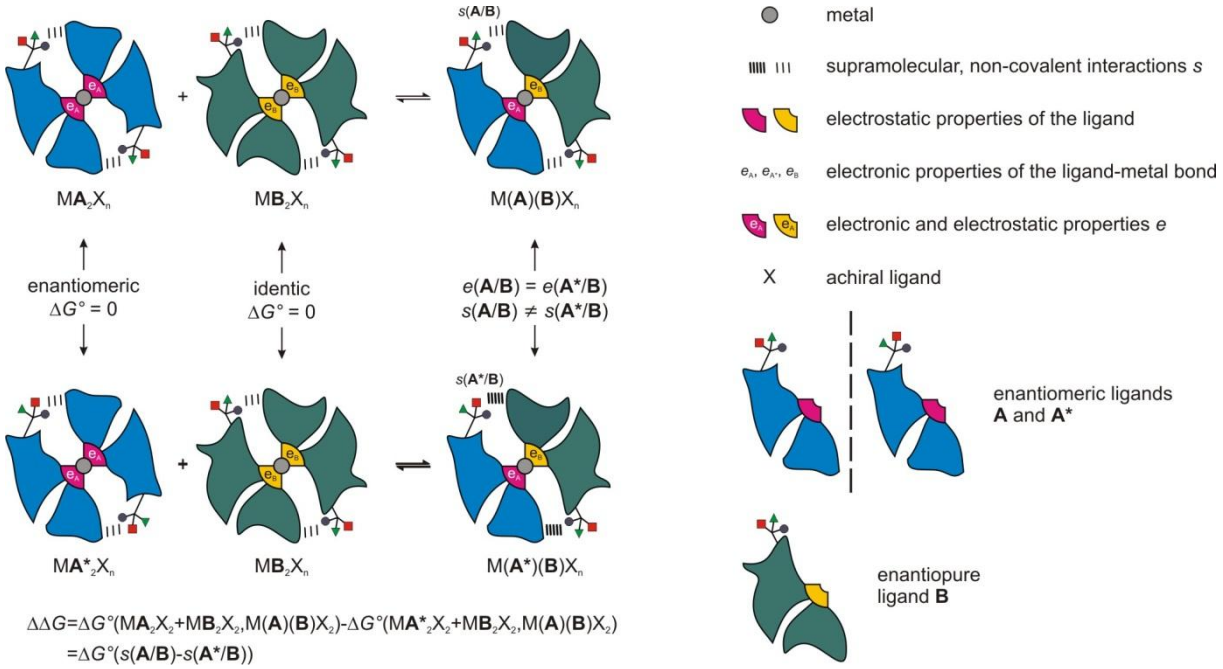

Scheme 4.1. The principle of the supramolecular balance for transition metal complexes: Two equilibria between homo- and heterocomplexes are linked energetically by combining one enantiopure ligand **B** (green) with two enantiomeric ligands **A** and **A*** (blue). Since identical or enantiomeric homocomplexes are formed, the free energy difference *ΔΔG* between the two equilibria directly provides the free energy difference of the two heterocomplexes. In case the heterocomplexes have identic stereoelectronic and electrostatic properties (*e*(**A**/**B**) = *e*(**A***/**B**)) the *ΔΔG* value directly reflects the difference in non-covalent supramolecular interactions *s*(**A**/**B**) and *s*(**A***/**B**).

a) Three chiral ligands, **A**, **A*** (enantiomer of **A**) and **B,** are chosen. For each ligand combination **A**/**B** and **A***/**B** an equilibrium between two homocomplexes - ML_2X_n and ML'_2X_n - and one heterocomplex $MLL'X_n$ is formed (see Scheme 4.1). For both equilibria the free energy $\Delta G°$ of the heterocomplex formation can be determined from the complex integrals according to $\Delta G° = -RT\ln K$.

b) The selection of two enantiomeric ligands (**A**, **A***) and one enantiopure ligand (**B**) allows for the energetic linkage of the two equilibria. For both ligand combinations homocomplex $M\mathbf{B}_2X_n$ is identical, while homocomplexes $M\mathbf{A}_2X_n$ and $M\mathbf{A}^*_2X_n$ are enantiomeric ($\Delta G = 0$). As a result, the free energy difference between both systems

($\Delta\Delta G$ = $\Delta G°$(**A**/**B**) - $\Delta G°$(**A***/**B**)) directly reflects the energy difference between the two heterocomplexes M(**A**)(**B**)X_n and M(**A***)(**B**)X_n.

So far this method is applicable without restrictions on the structure of the ligands or the transition metal complexes. However, the resulting $\Delta\Delta G$ encompasses energetic differences caused by both stereoelectronic and electrostatic properties *e* (σ-donor/π-acceptor properties, electrostatic interactions of the dipoles within each ligand) and supramolecular interactions (*s*) within one heterocomplex compared to the other. In order to measure pure supramolecular interactions, the electronic contributions have to be eliminated. Therefore,

c) ligands and transition metal complexes are selected, which provide identical stereoelectronic and electrostatic effects *e* but different supramolecular interactions *s* in the two heterocomplexes (*e*(**A**/**B**) = *e*(**A***/**B**); *s*(**A**/**B**) ≠ *s*(**A***/**B**)). As a result, the free energy difference between the two complex equilibria provides exclusively the energetic difference of supramolecular interactions in both heterocomplexes ($\Delta\Delta G$ = $\Delta G°$(*S*(**A**/**B**) - *S*(**A***/**B**)).

Two enantiomeric ligands **A** and **A*** possess by definition identical chemical properties in an achiral environment also including stereoelectronic properties such as σ-donor/π-acceptor character in metal complexes. However, in a chiral environment enantiomers can generally be discriminated by the formation of different interactions. In metal complexes such a chiral environment can easily be created by a simple combination with another chiral ligand, e.g. ligand **B**. Thus, supramolecular ligand-ligand interactions in the diastereomeric complexes M(**A**)(**B**)X_n and M(**A***)(**B**)X_n are expected to differ in their strength. In order to use both of these fundamental properties of enantiomeric ligands for the separation of electronic and supramolecular interactions in metal complexes, the electronic properties of **A** and **A*** have to stay identical within both diastereomeric complexes M(**A**)(**B**)X_n and M(**A***)(**B**)X_n. That means complexes with clearly defined coordination sites and with identical general structures must be formed. In addition, the orientation of the dipoles has to be retained within M(**A**)(**B**)X_n and M(**A***)(**B**)X_n to achieve identical electrostatic properties of the two complexes. One possible approach to fulfill these general requirements for the applicability of the transition metal balance is the selection of ligands and complexes, which meet the following structural criteria (see Scheme 4.1 for schematic illustration):

i) For **A**, **A*** and **B** ligands are selected which can be separated into “two spheres”: A small structurally rigid inner sphere, in which all heteroatoms are located encompassing the dipoles (see pink and yellow triangles in Scheme 4.1), and a larger nonpolar outer sphere, which is responsible for supramolecular non-covalent interactions.

ii) The moieties of the ligands, which contain the chiral center(s) and are involved into supramolecular interactions, should be flexibly connected to the inner sphere. That allows for different orientations of the chiral parts of **A**, **A*** and **B** without inducing torsional strains on the whole ligands.

If these structural criteria are fulfilled the direct involvement of the different chiral groups of **A** and **A*** into non-covalent interactions with the chiral moiety of ligand **B** in a transition metal complex causes a difference in the strength of supramolecular interactions $s_{(\mathbf{A/B})}$ and $s_{(\mathbf{A^*/B})}$. However, the formation of interligand interactions in the outer spheres should have no effect on the electrostatic properties in the inner spheres of **A**, **A*** and **B**, so that the electronic properties $e_{(\mathbf{A/B})}$ and $e_{(\mathbf{A^*/B})}$ of the two diastereomeric complexes M(**A**)(**B**)X_n and M(**A***)(**B**)X_n can be supposed to be identical.

Compared to the classical `molecular torsion balance` originally developed by Wilcox[25-26] the presented supramolecular balance for transition metal complexes has the advantage that non-covalent interactions within the complex are exchanged. Therefore, the usually extremely important solvation effects[15, 27] on intermolecular interactions can be neglected for our method.

Model system. This method was tested on Pd(II) complexes using combinations of the famous phosphoramidite ligands (S_a,R_c,R_c)-**1**,[28] (S_c,S_c)-**2*** and (R_c,R_c)-**2**[29] (see Figure 2b), which find broad applications in many asymmetric catalytic reactions.[28-34]

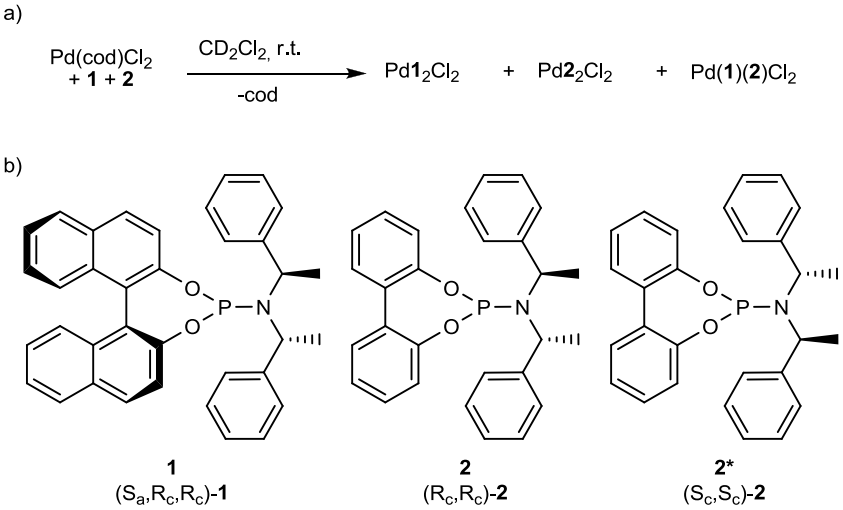

Scheme 4.2. a) General synthesis of the hetero- and homocomplexes and b) schemes of phosphoramidite ligand **1** and enantiomeric ligands **2** and **2*** used in this study.

Both ligands meet the structural requirements discussed above: All heteroatoms are located in a very small inner sphere (O_2PN moieties), whereas the extensive outer sphere allows the formation of CH-π and π-π interactions. The chiral centers are located in two amine side chains with high rotational flexibility, which is neither affected by complexation nor by aggregation.[35] Moreover, we could already observe a general affinity of these phosphoramidites to form non-covalent interligand interactions in the temperature dependent interconversion of different Cu complexes[35-36] and in aggregation studies of these ligands and their Cu, Pd and Ir complexes.[35]

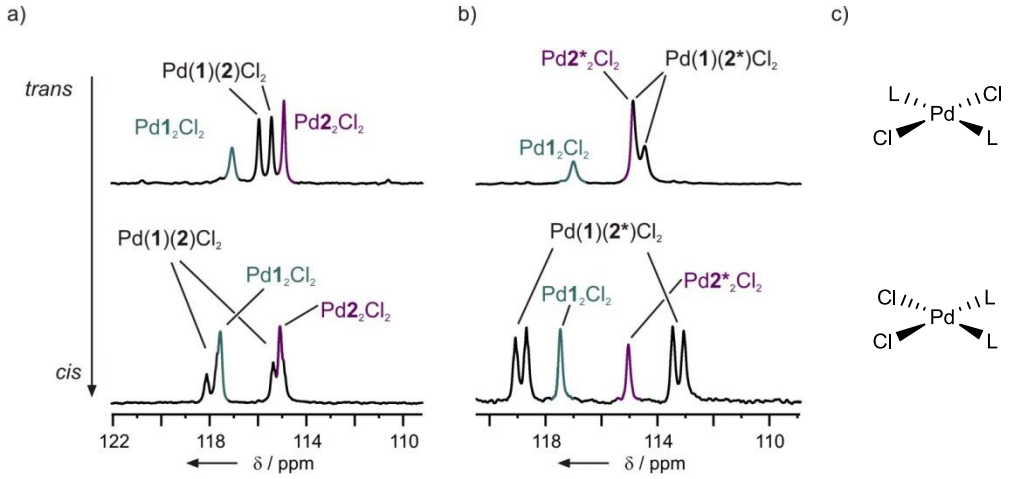

Figure 4.1. ^{31}P spectra of a) Pd(**1**)(**2**)Cl_2 and b) Pd(**1**)(**2***)Cl_2 and corresponding homocomplexes (colored) in exclusive *trans*-configuration (above) and after complete interconversion into *cis*-complexes (below) c) illustrated on the example of PdL_2Cl_2.

Retention of the general complex structure. Primarily the retention of the general complex structure upon ligand variation was investigated by a small screening of phosphoramidite Pd complexes using overall four different ligand combinations (see also chapter 3).[37] After complex synthesis for each investigated ligand combination one heterocomplex PdLL'Cl_2 and the corresponding two homocomplexes PdL_2Cl_2 and PdL'_2Cl_2 are formed. $^2J_{PP}$ scalar coupling constants between 1150 and 1180 Hz for all heterocomplexes verified the formation of exclusively *trans*-complexes, which completely, but slowly convert into *cis*-complexes with appropriate $^2J_{PP}$ coupling constants between 95 and 105 Hz.[38-42] This isomerization is shown on the ^{31}P spectra of the ligand combinations **1/2** and **1/2*** in Figure 4.1. In addition, the interaction pattern is extremely similar within all *cis*-complexes Pd(L)(L')Cl_2 and closely resembles the known crystal structure of *cis*-Pd**2***$_2Cl_2$.[43] Therefore, in the following all structural details will be discussed on modifications of this crystal structure (e.g. mirror image and/or extensions of aromatic systems, see Figure 4.2a).

The extremely high structural similarity of the complexes is explained best by the comparison of the ^{1}H spectra of the homocomplexes *cis*-Pd**1**$_2Cl_2$ and *cis*-Pd**2**$_2Cl_2$ with the heterocomplex *cis*-Pd(**1**)(**2**)Cl_2 shown in Figure 4.2b. For both homocomplexes only one set of signals is detected due to the high symmetry of the complexes. The ^{1}H spectrum of the heterocomplex Pd(**1**)(**2**)Cl_2, which contains also both homocomplexes, is almost an addition of the spectra of the corresponding homocomplexes reflecting the high structural similarity. In all complexes two separated sets of signals are detected for the two aromatic rings of each biaryl unit, which show a high chemical shift dispersion due to different non-covalent interactions obvious by the complex structures shown in Figure 4a. One half of the biphenol

or binaphthol unit (labeled 3, 4, 5, etc.) is involved in CH-π and π–π interactions with the amine moiety of the other ligand (see inter(**2**→**2**), inter(**1**→**1**), inter(**2**→**1**) and inter(**1**→**2**) in Figure 4.2a), whereas the second half of the biaryl units (labeled 3', 4', 5', etc.) shows π–π stacking with one phenyl group of the own ligand (see intra(**1**) and intra(**2**) in Figure 4.2a). In contrast, only one set of proton signals is observed for both amine side chains indicating a rotation around the P-N bond, which is fast on the NMR time scale (see signals a-f in Figure 4.2b). Next, the variation of the interligand interactions between the homocomplexes and the heterocomplex can be analyzed. In all complexes the CH and CH_3 group of one of the amine arms is located on the interligand interface and directed towards one half of the biaryl unit of the second ligand (see inter contacts in Figure 4a). The CH group and the CH_3 group of the second amine arm are not involved in interactions and directed towards the amine moiety. Since the amine moieties of the ligands **1** and **2** are identical, variations in the chemical shifts of the CH and CH_3 groups are determined by the interligand interactions. Thus, a change from homo- to heterocomplex under retention of the complex structure just exchanges the interacting biaryl groups for both, CH and CH_3 group, in the interligand interactions (see inter(**1**→**2**) and inter(**2**→**1**)). Exactly this structural exchange is reflected by the chemical shift changes observed in the ^1H spectra of the three complexes (see Figure 4.2b). The chemical shift assignment shows that the methine and methyl signals of ligand **1** and **2** in the heterocomplex change places compared to the corresponding homocomplexes (see signals a and b and dotted lines in Figure 4.2b).

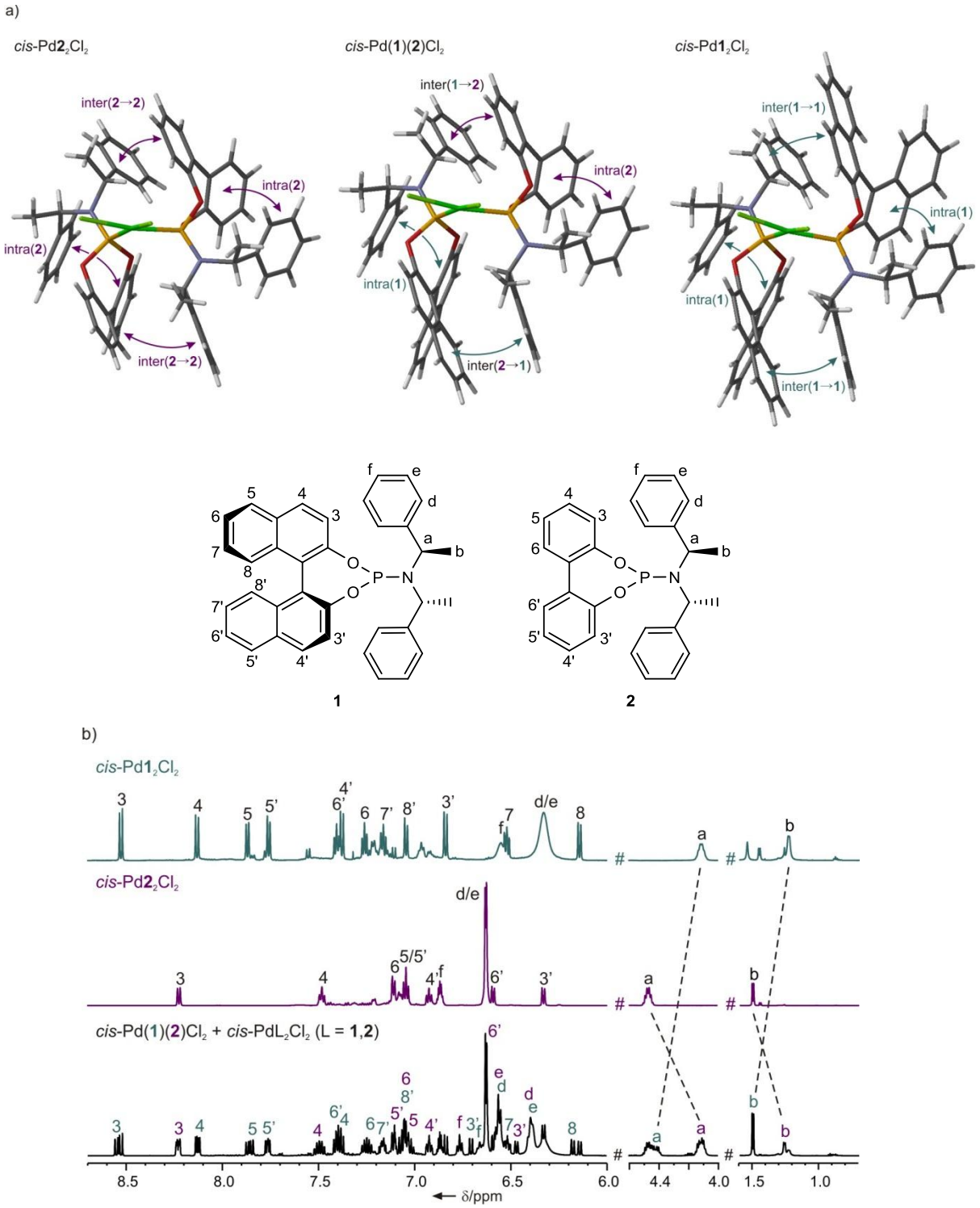

Figure 4.2. a) Inter- and intraligand interactions in *cis*-Pd**2**$_2$Cl$_2$, *cis*-Pd(**1**)(**2**)Cl$_2$ and *cis*-Pd**1**$_2$Cl$_2$ presented on structural models derived from the crystal structure of *cis*-Pd**2***$_2$Cl$_2$. b) The extreme similarity of the ^{1}H spectrum of *cis*-Pd(**1**)(**2**)Cl$_2$ with those of the homocomplexes *cis*-PdL$_2$Cl$_2$ (L = **1**, and **2**) reveals the close retention of the general complex structure and the interaction pattern in the hetero- and homocomplexes.

Proof of concept. After proving the fulfilment of all structural conditions discussed above, which guarantee no affection of electronic properties by the formation of supramolecular interactions, the free energy contribution of different non-covalent

interactions can be measured with the double equilibrium approach shown in Scheme 4.1. Using ligand combinations **1**/**2** and **1**/**2*** the simulations and integrations of the ^{31}P spectra indeed revealed different homo-to-heterocomplex ratios indicating a variation in supramolecular interactions (see Figure 4.1 and for simulations Figure 4.6 to Figure 4.8 in the Supporting Information). For ligand combination **1**/**2*** we observed a ratio of 1.0 : 0.9 : 4.5 for the two *cis*-homocomplexes to the *cis*-heterocomplex, whereas for ligand combination **1**/**2** the homo-to-heterocomplex ratio approximates statistical distribution (1.0 : 1.1 : 2.1). According to the formulas described above the free energy difference between the two heterocomplexes *cis*-Pd(**1**)(**2***)Cl_2 and *cis*-Pd(**1**)(**2**)Cl_2 can now be calculated to $\Delta\Delta G = \Delta G(s(\mathbf{2^*/1}) - s(\mathbf{2/1})) = -4.82$ kJ/mol (for detailed calculations see SI). That value directly describes the stabilization of *cis*-Pd(**1**)(**2***)Cl_2 compared to *cis*-Pd(**1**)(**2**)Cl_2 caused by additional non-covalent supramolecular interactions.

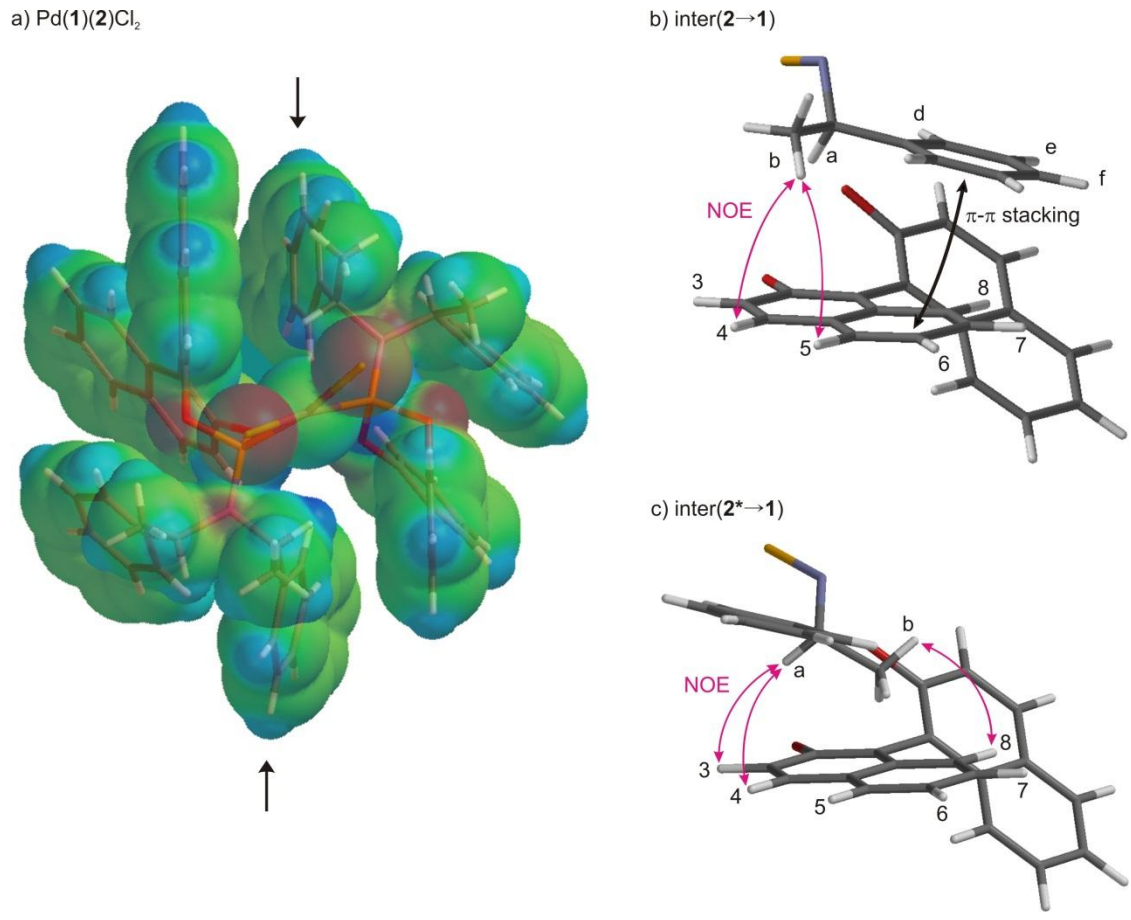

Figure 4.3. a) Molecular electrostatic potential surfaces plotted on the van der Waals' surface of *cis*-Pd(**1**)(**2**)Cl_2 (IsoVal -0.5) calculated at a AM1 level of theory. Positive regions are shown in blue, negative regions are shown in red. The tube representation and molecular electrostatic potential surface shows that the amine moieties composed of CH, CH_3 and phenyl groups form a large flat interligand interaction area (see arrows) with a maximum of the positive charge on the CH; b) details of the interligand interactions inter(**2**→**1**) with experimental NOE contacts; c) in the heterocomplex *cis*-Pd(**1**)(**2***)Cl_2 only the CH_3 and the phenyl group are exchanged in the amine moieties, which leads to an exchange of these groups in the interligand interactions inter(**2***→**1**).

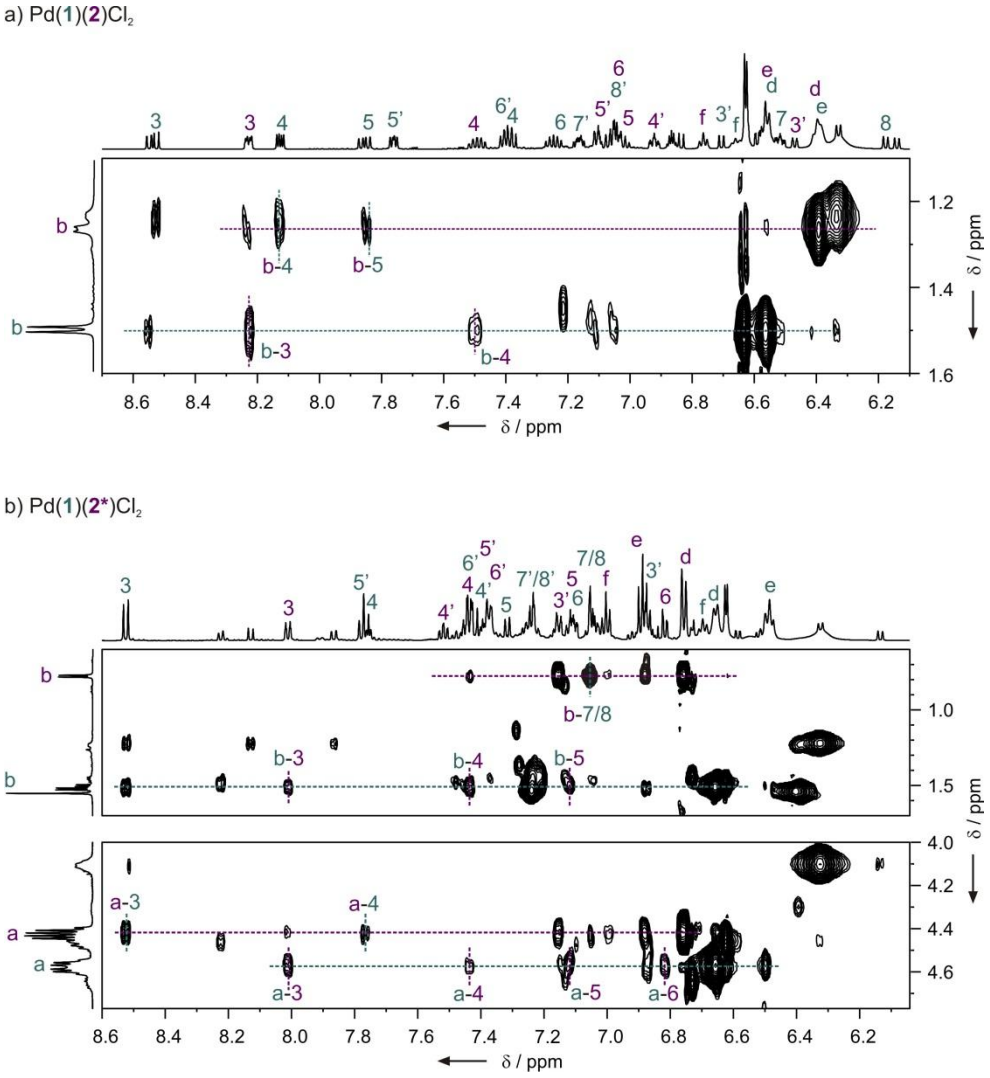

Figure 4.4. Sections of $^{1}H^{1}H$ NOESY spectra of a) *cis*-Pd(**1**)(**2**)Cl_2 and b) *cis*-Pd(**1**)(**2***)Cl_2 in which the observed interligand NOE cross peaks are highlighted (cross peaks of intraligand interactions or homocomplexes are not labeled).

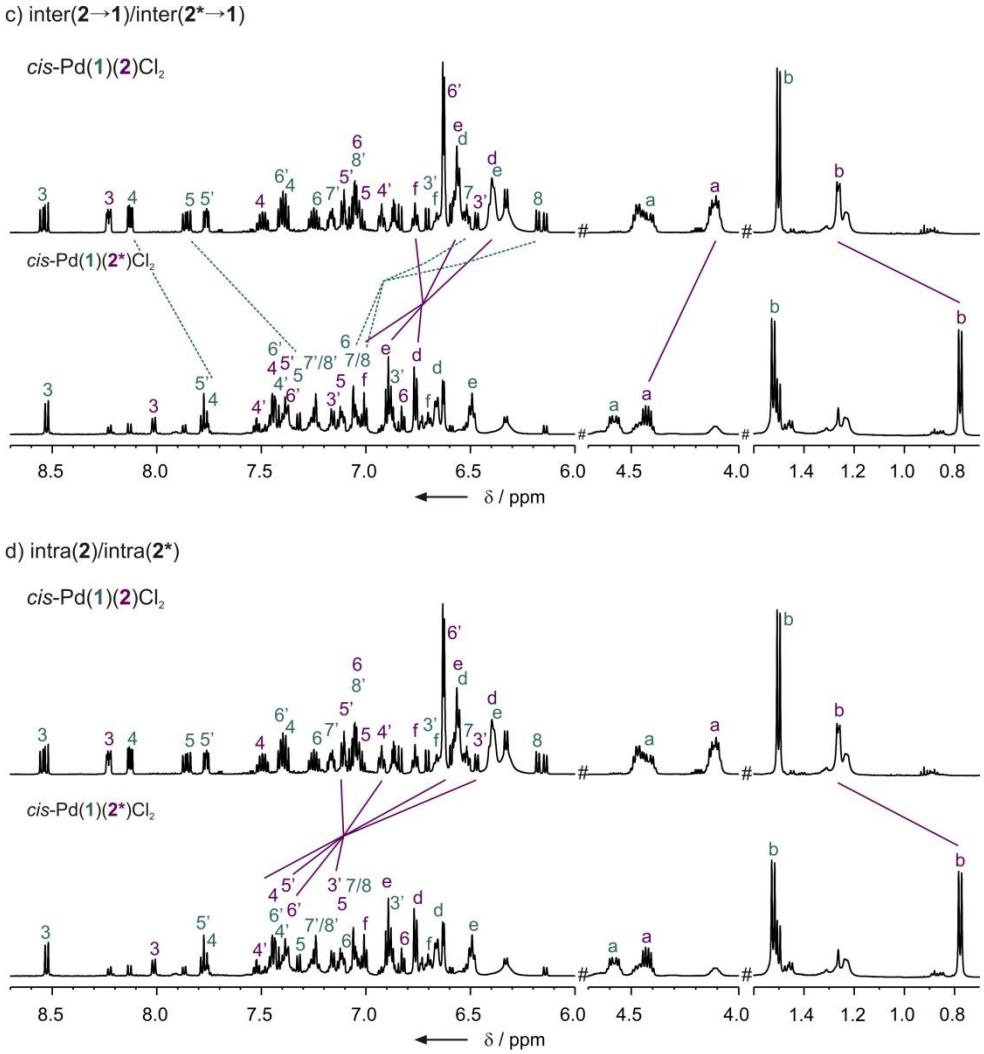

Figure 4.5. ^{1}H chemical shift analysis of *cis*-Pd(**1**)(**2**)Cl_2 and *cis*-Pd(**1**)(**2***)Cl_2 for the c) interligand interaction and d) intraligand interactions. Chemical shift changes Δδ between the two heterocomplexes, which confirm the mutual exchange of the CH_3 and the phenyl group are pointed out by colored lines.

Next ^{1}H^{1}H NOESY spectra and ^{1}H chemical shift changes Δδ were used to gain insights into the differences of non-covalent interactions between the two heterocomplexes. An overview of the expected structural changes will be discussed first based on the heterocomplex structure of *cis*-Pd(**1**)(**2**)Cl_2 (see Figure 4.2a) and its tube representation showing the electrostatic potential surface and contact areas of *cis*-Pd(**1**)(**2**)Cl_2 in an optimized view of the interligand interactions (see Figure 4.3a). The tube representation reveals that in *cis*-Pd(**1**)(**2**)Cl_2 one amine moiety composed of CH, CH_3 and a phenyl group forms a large, nearly planar surface area which can interact with the biaryl group of the second ligand via CH-π and π–π interactions. Within this contact area a maximum in the molecular electrostatic potential surface indicates that the CH group possesses the highest proton donating ability (dark blue in Figure 4.3a) i.e. the largest stabilizing effect for CH-π interactions. Concerning ligand **2** and **2*** the main difference between both ligands lies in

the configuration of their amine moiety which can be seen as a mutual exchange of the CH_3 and the phenyl group. Thus, under a retention of the general complex structure the CH_3 group of **2** in the interligand interactions inter(**2**→**1**) should be exchanged by the phenyl group and vice versa to give inter(**2***→**1**) (see Figure 4.3b and c). Indeed, the NOESY spectra and the chemical shift changes Δδ between *cis*-Pd(**1**)(**2**)Cl_2 and *cis*-Pd(**1**)(**2***)Cl_2 show exactly this group interchange accompanied by a minimal conformational reorientation to optimize the group interaction geometries (see Figure 4.3b and c for schematic representation): As to complex *cis*-Pd(**1**)(**2**)Cl_2, the methyl group of ligand **2** is located outside the naphthol plane of ligand **1** leading to NOE contacts to position 4/5 (see Figure 4.4a), whereas the methine group directly lies within the naphthol surface area in close approximation to quaterny carbons. Therefore, no interligand NOEs can be detected for the methine of ligand **2**. However, an involvement into pretty strong CH-π interaction could be proven by its significant upfield-shift. Aside from CH-π interactions π-π stacking between phenyl and naphthol group also contributes to interligand interactions in *cis*-Pd(**1**)(**2**)Cl_2, which can be realized by upfield-shifts of the ^1H signals of the phenyl group (d,e,f) and of the naphthol group (7, 8) (see Figure 4.4c). Compared to inter(**2**→**1**) there is no π-π stacking between the phenyl and the naphthol group in inter(**2***→**1**) of *cis*-Pd(**1**)(**2***)Cl_2 which is in good agreement with the observed ^1H chemical shifts for the phenyl signals (d,e,f) of ligand **2*** and the naphthol signals (7/8) of ligand **1** (highlighted by colored lines in Figure 4.4c). Instead, methyl and phenyl group change positions so that strong CH_3-π interactions are formed, which is in accordance with the significant upfield-shift of the methyl signal (b) and the observed interligand NOEs to the naphthol group (7/8) (Figure 4.4b and c). As to the CH group (a) its orientation has slightly shifted so that in *cis*-Pd(**1**)(**2***)Cl_2 NOE contacts to the binaphthol group of ligand **1** (3/4) can be observed (Figure 4.4b). In both heterocomplexes the CH group is involved into intraligand interactions which can also be seen on the significant downfield shift of more than 0.7 ppm by the *trans*-*cis*-isomerization (data not shown). However, the smaller downfield-shift of the CH signal in *cis*-Pd(**1**)(**2***)Cl_2 compared to *cis*-Pd(**1**)(**2**)Cl_2 indicates a slight reduction of CH-π interaction due to the reorientation discussed above (Figure 4.4c). In summary the π-π interactions between the terminal aromatic ring of one naphthol group of **1** and the phenyl group of **2** in *cis*-Pd(**1**)(**2**)Cl_2 are replaced by CH-π interactions with the methyl group of **2*** in *cis*-Pd(**1**)(**2***)Cl_2, and at the same time CH-π interaction between the methine and the naphthol group are slightly reduced.

Due to the symmetry of the two amine moieties in **2** and **2*** the identical structural change is also expected for the intraligand interactions between the second amine arm and the own biphenol unit in both complexes (see intra(**2**) in Figure 4.2a for visualization). Indeed, again π-π stacking in *cis*-Pd(**1**)(**2**)Cl_2 is replaced by CH_3-π interactions in *cis*-Pd(**1**)(**2***)Cl_2 confirmed by appropriate downfield-shifts of the biphenol part incorporated into intraligand interactions (3'-6') (Figure 4.4d). The remaining parts of the complexes which are not directly affected by the mutual group exchange in **2** and **2*** (e.g. intra(**1**), inter(**1**→**2**) and inter(**1**→**2***), see Figure 4a) show no significant structural changes indicated by very similar NOE contacts and ^1H chemical shifts.

Thus, the mutual exchange of the CH_3 and the phenyl group in the amine moieties of ligand **2** and **2*** causes a replacement of two strong π-π interactions in *cis*-Pd(**1**)(**2**)Cl_2 by two strong CH_3-π interaction in *cis*-Pd(**1**)(**2***)Cl_2, and, moreover, a substitution of two weak CH_3-π interactions by two weak π-π interactions. In addition, in inter(**2***→**1**) the CH-π interaction between the CH and the naphthol group is slightly reduced. Of course in a system with such multiple functional group interactions as described above, the experimentally determined $\Delta\Delta G$ value cannot directly be used to measure a single functional group interaction. However, the structural investigations show that effectively two phenyl groups are replaced by two CH_3 groups such as in a pseudo diastereotopic balance, which in a very rough approximation could be addressed as two additional CH-π interactions. Thus, the calculated $\Delta\Delta G$ value of -4.8 kJ/mol is in the right order of magnitude for the structural changes discussed above[17, 27, 44-45] approving the applicability of our method presented here.

4.4 Conclusion

In summary, to our knowledge for the first time a method is presented to determine experimentally and quantitatively the contribution of non-covalent interactions within transition metal complexes. In this general approach the $\Delta\Delta G$ value of two complex equilibria is used as a measure for the deviating non-covalent interactions within the two heterocomplexes. The two equilibria are energetically linked by the combination of one enantiopure ligand with two enantiomeric ligands leading to identical or enantiomeric homocomplexes. In addition, the selection of two enantiomeric ligands allows for the separation of non-covalent supramolecular interactions from stereoelectronic and electrostatic properties such as σ-donor/π-acceptor characters or dipole/dipole interactions provided that their identical electronic properties are retained in the two heterocomplexes. In addition, this method using deviating intracomplex interactions within two heterocomplexes has the advantage that solvation effects of the interacting functional groups are of minor importance. The applicability of this approach was proven on phosphoramidite palladium complexes with identical general structures. The mutual exchange of the CH_3 and the phenyl groups from one ligand to its enantiomer is directly reflected in the structural changes observed by NOE cross peaks and ^1H chemical shift changes Δδ. The experimentally determined $\Delta\Delta G$ value is in the right order of magnitude for the observed changes in the interaction pattern. However, the multiple functional group interactions obscure the $\Delta\Delta G$ assignment to a single interaction. In addition, this example proves for the first time that in solution the catalytically highly important and privileged class of phosphoramidite ligands show a pseudo bidentate character based on CH-π and π–π interactions.

4.5 Supporting Information

4.5.1 ^{31}P spectra simulation

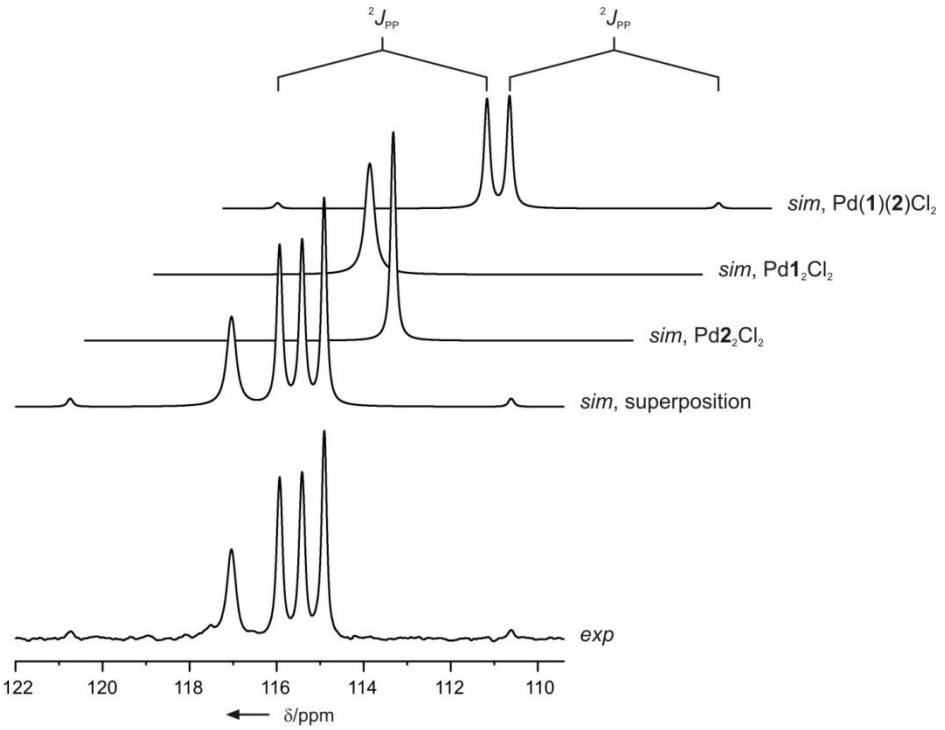

Figure 4.6. ^{31}P spectrum of a sample containing *trans*-Pd(**1**)(**2**)Cl_2 and corresponding homocomplexes *trans*-PdL_2Cl_2 (L = **1**, **2**) and simulations of the ^{31}P spectra of each *trans*-complex.

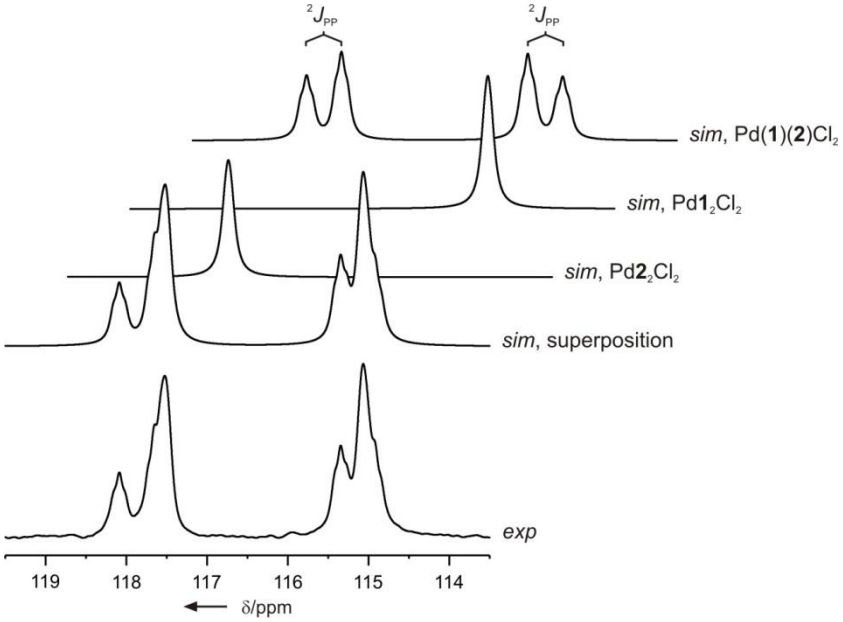

Figure 4.7. ^{31}P spectrum of a sample containing *cis*-Pd(**1**)(**2**)Cl_2 and corresponding homocomplexes *cis*-PdL_2Cl_2 (L = **1**, **2**) and simulations of the ^{31}P spectra of each *cis*-complex.

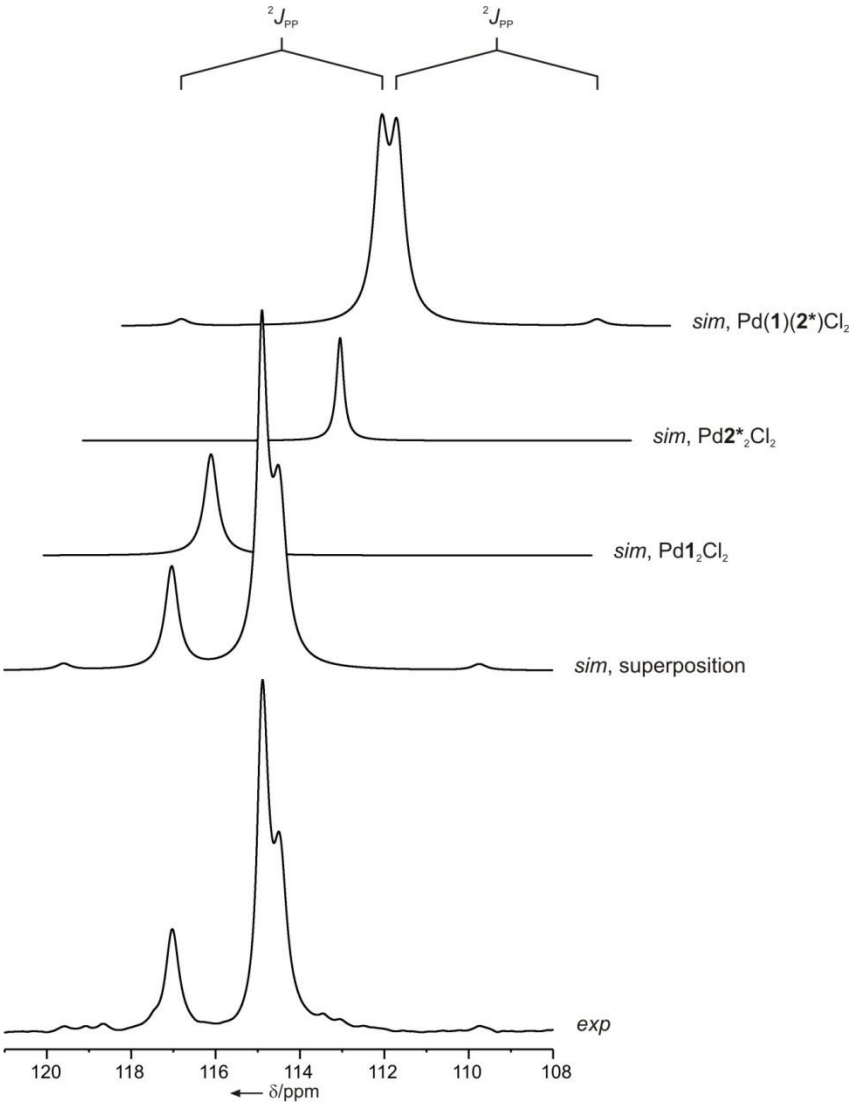

Figure 4.8. ^{31}P spectrum of a sample containing *trans*-Pd(**1**)(**2***)Cl_2 and *trans*-PdL_2Cl_2 (L = **1**, **2***) and already a small amount of the corresponding *cis*-complexes and simulations of the ^{31}P spectra of each *trans*-complex.

4.5.2 *ΔG°* calculations

$$Pd\mathbf{1}_2Cl_2 + Pd\mathbf{2}_2Cl_2 \rightleftharpoons Pd(\mathbf{1})(\mathbf{2})Cl_2$$

$$Pd\mathbf{1}_2Cl_2 + Pd\mathbf{2}^*_2Cl_2 \rightleftharpoons Pd(\mathbf{1})(\mathbf{2}^*)Cl_2$$

Table 4.1. Hetero-to-homo-complex ratios for *cis*- complexes of both ligand combinations **1**/**2** and **1**/**2*** determined by either ^{31}P signal integration or spectra simulation.

$Pd(\mathbf{1})(\mathbf{2})Cl_2$	$Pd\mathbf{1}_2Cl_2$	$Pd\mathbf{2}_2Cl_2$
0.51	0.23	0.26
$Pd(\mathbf{1})(\mathbf{2}^*)Cl_2$	$Pd\mathbf{1}_2Cl_2$	$Pd\mathbf{2}^*_2Cl_2$
0.71	0.16	0.13

$$K_{\mathbf{1/2}} = \frac{[\mathrm{Pd}(\mathbf{1})(\mathbf{2})\mathrm{Cl}_2]^2}{[\mathrm{Pd}\mathbf{1}_2\mathrm{Cl}_2]\cdot[\mathrm{Pd}\mathbf{2}_2\mathrm{Cl}_2]} \qquad K_{\mathbf{1/2}^*} = \frac{[\mathrm{Pd}(\mathbf{1})(\mathbf{2}^*)\mathrm{Cl}_2]^2}{[\mathrm{Pd}\mathbf{1}_2\mathrm{Cl}_2]\cdot[\mathrm{Pd}\mathbf{2}_2^*\mathrm{Cl}_2]}$$

$$\Delta G° = -\mathrm{RTln}K\,; \qquad \mathrm{R} = 8.314\frac{\mathrm{J\cdot mol}}{\mathrm{K}}, \mathrm{T} = 300\mathrm{K}$$

$$\Delta G°(\mathrm{Pd}(\mathbf{1})(\mathbf{2})\mathrm{Cl}_2) = -3.04\,{}^{\mathrm{kJ}}/_{\mathrm{mol}} \qquad \Delta G°(\mathrm{Pd}(\mathbf{1})(\mathbf{2}^*)\mathrm{Cl}_2) = -7.86\,{}^{\mathrm{kJ}}/_{\mathrm{mol}}$$

⇨ $\Delta\Delta G° = -4.82\,{}^{\mathrm{kJ}}/_{\mathrm{mol}}$

4.5.3 Sample preparation

All reactions were carried out under argon atmosphere in heat gun dried Schlenk flask using freshly distilled solvents. CD_2Cl_2 was distilled from CaH_2. Ligand **1** and **2** were prepared according to reported protocols[46] or bought from Sigma-Aldrich. Pd(cod)Cl_2 was bought from Alfa Aesar The samples were prepared at room temperature by adding solvent to a mixture of free ligand(s) and Pd(cod)Cl_2 using a total ligand-to-Pd ratio of 2:1. The solution was stirred for at least 2.5 h for *trans*-PdL_2Cl_2 and stored at room temperature to obtain *cis*-PdL_2Cl_2.

4.5.4 NMR data collection and processing

NMR spectra were recorded on a Bruker Avance DRX 600 (600.13 MHz) spectrometer equipped with a 5 mm broadband triple resonance z-gradient probe (maximum gradient strength 53.5 Gauss/cm) and a Bruker Avance III 600 (600.25 MHz) spectrometer, equipped with a TCI cryoprobe with z-gradient (53.5 G/cm). ^{1}H and ^{13}C chemical shifts were referenced to TMS, for ^{31}P chemical shifts the corresponding Ξ value was applied. Temperature stability was controlled by a BVT 3000 unit. All measurements were performed at 300 K. For the characterization of the different observed complex species detailed 2D NMR spectroscopic investigation have been performed: $^{1}H^{31}P$ HMBC, $^{1}H^{1}H$ COSY, $^{1}H^{1}H$ NOESY, $^{1}H^{13}C$ HSQC, $^{1}H^{13}C$ HMBC and *J*-resolved ^{31}P. For appropriate $^{1}H^{1}H$ NOESY measurements mixing times of 750 to 800 ms have been applied. NMR data were processed and evaluated with Bruker Topspin 2.1, ^{31}P spectra simulations were created using DAISY , a spectra simulation program included in Topspin 2.1. Figure 4.2a and Figure 4.3 were drawn and calculated with Spartan '04 V1.0.0. Molecular electrostatic potential surfaces plotted on the van-der Waals' surface of the complex (IsoVal -0.5) calculated at a AM1 level of theory. Positive regions are shown in blue (400 kJ mol^{-1}), negative regions are shown in red (-250kJ mol^{-1}).

For full signal assignment of complexes *cis*-Pd(**1**)(**2**)Cl_2 and *cis*-Pd(**1**)(**2***)Cl_2 see Supporting Information of chapter 3.

4.6 References

[1] M. Berthod, G. Mignani, G. Woodward, M. Lemaire, *Chem. Rev.* **2005**, *105*, 1801-1836.

[2] H. B. Kagan, P. Dang Tuan, *J. Am. Chem. Soc.* **1972**, *94*, 6429-6433.

[3] M. McCarthy, P. J. Guiry, *Tetrahedron* **2001**, *57*, 3809-3844.

[4] M. de Greef, B. Breit, *Angew. Chem. Int. Ed.* **2009**, *48*, 551-554.

[5] Y. Liu, C. A. Sandoval, Y. Yamaguchi, X. Zhang, Z. Wang, K. Kato, K. Ding, *J. Am. Chem. Soc.* **2006**, *128*, 14212-14213.

[6] C. Waloch, J. Wieland, M. Keller, B. Breit, *Angew. Chem.* **2007**, *119*, 3097-3099.

[7] J. Wieland, B. Breit, *Nat Chem* **2010**, *2*, 832-837.

[8] X.-B. Jiang, L. Lefort, P. E. Goudriaan, A. H. M. de Vries, P. W. N. M. van Leeuwen, J. G. de Vries, J. N. H. Reek, *Angew. Chem. Int. Ed.* **2006**, *45*, 1223-1227.

[9] S. A. Moteki, J. M. Takacs, *Angew. Chem. Int. Ed.* **2008**, *47*, 894-897.

[10] J. M. Takacs, D. S. Reddy, S. A. Moteki, D. Wu, H. Palencia, *J. Am. Chem. Soc.* **2004**, *126*, 4494-4495.

[11] B. Breit, *Angew. Chem. Int. Ed.* **2005**, *44*, 6816-6825.

[12] S. Carboni, C. Gennari, L. Pignataro, U. Piarulli, *Dalton Transactions* **2011**, *40*, 4355-4373.

[13] M. T. Reetz, *Angew. Chem. Int. Ed.* **2008**, *47*, 2556-2588.

[14] F. Hof, D. M. Scofield, W. B. Schweizer, F. Diederich, *Angew. Chem. Int. Ed.* **2004**, *43*, 5056-5059.

[15] S. L. Cockroft, C. A. Hunter, *Chem. Commun.* **2006**, 3806-3808.

[16] C. A. Hunter, J. K. M. Sanders, *J. Am. Chem. Soc.* **1990**, *112*, 5525-5534.

[17] S. L. Cockroft, J. Perkins, C. Zonta, H. Adams, S. E. Spey, C. M. R. Low, J. G. Vinter, K. R. Lawson, C. J. Urch, C. A. Hunter, *Org. Biomol. Chem.* **2007**, *5*, 1062-1080.

[18] A. L. Ringer, M. O. Sinnokrot, R. P. Lively, C. D. Sherrill, *Chem. Eur. J.* **2006**, *12*, 3821-3828.

[19] K. E. Riley, M. Pitoňák, P. Jurečka, P. Hobza, *Chem. Rev.* **2010**, *110*, 5023-5063.

[20] E. A. Meyer, R. K. Castellano, F. Diederich, *Angew. Chem. Int. Ed.* **2003**, *42*, 1210-1250.

[21] L. Serrano, A. Horovitz, B. Avron, M. Bycroft, A. R. Fersht, *Biochemistry* **1990**, *29*, 9343-9352.

[22] A. Horovitz, A. R. Fersht, *J. Mol. Biol.* **1990**, *214*, 613-617.

[23] P. J. Carter, G. Winter, A. J. Wilkinson, A. R. Fersht, *Cell* **1984**, *38*, 835-840.

[24] S. L. Cockroft, C. A. Hunter, *Chem. Soc. Rev.* **2007**, *36*, 172-188.

[25] E.-i. Kim, S. Paliwal, C. S. Wilcox, *J. Am. Chem. Soc.* **1998**, *120*, 11192-11193.

[26] S. Paliwal, S. Geib, C. S. Wilcox, *J. Am. Chem. Soc.* **1994**, *116*, 4497-4498.

[27] C. A. Hunter, *Angew. Chem. Int. Ed.* **2004**, *43*, 5310-5324.

[28] B. L. Feringa, M. Pineschi, L. A. Arnold, R. Imbos, A. H. M. de Vries, *Angew. Chem. Int. Ed.* **1997**, *36*, 2620-2623.

[29] A. Alexakis, S. Rosset, J. Allamand, S. March, F. Guillen, C. Benhaim, *Synlett* **2001**, 1375-1378.

[30] A. Alexakis, D. Polet, *Org. Lett.* **2004**, *6*, 3529-3532.

[31] G. P. Howell, A. J. Minnaard, B. L. Feringa, *Org. Biomol. Chem.* **2006**, *4*, 1278-1283.

[32] R. Imbos, A. J. Minnaard, B. L. Feringa, *Dalton Transactions* **2003**, 2017-2023.

[33] J. F. Jensen, B. Y. Svendsen, T. V. la Cour, H. L. Pedersen, M. Johannsen, *J. Am. Chem. Soc.* **2002**, *124*, 4558-4559.

[34] J. F. Teichert, B. L. Feringa, *Angew. Chem. Int. Ed.* **2010**, *49*, 2486-2528.

[35] K. Schober, E. Hartmann, H. Zhang, R. M. Gschwind, *Angew. Chem. Int. Ed.* **2010**, *49*, 2794-2797.

[36] H. Zhang, R. M. Gschwind, *Chem. Eur. J.* **2007**, *13*, 6691-6700.

[37] E. Hartmann, R. M. Gschwind, *in preperation* **2012**.

[38] F. B. Ogilvie, J. M. Jenkins, J. G. Verkade, *J. Am. Chem. Soc.* **1970**, *92*, 1916-1923.

[39] J. Mason, *Multinuclear NMR*, Plenum Press, New York and London, **1987**.

[40] J. G. Verkade, *Coord. Chem. Rev.* **1972**, *9*, 1-106.

[41] R. J. Goodfellow, B. F. Taylor, *J. Chem. Soc., Dalton Trans.* **1974**, 1676-1684.

[42] A. J. Carty, D. K. Johnson, S. E. Jacobson, *J. Am. Chem. Soc.* **1979**, *101*, 5612-5619.

[43] I. S. Mikhel, G. Bernardinelli, A. Alexakis, *Inorg. Chim. Acta* **2006**, *359*, 1826-1836.

[44] M. Nishio, *PCCP* **2011**, *13*, 13873-13900.

[45] M. Nishio, M. Hirota, Y. Umezawa, *The CH/π Interaction: Evidence, Nature, and Consequences*, Wiley, New York, **1998**.

[46] A. Alexakis, S. Rosset, J. Allamand, S. March, F. Guillen, C. Benhaim, *Synlett* **2001**, *9*, 1375-1378.

5 Investigation of the Umpolung Reaction Mechanism

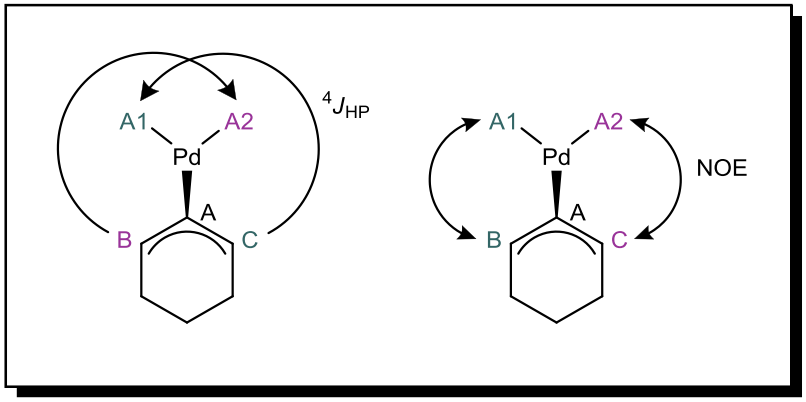

Evelyn Hartmann, and Ruth M. Gschwind

5.1 Abstract

The Pd-catalyzed Umpolung reaction is a promising new synthetic pathway for the allylation of ketones or aldehydes. Key step for this reaction is the Umpolung of the allyl from electrophilic to nucleophilic. Diverse reaction mechanisms and catalytic cycles have already been proposed for the Pd-catalyzed Umpolung reaction, however, up to now the mechanism is not clearly elucidated yet. Therefore, we present structural investigations on different intermediates formed during the reaction between 2-cyclohexenyl acetate and benzaldehyde. As catalysts a palladium salt in combination with two diastereomeric ligands **1** or **1'**, which provide different *ee*-values, have been used. Differences in number, preference and structure of the formed intermediates when using ligand **1** or **1'** are addressed. The formations of various π-allyl complex species are described and, moreover, the formation of a σ-allyl complex is discussed, which is supposed to be essential for the Umpolung of the allyl.

5.2 Introduction

In the field of asymmetric catalysis transition-metals combined with chiral ligands are one of the most effective and versatile approaches.[1] An often used catalyst for C-C bond forming reactions is palladium which finds broad application in today's synthesis.[2-5] In combination with chiral ligands – both monodentate and bidentate ligands – Pd catalysts achieve high enantioselectivities. However, although Pd catalysis has become standard application in synthesis, reaction mechanisms are not fully understood so far.[6-7] For most mechanisms the rate determining and selectivity discriminating step cannot clearly be identified. It is commonly accepted that two main steps in the catalytic cycle of all Pd catalyzed reactions are oxidative addition of one substrate and reductive elimination of the product and that both processes proceed in a *cis*-manner.[5, 8] However, in case of two monodentate ligands attached to palladium a *trans*-coordination of both ligands is usually observed after the oxidative addition of the substrate. This observation indicates a continuous change between *cis*- and *trans*-Pd complexes during the catalytic cycle.[9]

The oxidative addition of e.g. an allyl substrate, which is usually the first step in all catalytic cycles using palladium, leads to the formation of an allyl complex often followed by the attack of a nucleophile which is usually supposed to be the selectivity discriminating step. However, in presence of dialkyl zinc or trialkyl bor the allyl complex switches from electrophilic to nucleophilic.[10] Such a type of reaction is called Umpolung and is a promising new synthetic pathway for the allylation of ketones or aldehydes using Pd as catalyst.[10-15] An example for such an Umpolung developed by Zanoni is the enantioselective coupling reaction of 2-cyclohexenyl acetate with benzaldehyde using a Pd catalyst leading to a chiral allyl alcohol, however, with only moderate enantioselectivity.[14] Feringa improved reaction conditions including the replacement of the initial phosphorligand by phosphoramidite ligand **1** (Scheme 5.2) achieving *ee*-values up to 81%.[15] However, up to now the mechanism of the Umpolung reaction is not clearly elucidated and moreover the proposed mechanisms vary a lot. A continuous transmetalation of the phosphorligand between Pd and Zn during the catalytic cycle has been excluded by Feringa because of the known high stability of Pd complexes using phosphorligands. Furthermore a transmetalation of the allyl from Pd to Zn as initially supposed by Tamaru[13] can be excluded, because such a transmetalation step would lead to a loss of any chiral information on the substrate. A possible catalytic cycle of the Umpolung reaction proposed by Feringa including the enantioselectivity determining transition state of the insertion step is shown in Scheme 5.1.[15]

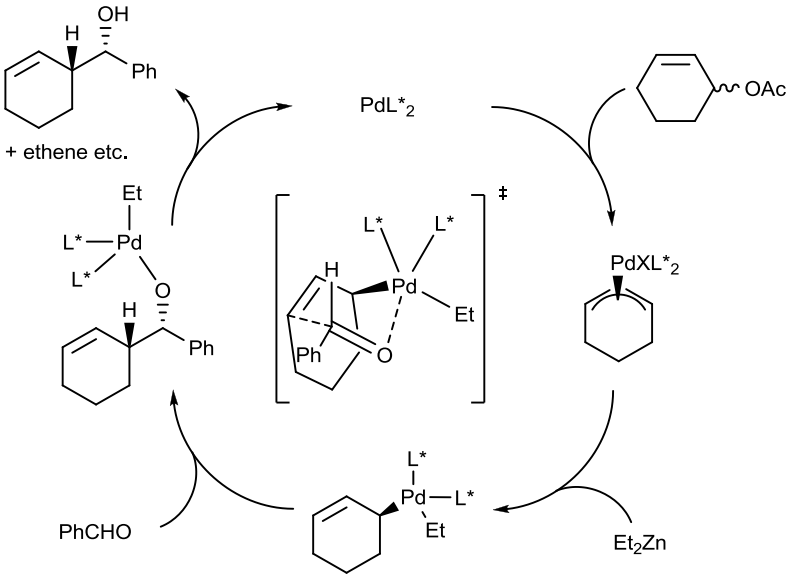

Scheme 5.1. Catalytic cycle proposed by Feringa.[15]

In the proposed catalytic cycle the first step is the classic oxidative addition of the allyl substrate to Pd(0). The formed π-allyl complex subsequently converts into a σ-complex by the further coordination of an ethyl group to palladium. Afterwards the electrophile – the benzaldehyde – is inserted into the σ-allyl palladium bond over a transition state shown in the middle of Scheme 5.1. After a reductive elimination of the product the active catalyst- a Pd(0) complex – is regained.

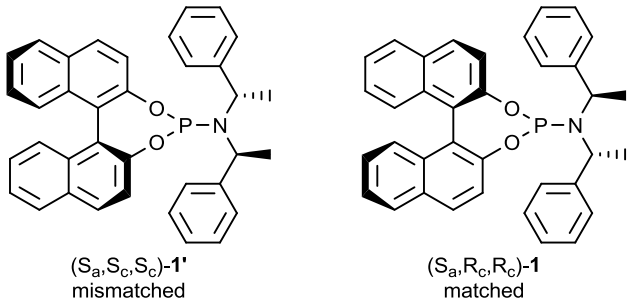

Scheme 5.2. Phosphoramidite ligands developed by Feringa used in this study.

Herein we present NMR spectroscopic studies on intermediates formed during the Umpolung reaction. For this purpose complexes, which are formed after the stepwise addition of the different substrates have been investigated. In order to isolate the diverse intermediates and to avoid a complete conversion a substoichiometric amount of Et_2Zn was added. To imitate standard reaction conditions[15] the samples were prepared and measured at 0°C in CD_2Cl_2. As a catalyst $Pd(cod)Cl_2$ with two equivalents of ligand **1** was used. Ligand **1** exists in two diastereomeric forms which differ only in the conformation of their binaphthol

group (Scheme 5.2). However, the orientation of the binaphthol moiety can have an either matched or mismatched effect on enantioselectivity leading to different *ee*-values of 70% for (S_a,R_c,R_c)-**1** but only 21% for (S_a,S_c,S_c)-**1'**.[15] Therefore differences in the mechanistic steps using ligand (S_a,R_c,R_c)-**1** and (S_a,S_c,S_c)-**1'** are also addressed.

5.3 Reduction of Pd(II)

5.3.1 Introduction

For the first step of the catalytic cycle – the oxidative addition of the substrate – Pd(II) has to be reduced to Pd(0) first. Preliminary studies excluded any reaction between Pd**1'**$_2$Cl$_2$ with the allyl substrate (for more details see SI). As Et_2Zn is the only reducing agent under reaction conditions, complex PdL_2Cl_2 (L = **1** or **1'**) was synthesized and a small amount of Et_2Zn was added to the solution. The proposed mechanism for the reduction of Pd(II) is a transmetalation followed by a reductive elimination:

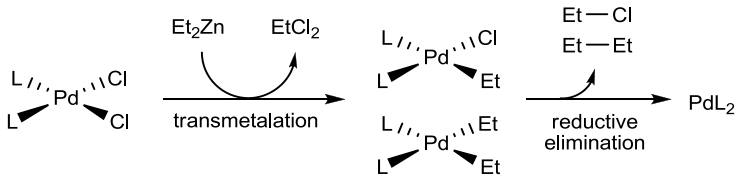

Scheme 5.3. Proposed mechanism of the reduction of Pd(II) to Pd(0) by Et_2Zn.

For both systems the reduction of Pd(II) could be observed on a blackening of the initially yellow solution after the addition of Et_2Zn upon the formation of Pd(0). Apart from the described reduction of Pd(II) an oxidation of both phosporamidite ligands could also be observed, but will not be considered in the following (for more details see SI).

NMR measurements were often limited only to the identification of specific groups attached to palladium in the different complexes. However, for most complexes the determination of the exact stoichiometric composition of the different complex species (i.e. number of phosphorligands, ethyl groups, chloride ligands, etc.) was hard to realize. Therefore, all complex structures mentioned in the following sections are proposals used to illustrate structural information obtained by NMR data under reserve that the actual stoichiometry might deviate.

5.3.2 Pd(S_a,S_c,S_c)-1'$_2$Cl$_2$ + Et$_2$Zn

^{31}P NMR investigations of a sample Pd**1**'$_2$Cl$_2$ + Et$_2$Zn showed that the amount of added Et$_2$Zn was - as intended - too small to reduce all of the Pd(II) complex (Figure 5.1).

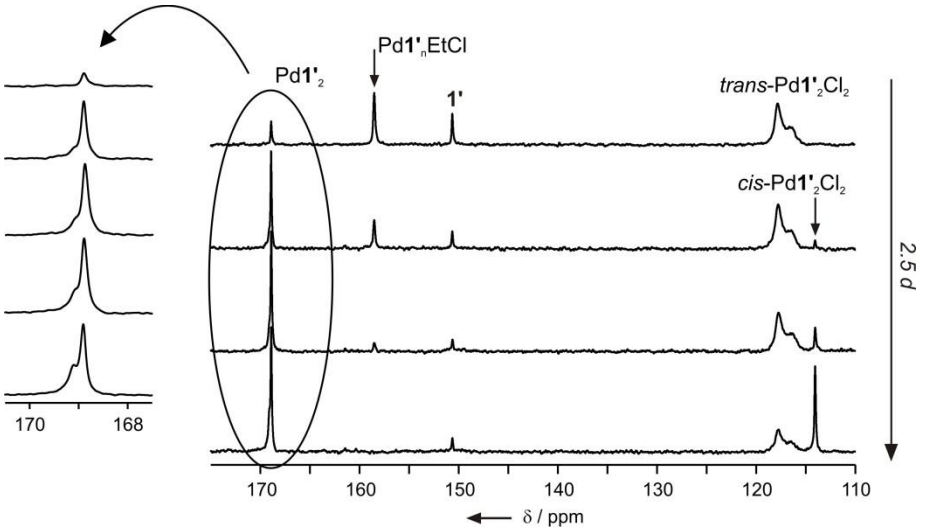

Figure 5.1. ^{31}P spectra of Pd**1'**$_2$Cl$_2$ measured in different time-intervals after the addition of Et$_2$Zn over a period of ca. 2.5 d.

Besides Pd**1'**$_2$Cl$_2$ and a small amount of free ligand **1'** two new complex species have been formed. One of the ^{31}P signals at $\delta(^{31}P)$ = 158.5 ppm have been assigned to an intermediate of the reduction reaction because its signal intensity had its maximum right after the addition of Et$_2$Zn but decreased afterwards until it has vanished completely within 24 h. The other new complex signal was assigned to the product of this reaction - a Pd(0) complex - as its intensity increased by and by until it reached a maximum. This complex underwent another conversion since its signal is shifted downfield by about 0.2 ppm.

As already mentioned a small amount of free ligand **1'** can be observed in the ^{31}P spectra which indicates that ligand is set free during the reduction of Pd(II). However, the amount of released ligand decreases again at the end of the reaction so that the ligand-to-Pd ratio of 2 : 1 should not have changed after the reduction but should still be valid for Pd(0). Therefore the Pd(0) complex(es) will be described as Pd**1'**$_2$ in the following.[16] Recent studies in our working group showed, that initially Pd(II)-complexes with a *trans*-configuration of the phosphoramidite ligands are formed which convert into *cis*-complexes afterwards attracted by the formation of weak CH-π and π-π interactions(see also chapter 3 and 4).[17] This process can be observed in the ^{31}P spectra as well on the conversion of the initially broad ^{31}P complex signal(s) at 117.5 ppm (conformational isomers of *trans*-complexes) into a sharp singlet at 114 ppm (one *cis*-Pd**1'**$_2$Cl$_2$ complex locked by weak

ligand-ligand interactions). In the ^{31}P spectra measured after the addition of Et_2Zn the ^{31}P signal of this *cis*-complex does not emerge until the reduction reaction is completed due to the run out of Et_2Zn. Therefore a conversion from *trans*- into *cis*-Pd**1**$_2Cl_2$ might be necessary for the transmetalation or at least the *cis*-complex reacts faster with Et_2Zn than the initially formed *trans*-complex.

Interestingly the *trans*-*cis*-isomerization is very fast under these conditions compared to isolated systems, so that after 2.5 d a large amount of *cis*-complex is present in solution. Thus, some species in the reaction mixture (free ligand, other complex species, small amount of toluene, etc.) strongly accelerates the isomerization.

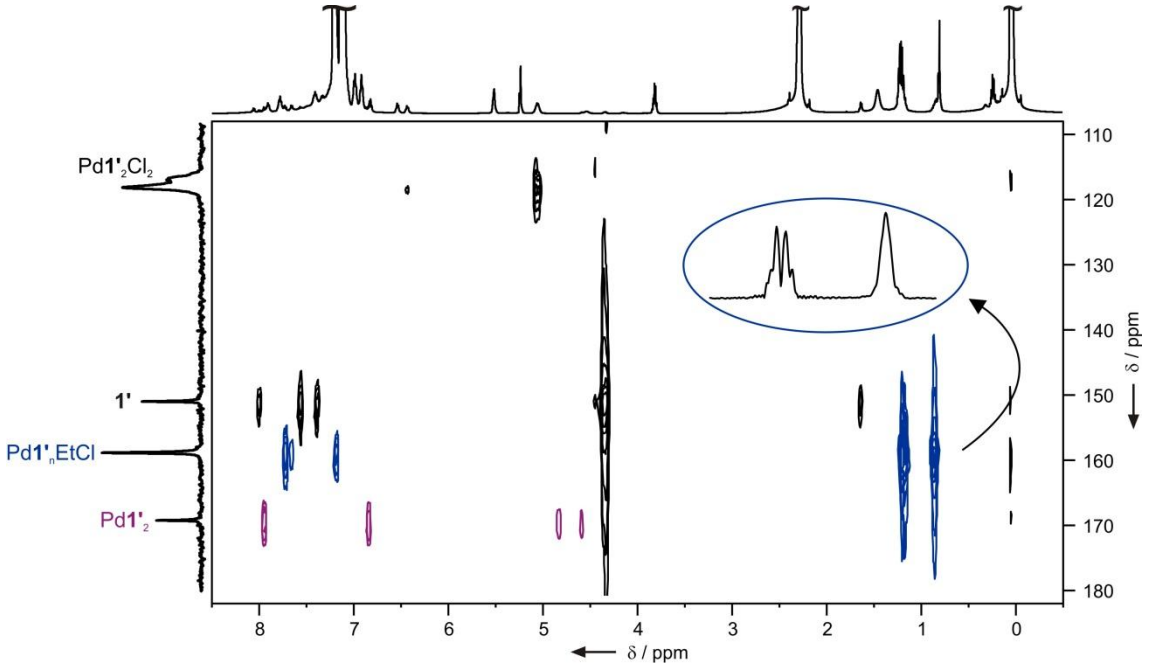

Figure 5.2. $^{1}H^{31}P$ HMBC of a sample Pd**1'**$_2Cl_2$ + Et_2Zn with a 1D excerpt of the ethyl cross signals of Pd**1'**$_n$EtCl.

$^{1}H^{31}P$ HMBC measurements confirmed the identification of the two new complex species as intermediate and Pd(0) complex (Figure 5.2): Two intensive cross signals of the intermediate in the region between $\delta(^{1}H)$ = 0.5 and 1.5 ppm proved the transmetalation of an Et group from Zn to Pd. Because of the different coupling pattern both cross signals have been assigned to the CH_2 and CH_3 group of one ethyl group (see 1D excerpt in Figure 5.2). However, if only one ethyl group was transmetalated to palladium leading to a complex structure of Pd**1**$_2$EtCl, two ^{31}P signals with a $^{2}J_{PP}$ doublet coupling should be observable. Therefore, either ligand exchange within this complex is fast on the NMR time scale or one ligand is temporary released. Another possibility might be the formation of oligomeric complex structures. For simplification the intermediate will be described as Pd**1'**$_n$EtCl in the

following. As to complex Pd**1'**$_2$ no cross signals to an ethyl group could be observed, but two fairly strong cross signals between δ(^{1}H) = 4.5 and 5 ppm. An excerpt of the ^{1}H spectrum in Figure 5.3 shows both signals:

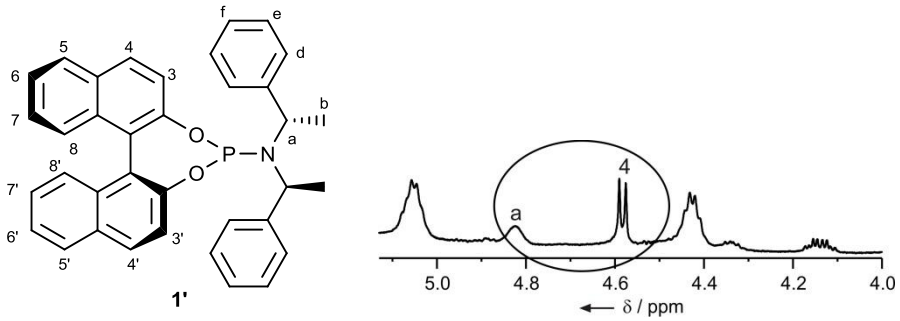

Figure 5.3. Section of a ^{1}H spectrum of a sample Pd**1'**$_2$Cl$_2$ + Et$_2$Zn in the region of the two cross signals of Pd**1'**$_2$ (the two ^{1}H signals giving the intensive cross signals in the ^{1}H^{31}P HMBC are encircled).

A combination of different 2D NMR measurements enabled an assignment of these signals to the methine group (a) and to an aromatic proton of the binaphthol moiety (4) of the phosphorligand. Despite this unusual chemical shift for aromatic protons the doublet was doubtlessly assigned to proton 4 because of 1) the typical ortho coupling constant of $^3J_{HH}$ = 8.84 Hz; 2) the appropriate chemical shift of the corresponding ^{13}C signal of δ(^{13}C) = 129.0 ppm in the ^{1}H^{13}C HSQC which is a typical value for 4 and 4', respectively, and 3) the cross signal to 3 in the ^{1}H^{1}H COSY. In addition, four equally strong NOEs between 4 and four other aromatic protons suggest the involvement into CH-π interactions, which might also explain the unusual ^{1}H chemical shift of 4.[18-20] A coordination of the aromatic compound to the metal centre via a weak η^2-arene-Pd bonding interaction as observed by Pregosin[21] could be excluded by inappropriate ^{13}C chemical shifts for such an η^2-arene-Pd coordination. These CH-π interactions are resolved again afterwards leading to the small downfield-shift of the ^{31}P complex signals by about Δδ(^{31}P) = 0.2 ppm (see excerpt in Figure 5.1). For the complex species with the downfield-shifted ^{31}P signal no unusual ^{1}H chemical shift of 4 in the aromatic region is observable any more. This break-up of probably CH-π interactions is very slow.

5.3.3 Pd(S_a,R_c,R_c)-$\mathbf{1}_2Cl_2$ + Et_2Zn

Investigations of a sample using the more selective ligand (S_a,R_c,R_c)-**1** revealed that several differences compared to the use of mismatched ligand (S_a,S_c,S_c)-**1'** can already be observed for the reduction of Pd(II). After the addition of Et_2Zn at least four new complex signals can be observed in the ^{31}P spectrum.

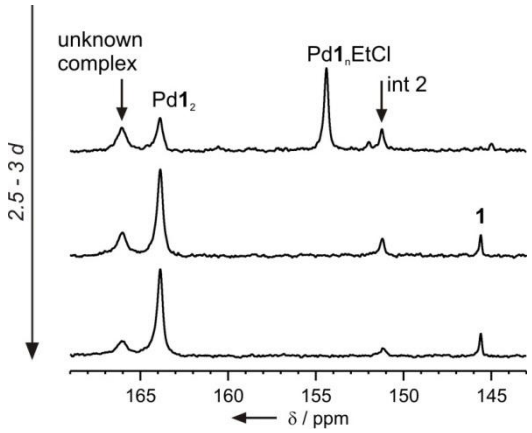

Figure 5.4. ^{31}P spectra of a sample Pd**1**$_2Cl_2$ measured in different time intervals after the addition of Et_2Zn over a period of 2.5 d.

The ^{31}P signal at δ(^{31}P) = 163.9 ppm can clearly be assigned to a stable Pd(0) complex, because its signal intensity increases until it reaches a maximum. Moreover, no cross signals to CH_2 and CH_3 groups could be detected in the $^1H^{31}P$ HMBC for this complex. Similar to Pd**1'**$_2Cl_2$ a small amount of ligand **1** is released during the reduction of Pd**1**$_2Cl_2$, but again it is too small to change the ligand-to-Pd ratio durable. Therefore the Pd(0) complex using ligand **1** will also be described as Pd**1**$_2$ in the following. The two complex signals at δ(^{31}P) = 154.4 and 151.2 ppm have been assigned to intermediates as their signal intensities have their maximum right after the addition of Et_2Zn and decrease afterwards by and by. Concerning the complex signal at δ(^{31}P) = 166.0 ppm its maximum signal intensity is also reached immediately after the addition of Et_2Zn and decreases afterwards which would be a typical feature of an intermediate. However, aside from its unusual ^{31}P chemical shift, no cross signals could be detected in the $^1H^{31}P$ HMBC. Thus there is no evidence of a transmetalation of Et groups for this complex species. Furthermore, a closer look at the shape of the ^{31}P signal indicates, that more than only one complex signal might overlap at that chemical shift. Thus, further ivestigations, e.g. by NMR measurements at low temperature, are necessary for a clear identification of that complex(es).

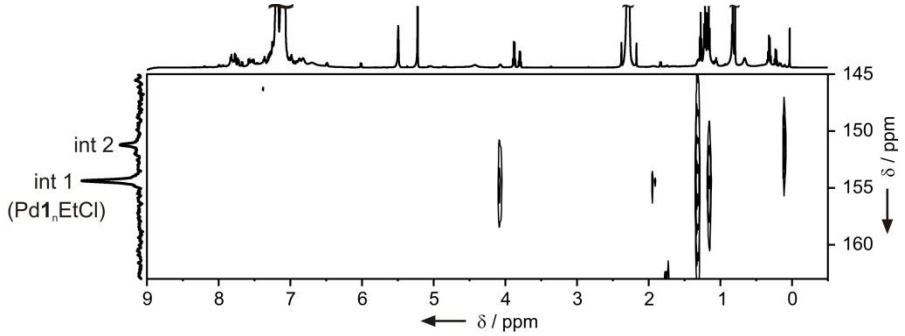

Figure 5.5. Section of a $^{1}H^{31}P$ HMBC in the region of intermediates Pd**1**$_n$EtCl and int 2.

In the $^{1}H^{31}P$ HMBC generally less cross signals are detected for (S_a,R_c,R_c)-**1** compared to ligand (S_a,S_c,S_c)-**1'**. Within ligand **1'** intraligand cross signals to the binaphthol group can be observed for most complexes. However, for complexes using ligand **1** intraligand cross signals are rather rare. In Pd**1**$_2$Cl$_2$ + Et$_2$Zn only intermediates int 1 and int 2 show some cross signals in the $^{1}H^{31}P$ HMBC for the most part in the region between $\delta(^{1}H)$ = 0 and 2 ppm (see Figure 5.5). For int 1 altogether four cross signals have been detected. The signal at $\delta(^{1}H)$ = 4.1 ppm probably belongs to the CH group of the phosphoramidite ligand. The significant upfield-shift of the methine signal hints at the involvement into CH-π interactions. Similar chemical shifts for the methine signal have also been observed for different *cis*-phosphoramidite palladium complexes locked by weak inter- and intraligand interactions (see also chapter 3 and 4).[17] The cross signals between $\delta(^{1}H)$ = 1 and 2 ppm can either derive from ethyl groups transmetalated to palladium or one of the cross signals might belong to the CH_3 group of ligand **1**. However, a repetition of the NMR measurements with optimized parameters is necessary to gain reliable results and more insight into the complex structure of int 1. Nevertheless, since ^{31}P chemical shift and cross signals of the ethyl group in the $^{1}H^{31}P$ HMBC are very similar to those of Pd**1'**$_n$EtCl, the same complex structure will be assigned to this intermediate in the following for simplification. Intermediate int 2 shows only one cross signal at about $\delta(^{1}H)$ = 0 ppm which again was assigned to an ethyl group. However more information about its complex structure could not be obtained by NMR.

5.3.4 Summary

NMR investigations of the reduction of PdL_2Cl_2 (L = **1** or **1'**) by Et_2Zn proved for both systems the transmetalation of an ethyl group from Et_2Zn to Pd(II) leading to the major intermediate PdL_nEtCl. In case of ligand **1** two further complex species occur, of which one has also been assigned to an intermediate containing an ethyl group. In both systems ligand is release during the reaction. However, the amount of free ligand decreases again at the end of the reduction. Moreover, the amount of released ligand is too small to cause a change of the initial ligand-to-Pd ratio of 2 : 1, so that the Pd(0) complexes have been described as PdL_2. For ligand **1'** (temporary) CH-π stacking could be observed in Pd**1'**$_2$. Furthermore it was shown that only the *cis*-isomer of PdL_2CL_2 reacts with Et_2Zn or at least it is reduced faster than its *trans*-isomers.

5.4 Oxidative Addition

5.4.1 Introduction

After the reduction of Pd(II) the reaction between the different Pd(0) complexes and cyclohexenyl acetate has been investigated. After the oxidative addition of the substrate a π-allyl Pd complex should be formed, which – according to Feringa's proposed catalytic cycle (see also Scheme 5.1) – subsequently converts into a σ-allyl complex in the presence of Et_2Zn. The formation of this σ-complex is essential for the Umpolung of the allyl species from electrophilic to nucleophilic:

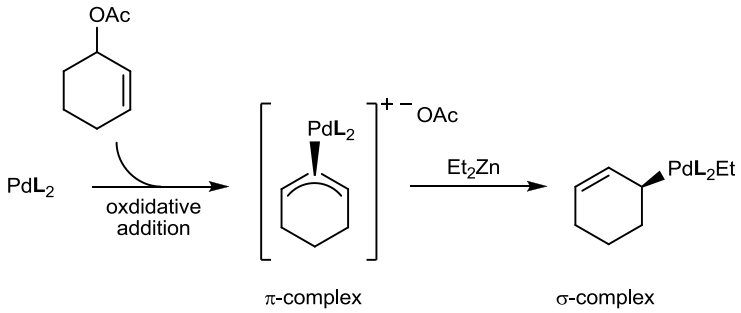

Scheme 5.4. Proposed mechanism of the oxidative addition of the substrate to Pd(0) leading to a π-allyl complex followed by a conversion into a σ-allyl complex in the presence of Et_2Zn.[15]

After the synthesis of PdL_2Cl_2 (L = **1** or **1'**) an excess of the substrate 2-cyclohexenyl acetate was added first followed by the addition of Et_2Zn as starting point of the reaction.[22]

In the following chapters again various complex structures will be proposed. However, these structures are not meant to describe the exact and complete complex structures of the detected intermediates but are only used to illustrate distinct structural information obtained from NMR data. Moreover most of the complexes will be described and discussed as pure π-allyl complexes regarding exclusively a η^3-coordination of the allyl to palladium for simplification. The possibility of a η^1-η^3 allyl isomerization will be neglected:

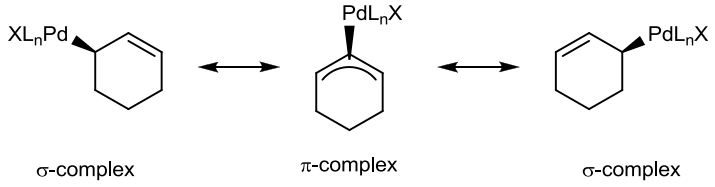

Scheme 5.5. Coordination of cyclohexenyl to palladium via a σ- or π-bond.

For the identification of a σ-complex as proposed by Feringa a well-defined double bond (character) with appropriate ^{1}H and ^{13}C chemical shifts must be verifiable.

A rough overview about the number of newly formed complexes and first structural information about these complexes were obtained from ^{31}P signals and their coupling patterns. However, for the identification of the individual components within the different complexes we mainly concentrated on cross signals in the $^{1}H^{31}P$ HMBC which gave information about cyclohexenyl and/or ethyl groups coordinated to palladium. In addition ^{13}C chemical shifts of the allyl-CH groups and moreover the difference $\Delta\delta(^{13}C)$ between C_B and C_C was used to identify ligands in *trans*-position based on NMR studies of different π-allyl complexes reported by Pregosin also using phosphoramidite ligands:[23-25]

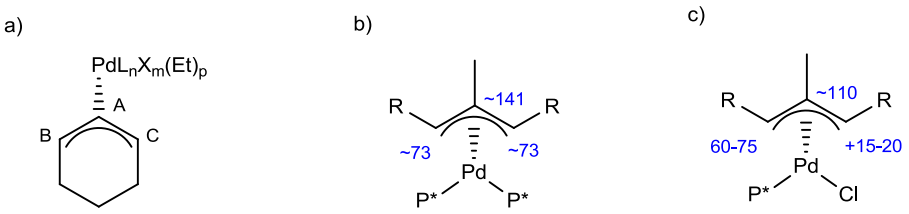

Scheme 5.6. a) Cyclohexenyl Pd complex including all possible ligands and nomenclature of the allyl group; b) and c) chemical shifts of different allyl Pd complexes reported by Pregosin.[23]

The range of possible ligands include phosphoramidites (L = **1** or **1'**), chloride (Cl) or ethyl groups (Et) (Scheme 5.6a). In case of similar ^{13}C chemical shifts for C_B and C_C with only small $\Delta\delta(^{13}C)$ values identical ligands are very likely to be coordinated in *trans*-position to C_B and C_C (Scheme 5.6b), whereas different ligands lead to a clear difference in the ^{13}C chemical shifts due to differently strong *trans*-effects of the ligands (Scheme 5.6c). As phosphoramidites have a stronger *trans*-effect than Cl-ligands they consequently cause a stronger downfield-shift of the CH-group in *trans*-orientation compared to chloride.

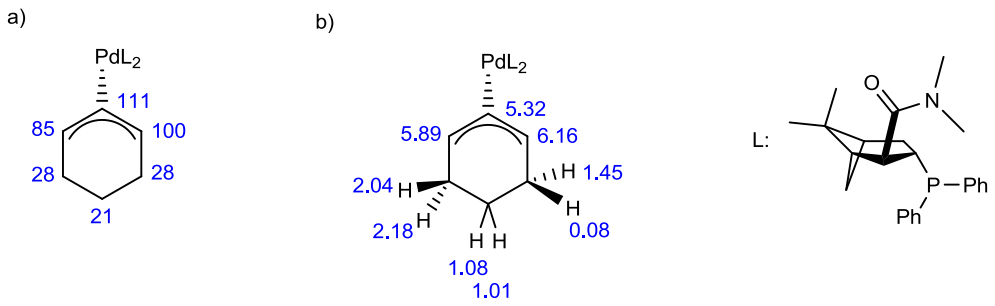

Scheme 5.7. π-cyclohexenyl palladium complex using monodentate ligand L characterized by NMR including a) ^{13}C chemical shift and b) ^{1}H chemical shift assignment.

In addition, a π-allyl complex gained after the oxidative addition of cyclohexenyl acetate to a palladium catalyst using monodentate phosphorligand L was characterized by NMR by the group of Prof. Thiele (see Scheme 5.7).[26] The obtained chemical shifts - especially those of the CH_2 groups of the cyclohexenyl - have been compared with our results.

5.4.2 Pd(S_a,S_c,S_c)-1'$_2$Cl$_2$ + cyclohexenyl acetate + Et$_2$Zn

After the addition of 2-cyclohexenyl acetate and Et$_2$Zn to Pd**1'**$_2$Cl$_2$ the formation of at least four new complex species (a, b and A, B) could clearly be observed in ^{31}P spectra:

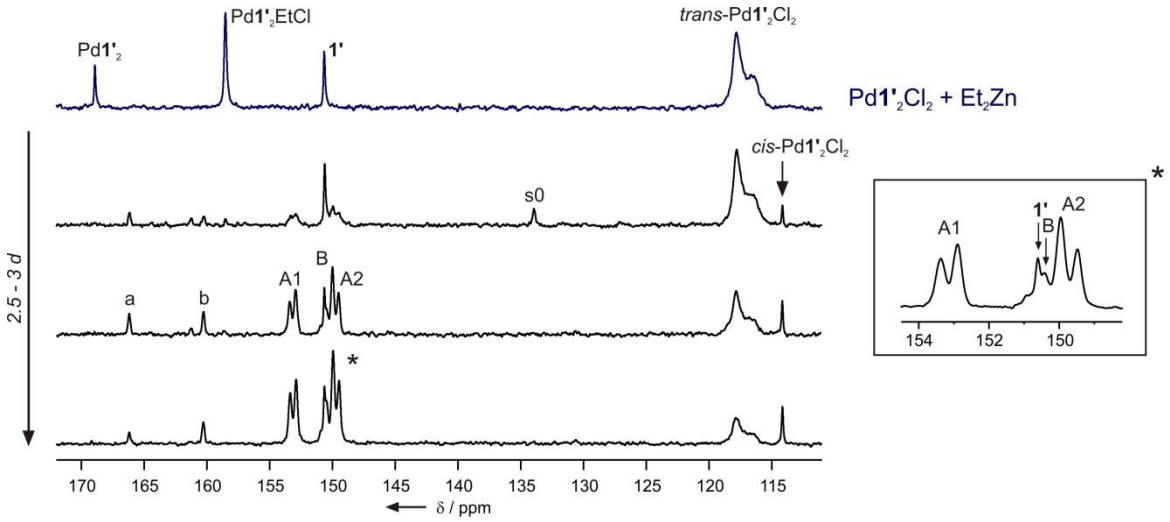

Figure 5.6. ^{31}P spectra of Pd**1'**$_2$Cl$_2$ measured in different time intervals after the addition of cyclohexenyl acetate and Et$_2$Zn over a period of ca. 2.5 to 3 d (black) and an excerpt of the region of complexes A and B (right). For comparison a ^{31}P spectrum of Pd**1'**$_2$Cl$_2$ + Et$_2$Zn is also shown (blue).

Surprisingly the reaction starts only very slowly. In the ^{31}P spectrum measured ca. 10-15 min. after the addition of Et$_2$Zn for the most part Pd**1'**$_2$Cl$_2$, a small amount of *cis*-Pd**1'**$_2$Cl$_2$ and only very tiny signals at higher ppm-values could be observed (spectrum not shown). Again a substoichiometric amount of Et$_2$Zn was added, so that the ^{31}P signals of some amount of Pd**1'**$_2$Cl$_2$ are still observable. The ^{31}P signals of the newly formed complex species – different allyl Pd complexes - are mainly concentrated in the region between $\delta(^{31}P)$ = 149 and 154 ppm (A and B) as well as between $\delta(^{31}P)$ = 160 and 166 ppm (a and b). Only one signal at $\delta(^{31}P)$ = 134 ppm (s0) lies outside these two regions. As this ^{31}P signal is only observable at the beginning of the reaction it was actually assigned to an intermediate of the oxidative addition. All complex species give one singlet each in the ^{31}P spectrum with exception of complex A showing two doublets (A1 and A2) with a coupling constant of $^2J_{PP} \approx 114$ Hz, which is a typical value for a *cis*-orientation of two phosphorligands.[27-30] Apart from the allyl complexes a not negligible amount of free ligand occurs indicating that ligand **1'** is released during the formation of the different allyl complexes probably connected with a (durable) reduction of the initially ligand-to-Pd ratio of 2:1 for some complex species. In the presence of an excess of cyclohexenyl acetate the ^{31}P signal of reduced Pd**1'**$_2$ cannot be observed, only a small amount of intermediate of the reduction Pd**1'**$_2$EtCl can be observed at the beginning. Therefore, either the oxidative addition of

cyclohexenyl acetate to Pd**1'**$_2$ is too fast to detect any ^{31}P signal of Pd**1'**$_2$ complex or/and the intermediate Pd**1'**$_2$EtCl itself reacts with the cyclohexenyl acetate.

^{1}H^{31}P HMBC measurements revealed that even more new complex species than those observable in 1D spectra have been formed.

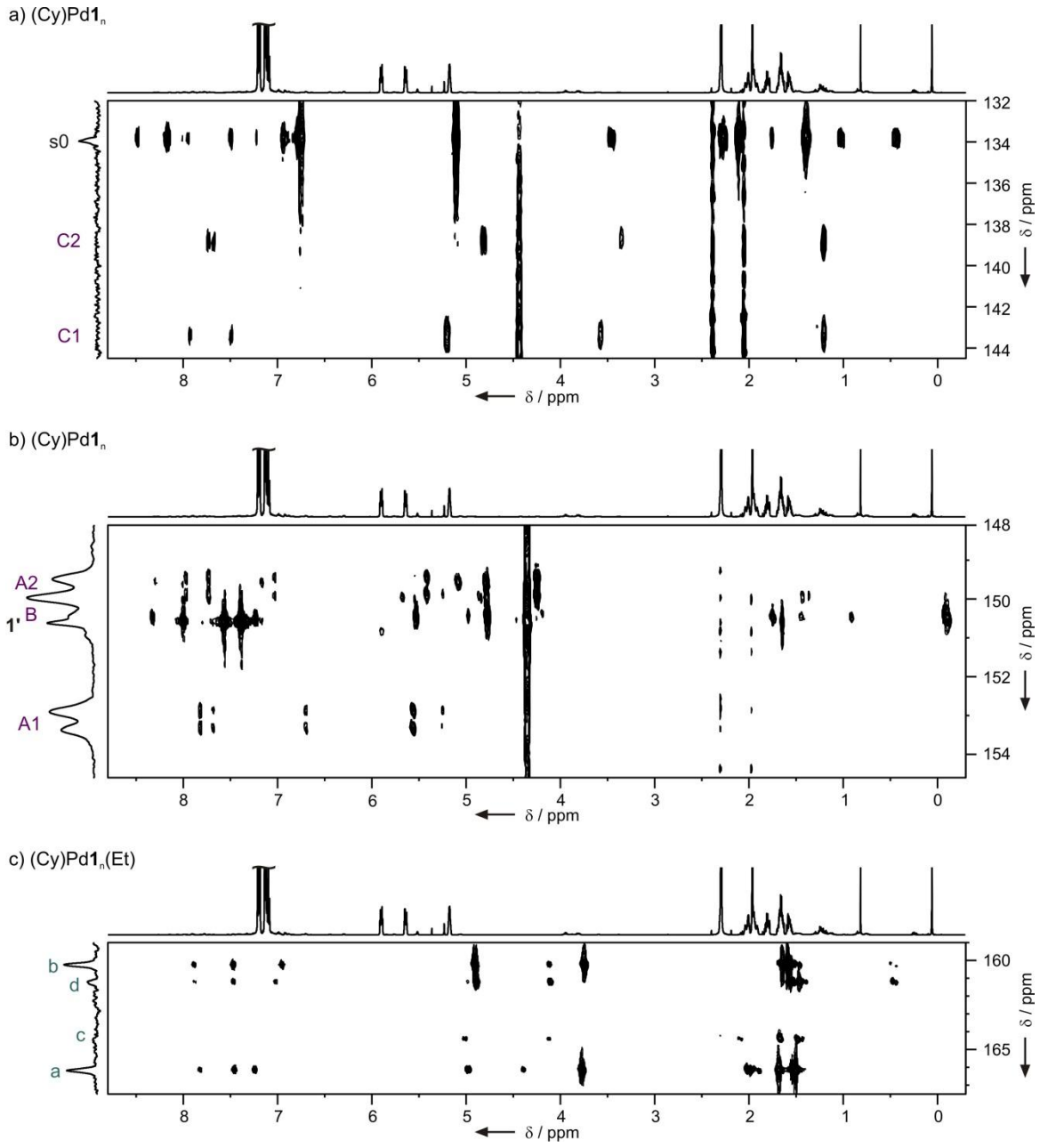

Figure 5.7. Sections of ^{1}H^{31}P HMBC in the region of allyl complexes a) and b) without an Et-group and c) with Et-groups coordinated to Pd.

Apart from the already mentioned allyl complex species A and B further cross signals in that region indicate the formation of another two complex species, the ^{31}P signals of which both completely overlap with that of A1 (Figure 5.7b). However, as number and

intensities of these cross signals are too small to give reliable structural information, these two complex species will not be discussed further. In the region of allyl complexes a and b also two more complex species c and d have been formed (Figure 5.7c). Their cross signals in the $^{1}H^{31}P$ HMBC are very similar to those of a and b indicating a high structural similarity between complexes a and c and between b and d.

Another two rows of cross signals (C1 and C2 in Figure 5.7a) prove the formation of another complex species referred to as complex C with two ^{31}P signals at $\delta(^{31}P)$ = 139.9 and 143.5 ppm showing a doublet splitting (resolution in Figure 5.7a is too low to discern the coupling pattern). The $^{2}J_{PP}$ coupling constant of ~154 Hz indicates a (widened) *cis*-orientation of both phosphorligands similar to complex A. However, complex C and complex species labeled s0 entirely deviate in their ^{1}H chemical shifts from the other allyl complexes and therefore they will be discussed separately later on.

The formed allyl complexes (A, B, a-d) show several - partially very strong - cross signals between $\delta(^{1}H)$ = 3.5 and 6.0 ppm which could be assigned to CH groups of cyclohexenyl coordinated to palladium which in turn clearly proved the addition of cyclohexenyl acetate to palladium. Strikingly, CH signals of the cyclohexenyl in complexes A and B are shifted a little bit downfield by about $\Delta\delta(^{1}H) \approx 0.6$ ppm compared to those in complexes a-d. In addition complexes a-d show two very intensive cross signals each between $\delta(^{1}H)$ = 1.5 and 1.7 ppm which could be assigned to ethyl groups. Similar signals could not be observed for complexes A or B. Therefore, A and B are allyl Pd complexes without ethyl group ((Cy)Pd**1'**$_n$), whereas in complexes a-d aside from cyclohexenyl an ethyl group is also coordinated to Pd ((Cy)Pd**1'**$_n$(Et)).

Complex A. Complex A is one of the major products of the oxidative addition. The two doublet signals at $\delta(^{31}P)$ = 153.6 and 149.7 ppm ($^{2}J_{PP} \approx 114$ Hz, A1 and A2) already expose that this complex contains altogether two phosphorligands **1'** and one cyclohexenyl group. Strong cross signals can be observed in the $^{1}H^{31}P$ HMBC of A1 at $\delta(^{1}H)$ = 5.41 ppm and of A2 at $\delta(^{1}H)$ = 5.55 as well as one common weaker cross signal at $\delta(^{1}H)$ = 5.24 ppm (Scheme 5.8a and b). The allyl ^{1}H signals which show intensive cross signals in the $^{1}H^{31}P$ HMBC to only one particular ligand show cross signals in the $^{1}H^{1}H$ NOESY spectrum to the binaphtol group of the corresponding other ligand (compare Scheme 5.8b and c).

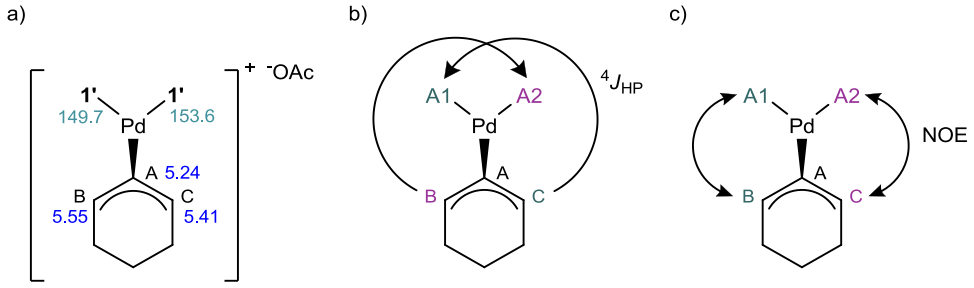

Scheme 5.8. Proposed complex structure of complex A with a) ^{31}P signal assignment to both ligands and ^{1}H signal assignment to allyl-CH groups, b) illustration of the strong $^{4}J_{HP}$ couplings between ligand A1 and A2 and the ally-CH group in *trans*-position and c) illustration of NOEs between ligand A1 and A2 and the ally-CH group in *cis*-position observed in the corresponding 2D NMR spectra.

All these observations indicate that the arrangement of the cyclohexenyl and of both ligands within complex A must be quite fix and inflexible. As a result a pretty strong $^{4}J_{HP}$ coupling between one phosphor ligand and the CH group of the cyclohexenyl in *trans*-orientation can evolve observable by strong cross signal in the $^{1}H^{31}P$ HMBC, whereas the $^{4}J_{HP}$ coupling to the other phosphor ligand in *cis*-orientation is too small to give any cross signal in the $^{1}H^{31}P$ HMBC at all. However, due to their spatial proximity NOEs can be detected between each allyl-CH group and aromatic protons of the phosphor ligand in *cis*-orientation. The coordination of the allyl group (Cy) to palladium via a (delocalized) η^3-coordination in a trigonal planar complex as shown in Scheme 5.8 is in good agreement with the different π-allyl Pd complexes also using phsophoramidite ligands described by Pregosin.[23-25] In addition, the ^{13}C chemical shifts of C_B and C_C are almost identical ($\delta(^{13}C)$ = 88 and 92 ppm, for detailed signal assignment see SI) which excludes a η^1-coordination of the allyl via a σ-bond and moreover also confirms that one phosphorligand must be *trans* to both allyl-CH groups B and C. A possible fourth ligand in this complex would have to be arranged between both phosphorligands, otherwise the complex symmetry was destroyed and C_B and C_C would not have the same ^{13}C chemical shift. However, that would lead to a *trans*-orientation of both phosphorligands, which in turn would cause a much larger coupling constant $^{2}J_{PP}$ (coupling constants of two phosphorligands in *trans*-coordination are usually between 800-1200 Hz). Thus, a fourth ligand within complex A can be excluded. Concerning the CH_2 groups of the cyclohexenyl their ^{1}H chemical shifts range between 0.4 and 2.3 ppm which is in good agreement with the results of the cyclohexenyl palladium complex characterized by the group of Prof. Thiele (Scheme 5.7b).[26]

As already mentioned above recent studies in our working group revealed the affinity of phosphoramidites such as ligand **1'** to form weak ligand-ligand interactions (see also chapter 3 and 4).[17] Thus, because of the *cis*-orientation of both ligands **1'** in complex A the possible formation of inter- and intraligand interactions between A1 and A2 was also

investigated. However, no interligand NOEs between the two phosphoramidites could be observed. Only the upfield shift of the methine and methyl signals of ligand A1 indicates the formation of weak CH-π interactions between the amine group of A1 and the binaphthol group of A2 or of the own ligand.

Complex B. Complex B also contains one allyl (Cy) and no ethyl (Et) group as complex A, but gives only one singlet in the ^{31}P spectrum. Thus, complex B possesses only one phosphorligand or - in case of two phosphorligands per complex - a fast ligand exchange within the complex causes an averaging of the ^{31}P signals. A reliable integration in both 1D and $^{1}H^{13}C$ HSQC spectra and therefore a reliable determination of the number of ligand **1'** in complex B was not possible due to severe signal overlap. However, a difference in the ^{13}C chemical shifts $\Delta\delta(^{13}C)$ of over 19 ppm between C_B and C_C confirms that two ligands with different *trans*-effects must be located opposite to allyl-CH groups B and C:

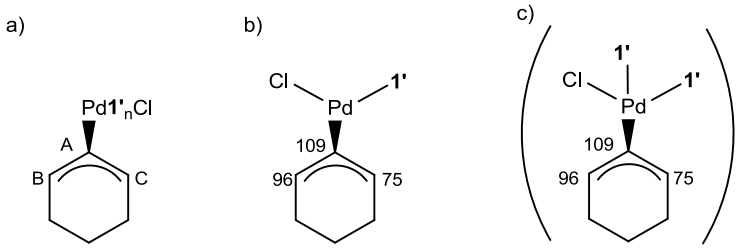

Scheme 5.9. a) Nomenclature of allyl-CH signal assignment for (Cy)Pd**1'**$_n$Cl (n = 1 or 2) and ^{13}C signal assignment for complex B assuming that b) n = 1 or c) n = 2.

According to Pregosin[23] a combination of phosphorligand and chloride ligand (Cl) leads to values up to 20 ppm for $\Delta\delta(^{13}C)$ (see also Scheme 5.6). If indeed a chloride ligand is still coordinated to palladium, complex B was probably not formed by an oxidative addition of cyclohexenyl acetate to complex Pd**1'**$_2$. More likely is a transmetalation of one ethyl group from Et_2Zn to Pd**1'**$_2Cl_2$ followed by a substitution of this ethyl group by cyclohexenyl, eventually under the release of one phosphorligand (see Scheme 5.10).

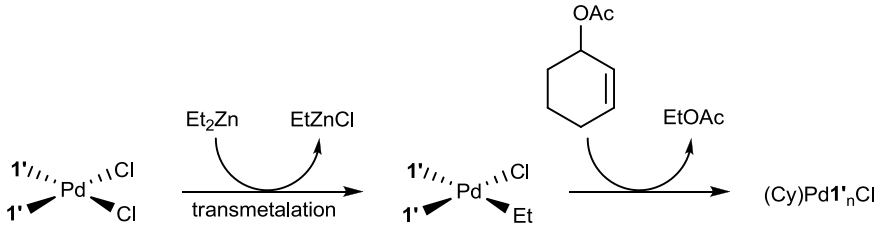

Scheme 5.10. Proposed mechanism for the formation of complex B.

A closer look at the cross signal intensities for complex B in the $^{1}H^{31}P$ HMBC reveals that the cross signal to H_B is very intensive and between $\delta(^{1}H) = 0$ and 2 ppm even cross signals to CH_2 groups of the allyl can be observed (for a detailed signal assignment see SI), which again are in good agreement with the results of the cyclohexenyl palladium complex characterized by the group of Prof. Thiele.[26] However for H_C no cross signal at all can be detected. Therefore, a trigonal planar complex structure with n = 1 becomes more likely than a complex structure with two fast exchanging phosphorligands (compare Scheme 5.9b and c). The $^{4}J_{HP}$ coupling between H_B and the phosphorligand in *trans*-position is quite strong leading to an intensive cross signal in the $^{1}H^{31}P$ HMBC. However, because of the (exclusive) *cis*-position of ligand **1'** referred to H_C $^{4}J_{HP}$ coupling between **1'** and H_C becomes too small to see any cross signal in the $^{1}H^{31}P$ HMBC. In case of a second phosphorligand at least a small cross signal to H_C should be observable in the $^{1}H^{31}P$ HMBC as this second phosphorligand is not in *cis*-orientation to H_C.

Complexes a-d. According to the results discussed so far, complexes a-d can be summarized and structurally described as (Cy)Pd**1'**$_n$(Et). The coordination of both cyclohexenyl (Cy) and ethyl (Et) group was proven by $^{1}H^{31}P$ HMBC in combination with other 2D NMR measurements (for a more detailed signal assignment see SI). Each complex a-d shows only one singlet in the ^{31}P spectra. Integration of the complex signals also exclude that two signals belong to one common (maybe Cl-bridged dinuclear) Pd complex. Thus ^{31}P signals a-d belong to four different complex species. The fact that all complex signals are singlets again indicates that these complexes either contain only one phosphoramidite ligand (n = 1) aside from one cyclohexenyl and one ethyl group leading to a trigonal planar complex structure or - in case of n = 2 – ligand exchange within the complexes is fast on the NMR time scale. Low signal intensities for complexes a-d and severe signal overlap denied a reliable integration in both 1D and $^{1}H^{13}C$ HSQC spectra and therefore a clear determination of n was not possible. Although Feringa proposed a conversion of a π- into a σ-allyl complex after the addition of an ethyl (Et) group (see Scheme 5.1and Scheme 5.4), ^{13}C signal assignment revealed that complexes a-d do not possess a clearly defined double bond but that they still possess a high π-complex character.[23]

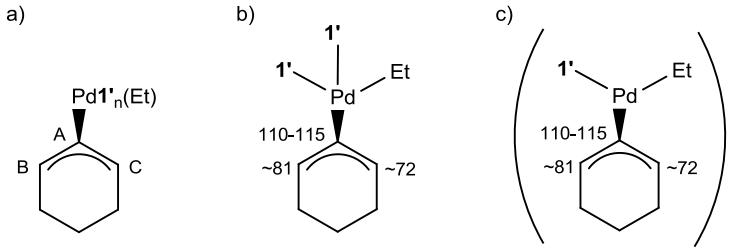

Scheme 5.11. a) Nomenclature of allyl-CH signal assignment for (Cy)Pd**1'**$_n$(Et) and b) ^{13}C signal assignment to the allyl in complexes a-d for b) n = 2 and c) n = 1.

For complexes a-d ^{13}C signals of C_A vary between 110 and 115 ppm, whereas the ^{13}C chemical shifts of C_B and C_C are almost identical for all four complexes at 81 and 72 ppm, respectively (see Scheme 5.11a for nomenclature and b and c for signal assignment). A closer look at signal intensities in the ^{1}H^{31}P HMBC reveals that cross signals to H_C are in general stronger than those to H_B. Therefore a complex structure is proposed with one phosphorligand in pseudo-*trans* orientation to H_C and the ethyl group *trans* to H_B. A second ligand **1'** in complexes a-d seems quite likely (Scheme 5.11b), because in case of trigonal planar complexes such as complex A and probably B no cross signals between the phosphorligands and the ally-CHs in *cis*-position (H_C) could be observed.

Complex C. Apart from two phosphorligands complex C contains no ethyl group but one cyclohexenyl group according to ^{1}H^{31}P HMBC. In addition the $^2J_{PP}$ coupling constant of 154 Hz indicates a *cis*-configuration of both phosphoramidite ligands. However, ^{1}H signal assignment revealed a significant upfield-shift of the allyl CH signals, especially for H_A, compared to all allyl complexes discussed so far.

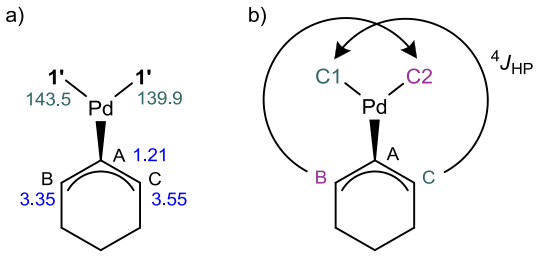

Scheme 5.12. Proposed complex structure of complex C with a) ^{31}P signal assignment to both ligands and ^{1}H signal assignment to allyl-CH groups and b) illustration of the strong $^4J_{HP}$ couplings between ligands C1 and C2 and the ally-CH groups in *trans*-position.

Similar to complex A phosphoramidite ligands C1 and C2 show only one (strong) cross signals to either H_B or H_C (to the one in *trans*-position, see Scheme 5.12b) but both ligands show one common (weaker) cross signal to H_A. Unfortunately the amount of complex C was too low to determine ^{13}C chemical shifts due to low signal intensity. Therefore no more structural information could be obtained from NMR data and no

plausible explanation for the upfield-shifts of ^{1}H signals H_A, H_B and H_C compared to the allyl complexes discussed so far can be proposed.

Complex s0. Although cross signals in the $^{1}H^{31}P$ HMBC are quite strong for this complex species, the species was too transient to obtain any detailed information about its structure by NMR so far. However, chemical shifts of the $^{1}H^{31}P$ HMBC cross signals indicate a still intact double bond of the cyclohexenyl. In addition, strong cross signals in the region between 1.5 and 2 ppm and the shape of these signals in the 1D excerpt of the $^{1}H^{31}P$ HMBC indicate that this complex species also contains an ethyl groups. Therefore it might describe the formation of a σ-Pd complex as proposed by Feringa:[15]

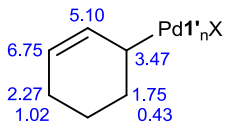

Scheme 5.13. Proposed structure for complex s0 of the oxidative addition step.

Nevertheless further investigations optimized on this complex species will be necessary to prove the exact complex structure.

5.4.3 Pd(S_a,R_c,R_c)-$\mathbf{1}_2Cl_2$ + cyclohexenyl acetate + Et_2Zn

After the addition of a shortfall of Et_2Zn to a solution of Pd$\mathbf{1}_2Cl_2$ and cyclohexenyl acetate the formation of three allyl complexes (a, b and A) could be observed by means of three sharp singlets in the ^{31}P spectra:

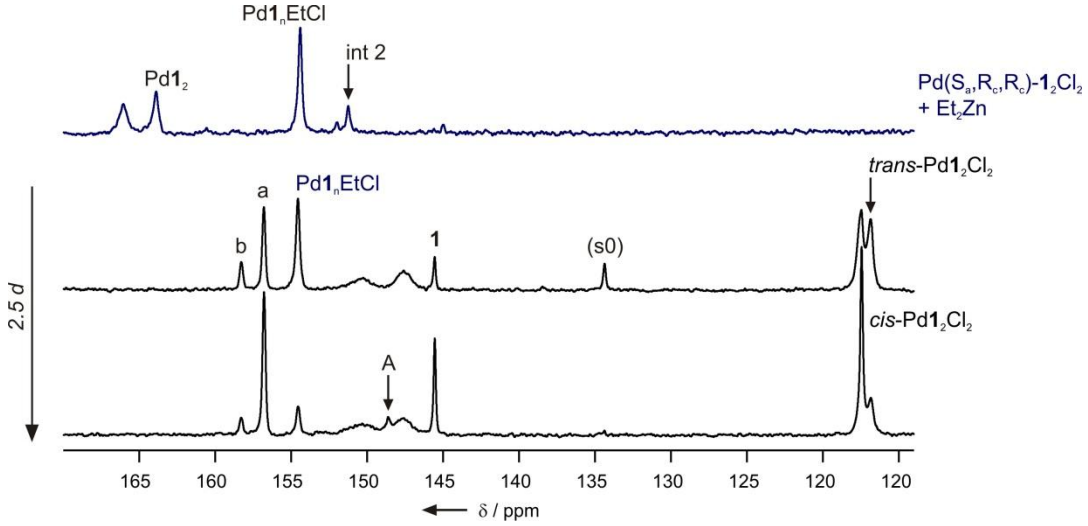

Figure 5.8. ^{31}P spectra of Pd$\mathbf{1}_2Cl_2$ measured in different time intervals after the addition of cyclohexenyl acetate and Et_2Zn over a period of 2.5 d (black). For comparison a ^{31}P spectrum of Pd$\mathbf{1}_2Cl_2$ + Et_2Zn is also shown (blue).

Apart from these three complex signals two further broad signals at $\delta(^{31}P)$ = 147.6 and 150.4 ppm appear. However, these two ^{31}P signals are too broad to give any cross signals in the $^{1}H^{31}P$ HMBC so that no ^{1}H signal assignment was possible and therefore no further information about the complex structure could be obtained. Thus, these complex species will not be discussed in the following. Surprisingly, one intermediate Pd$\mathbf{1}_2$EtCl of the previously investigated reduction of Pd$\mathbf{1}_2Cl_2$ also exists in solution to a quite large amount at the beginning and its ^{31}P signal decreases only very slowly.[31] Additionally the release of ligand **1** could be observed and the ^{31}P signal of another complex species at $\delta(^{31}P)$ = 134 ppm was observable for a short time at the beginning of the reaction. However, almost no cross signals in the $^{1}H^{31}P$ HMBC could be detected for this complex species and therefore no structural information about it could be obtained experimentally. As its ^{31}P chemical shift is almost identical with that of s0 using ligand **1'**, which might be a σ-allyl complex, it is very likely that the structures of both intermediates are also similar.

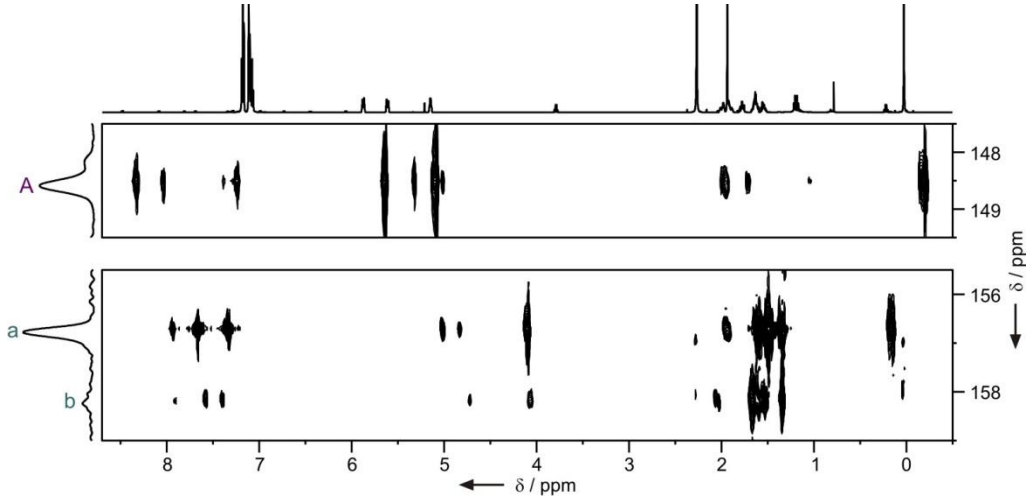

Figure 5.9. Sections of $^{1}H^{31}P$ HMBC in the region of allyl complexes a) without an Et-group and b) with Et-groups coordinated to Pd.

In the $^{1}H^{31}P$ HMBC cross signals to the allyl-CH groups can be observed for complexes A, a and b, which again confirms the addition of cyclohexenyl to Pd (Figure 5.9). Complex species a and b also show strong cross signals in the region between $\delta(^{1}H)$ = 0 and 2 ppm (Figure 5.9b), which could be assigned to ethyl groups on the one side and to CH_2 groups of cyclohexenyl on the other side. Complex A also shows strong cross signals between $\delta(^{1}H)$ = -0.5 and 2 ppm which could be assigned exclusively to CH_2 groups of the cyclohexenyl group (for more detailed signal assignment see SI), which is also in good agreement with the results of the cyclohexenyl palladium complex characterized by the group of Prof. Thiele (Scheme 5.7b).[26] Similar to the previously investigated system using ligand **1'** the ^{31}P complex signals of allyl complexes containing an ethyl group (a and b) are shifted a little bit downfield compared to the allyl complex without ethyl group (A). Moreover the allyl ^{1}H signals of complex A are shifted downfield compared to those of complexes a and b.

Complexes a and b. As already mentioned complexes a and b contain both a cyclohexenyl (Cy) and an ethyl group (Et) and therefore can be summarized and described as (Cy)Pd**1**$_n$Et. For complex a an integration of CH cross signals in the $^{1}H^{13}C$ HSQC[32] revealed a ratio of cyclohexenyl to ligand **1** of 1 : 2. Integration of ^{31}P signals also confirmed that the amount of released ligand is too small for a durable decrease in ligand-to-Pd ratio to (Cy)Pd**1**$_1$Et for complex a. Therefore complex a has a composition of (Cy)Pd**1**$_2$Et. In addition ^{13}C signal assignment revealed that chemical shifts of the allyl-groups are quite similar for both complexes a and b (see Scheme 5.14b and c). Therefore n = 2 was also assumed for complex b.

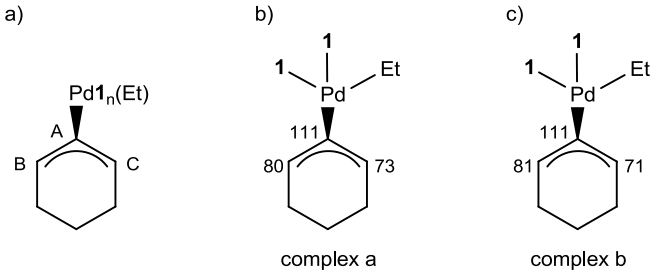

Scheme 5.14. a) Nomenclature of allyl-CH signal assignment for (Cy)Pd**1**$_n$Et in general; ^{13}C signal assignment for b) complex a and c) complex b assuming that n = 2. Ligand arrangement was chosen based on signal intensities in ^{1}H^{31}P HMBC.

A closer look at the intensities of the cross peaks in the ^{1}H^{31}P HMBC revealed, that cross signals between phosphorligand **1** and H_C are much stronger than those to H_B in both complexes which indicates that one phosphorligand is in *trans*-orientation to CH_C while the ethyl group is *trans* to CH_B (Scheme 5.14b and c). Such an arrangement would also be in agreement with a $\Delta\delta(^{13}C)$ of up to 10 ppm between C_B and C_C.

For investigations on the oxidative addition using ligand **1'** (chapter 0) complexes a to d showed the same characteristics in ^{13}C chemical shifts and cross signal intensities in the ^{1}H^{31}P HMBC as complexes a and b using ligand **1**. Therefore, the results obtained for complex a using ligand **1** can be transferred to complexes a-d using ligand **1'** which confirms the already proposed complex structure of (Cy)Pd**1'**$_2$Et for complexes a-d.

Complex A. As already mentioned complex A possesses no ethyl group and therefore is described as (Cy)Pd**1**$_n$. Integration of ^{1}H^{13} HSQC revealed that n = 1. In addition a difference in the ^{13}C chemical shift $\Delta\delta(^{13}C)$ of 21 ppm between C_B and C_C and cross signal intensities in ^{1}H^{31}P HMBC spectrum propose a ligand arrangement in a trigonal planar complex A as shown in Scheme 5.15b with one chloride ligand *trans* to CH_C and with phosphorligand **1** *trans* to CH_B according to the same argumentation as for complex B ((Cy)Pd**1'**Cl) in chapter 0.

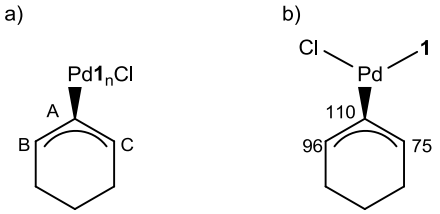

Scheme 5.15. a) Nomenclature of allyl-CH signal assignment for (Cy)Pd**1**$_n$ and b) ^{13}C signal assignment and proposed structure of complex A based on cross signal intensities in ^{1}H^{31}P HMBC.

5.4.4 Summary

For both systems using ligand **1'** or **1** the formation of allyl complexes (Cy)PdL_2(Et) and (Cy)PdLCl could be observed. Furthermore, when using ligand **1'** two complexes [CyPd**1'**$_2$]$^+$ could be identified with a fix arrangement of both ligands and the cyclohexenyl group. Hints for weak interligand interactions between the two phoshoramidites have been found for one of these complexes but the formation of interactions could not clearly be proven. For both systems the release of ligand and the temporary formation of a complex species s0 with δ(^{31}P) = 134 ppm was observed. Cross signals in the ^{1}H^{31}P HMBC suggest an intact double bond of cyclohexenyl within this complex species, which indicates the formation of a σ-complex.

Complexes (Cy)PdLCl are very likely to be formed out of PdL_nEtCl (intermediate of the reduction of PdL_2Cl_2). When using ligand **1** a large and pretty stable amount of Pd**1**$_n$EtCl was observable in the ^{31}P spectra, whereas when using ligand **1'** only a very small amount of Pd**1'**$_n$EtCl was observed only at the beginning of the reaction. Another striking difference between the two systems is their preference to form different allyl complex species: When using ligand **1'** allyl complexes without ethyl group - (Cy)Pd**1'**Cl and [CyPd**1'**$_2$]$^+$ - are formed in preference, whereas when using ligand **1** allyl complex (Cy)Pd**1**$_2$Et is the major product.

For the identification of the correct complex formula integration of ^{1}H^{13}C HSQC - if possible – was used to determine the number of ligand L within one allyl complex species. In addition ^{13}C chemical shifts and cross signal intensities in the ^{1}H^{31}P HMBC have been used for the identification of ligand configurations within the complexes. Following trends could be observed: 1) ^{31}P complex signals of allyl complexes containing an ethyl group are shifted downfield compared to those without an ethyl group and 2) ^{1}H allyl signals of complexes containing an ethyl group are shifted a little bit upfield compared to those without an ethyl group. With exception of complex species s0, all complexes have been interpreted as π-complexes based on studies on different allyl Pd complexes reported by Pregosin.[23-25] ^{1}H chemical shifts of the CH_2 groups of the cyclohexenyl range over the same chemical shift dispersion as those of a cyclohexenyl palladium complex characterized by the group of Prof Thiele.[26] Further investigations on the complex structure of s0 are needed, in order to verify if that transient complex species is really a σ-complex which would correspond to the key-intermediate proposed by Feringa.[15]

5.5 Insertion of Benzaldehyde

5.5.1 Introduction

The last investigated step in this study is the proposed insertion of benzaldehyde into a σ-allyl palladium bond followed by the release of product:

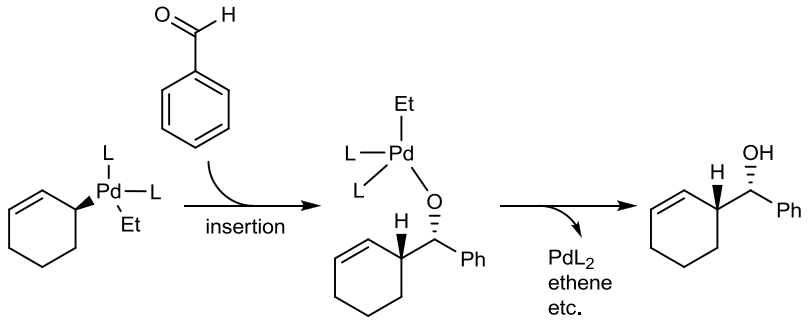

Scheme 5.16. Last step in the catalytic cycle proposed by Feringa: Insertion of benzaldehyde into the Pd-allyl bond followed by the release of product and recovery of the catalyst.[15]

According to literature[15] the η^3-allyl Pd complex have to convert into a η^1-allyl Pd complex in order to undergo an electrophilic allylation of the benzaldehyde. The insertion of benzaldehyde into this σ-allyl Pd bond leads to a chiral alcohol (Scheme 5.16).

Again complex PdL_2Cl_2 was synthesized first, followed by the addition of an excess of both 2-cyclohexenyl acetate and benzaldehyde. Et_2Zn was added subsequently as starting point of the reaction.

5.5.2 Pd(S_a,S_c,S_c)-1'$_2$Cl$_2$ + cyclohexenyl acetate + benzaldehyde + Et$_2$Zn

^{31}P NMR measurements showed that in a sample containing all reactants mainly products of the reduction of Pd**1'**$_2$Cl$_2$ and a large amount of allyl complexes (A-C) exist in solution (for comparison see the colored ^{31}P spectra in Figure 5.10).

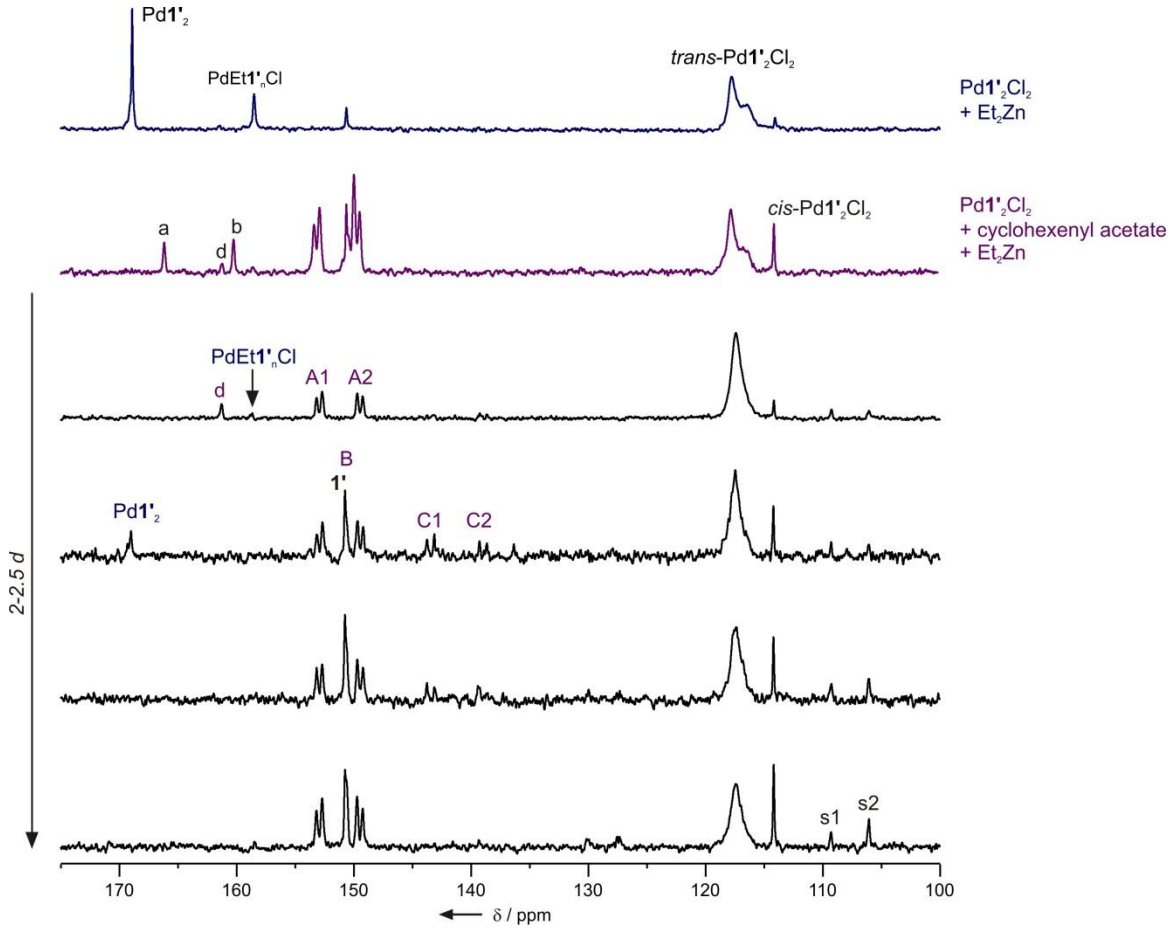

Figure 5.10. ^{31}P spectra of a sample containing Pd**1'**$_2$Cl$_2$ and an excess of cyclohexenyl acetate and benzaldehyde measured in different time intervals after the addition of Et$_2$Zn over a period of ca. 2.5 d (black). For comparison a ^{31}P spectrum of Pd**1'**$_2$Cl$_2$ + Et$_2$Zn (blue) and of a sample Pd**1'**$_2$Cl$_2$ + cyclohexenyle acetate + Et$_2$Zn (purple) is also shown.

At the beginning a small amount of complexes d, PdEt**1'**$_n$Cl$_2$ and Pd**1'**$_2$ are observable in the ^{31}P spectra. In addition a large and stable amount of complexes A and B and also of released ligand **1'** can be observed. Apart from these already known complex species two new ^{31}P complex signals at δ(^{31}P) = 106.1 and 109.3 ppm (s1 and s2) appear. After the run out of Et$_2$Zn, which defines the end of the reaction, no Pd**1'**$_2$ is formed, but only allyl Pd complexes and the two new complex species s1 and s2 exist in solution.

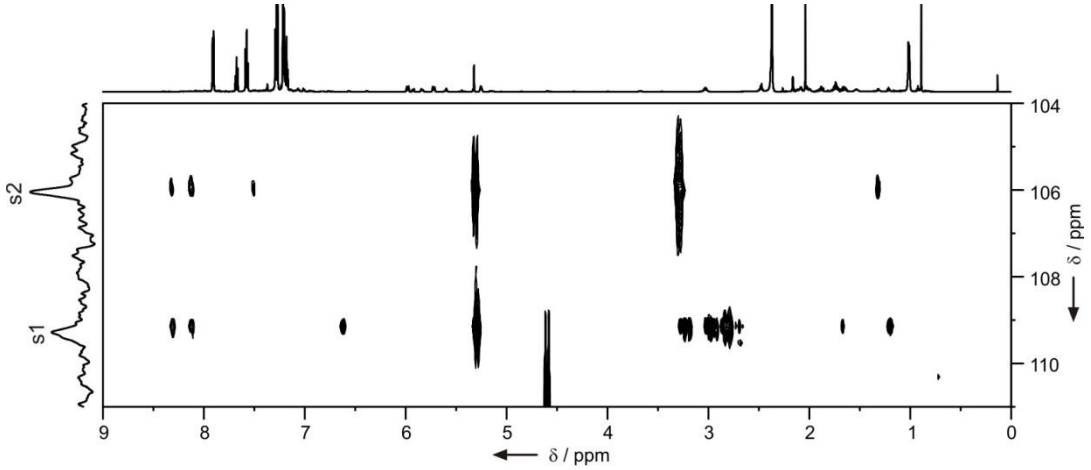

Figure 5.11. Section of a $^{1}H^{31}P$ HMBC in the region of the newly formed complex species s1 and s2.

Cross signals in the $^{1}H^{31}P$ HMBC are quite similar for s1 and s2 (see Figure 5.11), especially signals in the aromatic region are almost identical for s1 and s2. However for s1 more cross signals are observable in total.

Complex s1. For s1 the formation of a σ-complex is proposed with an intact double bond according to appropriate ^{1}H chemical shifts which are very similar to those of the intermediate of the oxidative addition (see Scheme 5.17 and compare Scheme 5.13 in section 0). Unfortunately ^{13}C signal assignment was not possible due to too low signal intensities. The strong cross signals between δ(1H) = 2.8 and 3 ppm have been assigned to ethyl groups.

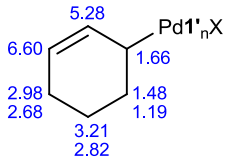

Scheme 5.17. Proposed complex structure and ^{1}H signal assignment for s1 a) as cyclohexenyl Pd complex and b) after the insertion of benzaldehyde.

Interestingly no evidence for the insertion of benzaldehyde into the Pd-allyl bond could be found. However, as complex s1 is only formed in the presence of benzaldehyde it is very likely that s1 at least interacts with benzaldehyde.

Complex s2. As already mentioned cross signals in the $^{1}H^{31}P$ HMBC of s2 are very similar to those of s1 but to a less number and different intensity. Unfortunately no structural information could be obtained for s1 by NMR.

The observed allyl complex species formation observed in Figure 5.10 can be interpreted in two ways: 1) Complexes PdEt**1'**$_n$Cl$_2$, Pd**1'**$_2$ and (Cy)Pd**1'**$_2$(Et) (complexes a-d) are the reactive intermediates and the reaction with benzaldehyde is much faster than the formation of these complexes so that no ^{31}P signals of these complexes can be detected or 2) complexes A and B (allyl complexes without Et groups) are the reactive intermediates, but the interaction with benzaldehyde (formation of s1 and s2) is the rate-determining step of the reaction and therefore much slower than the formation of A and B. Therefore their complex signals can be observed over the whole reaction time period in the ^{31}P spectra.

5.5.3 Pd(S_a,R_c,R_c)-1_2Cl_2 + cyclohexenyl acetate + benzaldehyde + Et_2Zn

In the ^{31}P spectra of a sample containing all reactants using ligand **1** no new complex signals could be detected.

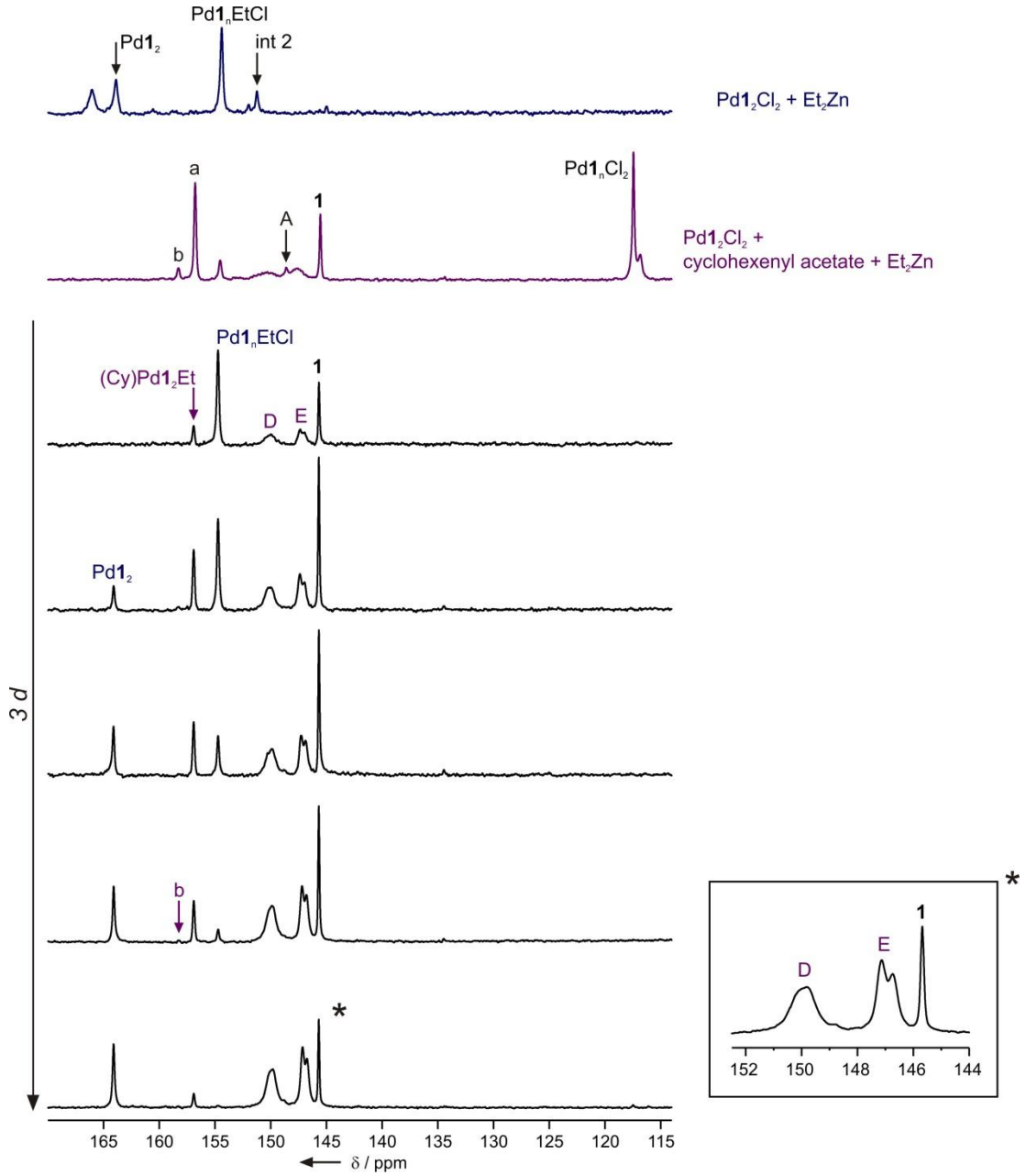

Figure 5.12. ^{31}P spectra of a sample containing Pd**1**$_2Cl_2$ and an excess of cyclohexenyl acetate and benzaldehyde measured in different time intervals after the addition of Et_2Zn over a period of 3 d (black) and an excerpt of the region of complexes D and E (right). For comparison a ^{31}P spectrum of Pd**1**$_2Cl_2$ + Et_2Zn (blue) and of a sample containing Pd**1**$_2Cl_2$ + cyclohexenyle acetate + Et_2Zn (purple) is also shown.

Immediately after the addition of Et_2Zn a large amount of Pd**1**$_n$EtCl and free ligand **1** and a small amount of the allyl complex (Cy)Pd**1**$_2$Et exist in solution. However, the ^{31}P signals of Pd**1**$_n$EtCl and (Cy)Pd**1**$_2$Et decrease by and by probably caused by the run out of

Et_2Zn. At the same time Pd**1**$_2$ is formed and the amount of free ligand and of the allyl complexes with the broad signals between δ(^{31}P) = 146 and 151 ppm (D and E) increases. Therefore it is very likely that both Pd**1**$_n$EtCl and (Cy)Pd**1**$_2$Et are the reactive complex species in the Umpolung reaction, whereas Pd**1**$_2$ is released during the last step of the catalytic cycle unable to continue without Et_2Zn. The increase of complex D and E might either also be ascribed to the run out of Et_2Zn or complex D and E are per se unreactive complex species. Nevertheless the reaction of the allyl complexes with benzaldehyde is too fast to detect any intermediate. In the ^{1}H^{31}P HMBC also no new complexes could be detected.

Although the amount of complexes D and E is much larger than during the investigation of the oxidative addition step, still no cross signals can be observed in the ^{1}H^{31}P HMBC and therefore no new structural information could be obtained. However, signal E turned out to be either a doublet signal or two overlapping singlets (see Figure 5.12 right).

5.5.4 Summary

NMR investigation of the last step of the catalytic cycle was rather unrewarding. Only for ligand **1'** two new complex species could be found. For the first time a η^1-coordination of cyclohexenyl to Pd was proposed with a well-defined double bond and appropriate ^{1}H chemical shifts. Surprisingly no ethyl group and no benzaldehyde could clearly be identified within this complex. However, in the absence of benzaldehyde s1 and s2 are not formed, therefore it is very likely that both complexes also contain or at least interact with benzaldehyde.

After the run out of Et_2Zn complexes (Cy)Pd**1'**$_2$, (Cy)Pd**1'**$_n$Cl and new complexes s1 and s2 are observable in the ^{31}P spectrum when using ligand **1'**, whereas for ligand **1** Pd**1**$_2$ (and allyl complexes of unknown structure) is formed to a large amount.

5.6 Conclusion and Outlook

In summary the diverse steps of the Pd-catalyzed Umpolung reaction were investigated and structural investigations on intermediates of the single steps of the catalytic cycle by NMR are reported. This study also addressed the differences between the use of two diastereomeric ligands **1** and **1'** providing different *ee*-values in the Umpolung reaction. The transmetalation of an ethyl group from zinc to palladium for the reduction of Pd(II) to Pd(0) was proven by $^{1}H^{31}P$ HMBC spectroscopy. Another focus of this study laid on the investigation of the oxidative addition step. The formation of several π-allyl complexes was described and typical ^{1}H and ^{31}P chemical shift ranges for the different complex species were presented. Diverse allyl Pd complexes containing both cyclohexenyl and an ethyl group were characterized with a η^3-coordination of the allyl. Moreover, it could be shown that different complex species - π-allyl complexes with or without an ethyl group attached to palladium – are preferably formed when using ligand **1** or **1'**. Furthermore the formation of σ-allyl complexes, which is the crucial step for the Umpolung of the allyl from electrophilic to nucleophilic, could be detected when using ligand **1'**.

Despite the vast amount of spectroscopic data further investigations are necessary to get more detailed structural information about the different intermediates and to gain some insight into the reaction mechanism. Especially for the last step – the insertion of the benzaldehyde followed by the release of product – further NMR data are needed. In addition low temperature NMR investigations when using ligand **1** and further optimization of the acquisition parameters will be necessary. The preparation of samples with exact defined stoichiometric ratios of the different starting materials is now possible due to the availability of appropriate tools. With the possibility to measure out solutions in µL amounts under Argon atmosphere the exact amount of Et_2Zn for the different steps of the catalytic cycle – for example the reduction of Pd(II) – can be determined.

5.7 Supporting Information

5.7.1 Pd1'$_2$Cl$_2$ + 2-Cyclohexenyl acetate

In order to test if there is any reaction between Pd(II) and cyclohexenyl acetate a sample containing Pd**1'**$_2$Cl$_2$ was investigated.

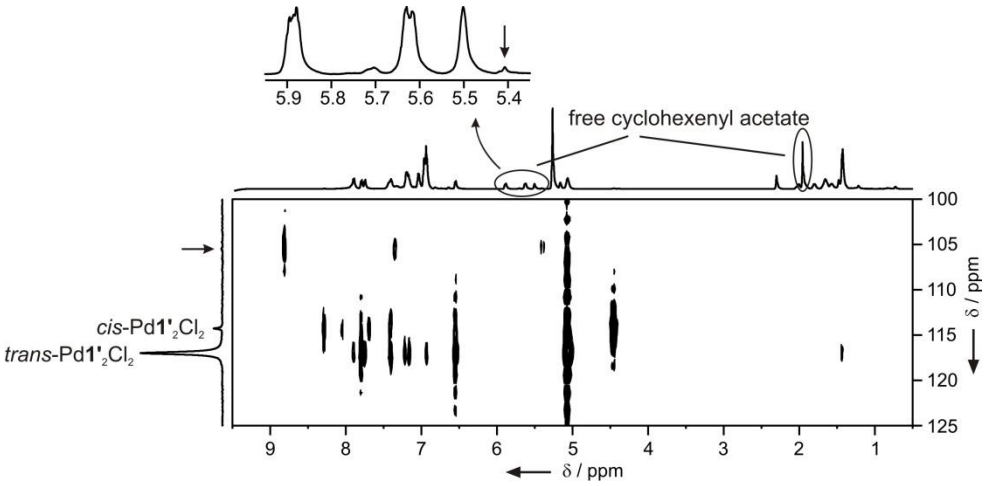

Figure 5.13. Section of a $^{1}H^{31}P$ HMBC in the region of Pd**1'**$_2$Cl$_2$ complexes and of the complex interacting with cyclohexenyl acetate. An excerpt of ^{1}H spectrum shows the signals of free and interacting cyclohhexenyl acetate.

In the ^{31}P spectra only signals of *trans*- and *cis*-Pd**1'**$_2$Cl$_2$ were observed, but no new signals could be detected. However, in the $^{1}H^{31}P$ HMBC a row of cross signals at $\delta(^{31}P)$ = 105.2 ppm (see arrow in Figure 5.13) indicates that a small amount of Pd**1'**$_2$Cl$_2$ interacts with cyclohexenyl acetate. One of the cross signals at $\delta(^{1}H)$ = 5.4 ppm is very similar in shape and chemical shift to one signal of free cyclohexenyl acetate $\delta(^{1}H)$ = 5.5 ppm (see ^{1}H excerpt in Figure 5.13). However, as the amount of the interacting complex is only small and moreover did not increase within a period of 24 h an actual reaction between Pd(II) and cyclohexenyl acetate was excluded.

5.7.2 Oxidation of phosphoramidite ligands

Aside from Pd(0) complexes and corresponding intermediates two other (complex) species are formed after the addition of Et$_2$Zn to Pd**1**$_2$Cl$_2$ with unusual ^{31}P chemical shifts of ~12 and ~70 ppm.

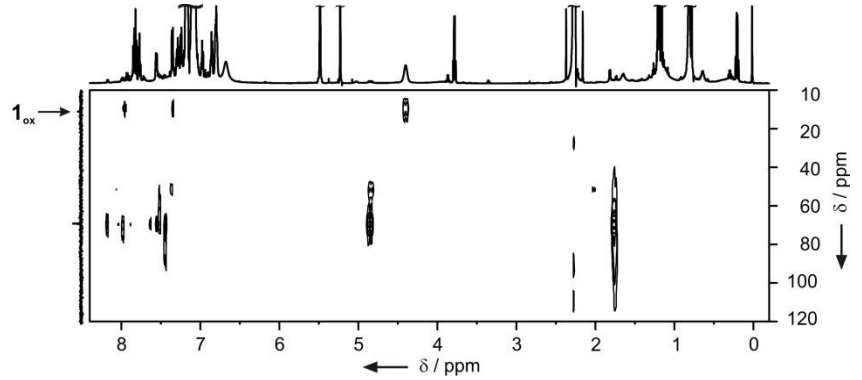

Figure 5.14. Section of a $^{1}H^{31}P$ HMBC in the region of the oxidized ligand and unknown complex species of a sample containing Pd**1**$_2$Cl$_2$ and Et$_2$Zn.

Both ^{31}P signals show intensive cross signals in the aromatic region as well as very strong cross signals to the methine and partially the methyl groups (Figure 5.14). Consequently decomposition products of the ligands can be excluded. Analogous (complex) species with almost identical chemical shifts are also observable when using ligand **1'** (data not shown). It turned out that one of these species ($\delta(^{31}P) \approx 10$ ppm) was also formed in a sample containing only free ligand **1'** and Et$_2$Zn (Figure 5.15). However, no structural information about the second (complex) species could be obtained.

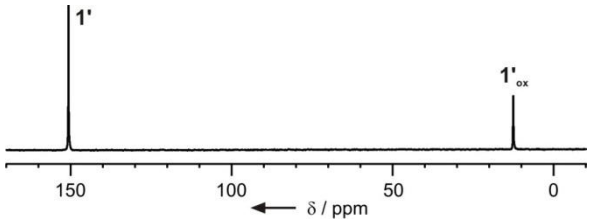

Figure 5.15. ^{31}P spectrum of ligand **1'** after the addition of Et$_2$Zn.

Due to its ^{31}P chemical shift of ~10 ppm this signal was assigned to oxidized phosphoramidite ligands $\mathbf{1_{ox}}$ and $\mathbf{1'_{ox}}$ which was also confirmed by observations made by Feringa.[33]

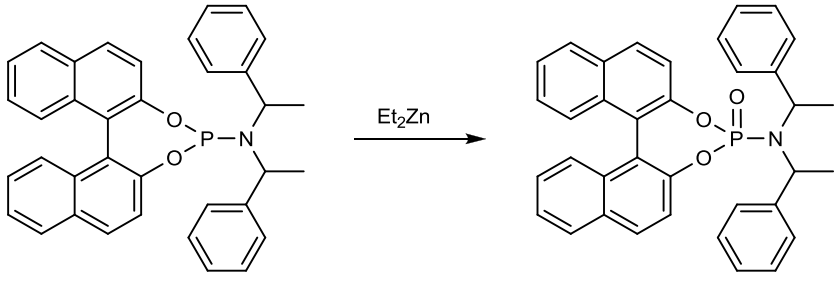

Scheme 5.18. Proposed oxidation of phosphoramidite ligands **1** and **1'** in the presence of Et$_2$Zn

5.7.3 Synthesis of 2-cyclohexenyl acetate[34]

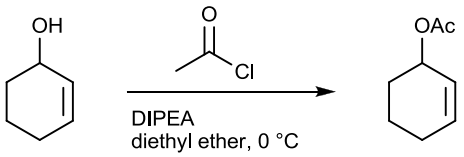

To a solution of 2-cyclohexen-1-ol (5.0 mL, 51 mmol) in 100 mL dry diethyl ether N,N-diisopropylethylamine (DIPEA) (26.5 mL, 153 mmol) and acetyl chloride (4.35 mL, 61.2 mmol) was added at 0°C. After stirring over night at room temperature the reaction mixture was quenched with 10 % aqueous citric acid (30 mL). After washing the etheral layer with brine (2 x 20 mL) it was dried with MgSO4 and filtered. After evaporation of the solvent the crude product was purified by flash column chromatography.

5.7.4 Sample preperation

All reactions were carried out under argon atmosphere in heat gun dried Schlenk flasks using freshly distilled solvents and benzaldehyde. CD_2Cl_2 was distilled from CaH_2. Ligand **1** and **1'** were prepared according to reported protocols[Lit] or bought from Sigma-Aldrich. Pd(cod)Cl_2 was bought from Alfa Aesar. The samples were prepared by adding solvent to a mixture of free ligand and Pd(cod)Cl_2 with a total ligand-to-Pd ration of 2:1. The solution was stirred at room temperature for at least 2-2.5 h before adding and excess of cyclohexenyl acetate and benzaldehyde at 0°C. After further 10 min of stirring Et_2Zn was added as starting point of the reaction. The exact amount of reactants could not be determined due to improper equipment. Sample concentrations used for NMR studies varied between 0.02 and 0.03 M.

5.7.5 NMR data collection and processing

NMR spectra were recorded on a Bruker Avance DRX 600 (600.13 MHz) spectrometer equipped with a 5 mm broadband triple resonance z-gradient probe (maximum gradient strength 53.5 Gauss/cm) and a Bruker Avance III 600 (600.25 MHz) spectrometer, equipped with a TCI cryoprobe with z-gradient (53.5 G/cm). ^{1}H and ^{13}C chemical shifts were referenced to TMS, for ^{31}P chemical shifts the corresponding Ξ value was applied. All measurements were performed at 273 K unless stated otherwise. For the characterization of the different observed complex species detailed 2D NMR spectroscopic investigation have been performed: $^{1}H^{31}P$ HMBC, $^{1}H^{1}H$ COSY, $^{1}H^{1}H$ NOESY, $^{1}H^{13}C$ HSQC, and $^{1}H^{13}C$ HMBC. For appropriate $^{1}H^{1}H$ NOESY measurements mixing times of 750 to 800 ms have been applied. NMR data were processed and evaluated with Bruker Topspin 2.1.

5.7.6 NMR data

Free cyclohexenyl acetate

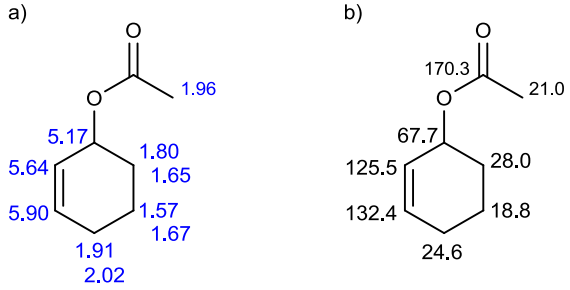

Scheme 5.19. a) ^{1}H and b) ^{13}C signal assignment of free cyclohexenyl acetate.

For NMR data following numbering for the cyclohexenyl group in the different complex species have been applied.

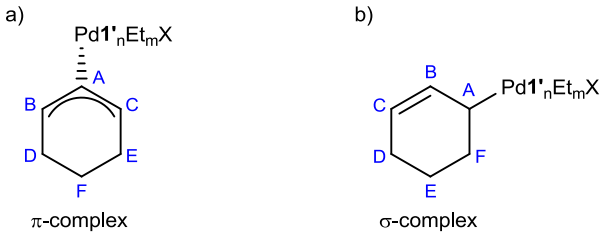

Scheme 5.20. Labeling of cyclohexenyl acetate in a π- or σ-allyl Pd complex.

Investigations using ligand (S_a,S_c,S_c)-1'

Table 5.1. Summary of NMR data of sample Pd**1'**$_2$Cl$_2$ + Et$_2$Zn.

Species	ligand **1'**				ethyl
	δ(^{31}P)/[ppm]	δ(^{1}H)/[ppm]			δ(^{1}H)/[ppm]
		CH_{aromat}	CH	CH_3	
Pd**1'**$_n$EtCl	158.5	7.71 7.65 7.17 6.54	4.55	0.81	1.18 0.85
Pd**1'**$_2$	168.9	7.94 6.83 4.59	4.82	0.32	
1'$_{ox}$	10.5	8.02 7.88 7.49 7.13	4.52	1.61	
unknown species	70.6		4.85	1.77	

Table 5.2. NMR data of different π-allyl Pd complexes formed in a sample Pd**1'**$_2$Cl$_2$ + cyclohexenyl acetate + Et$_2$Zn.

Species		ligand **1'**				cyclohexenyl						ethyl
		δ(^{31}P) [ppm]	δ(^{1}H)/(δ(^{13}C)) [ppm]			δ(^{1}H)/(δ(^{13}C)) [ppm]						δ(^{1}H) [ppm]
						-CH			-CH$_2$			
			CH$_{aromat}$	CH	CH$_3$	A	B	C	D	E	F	
A1	(Cy)Pd**1'**$_2$	149.7	8.05 7.81 7.11	4.33 (54.3)	0.85 (19.7)	5.34 (114.7)	5.65 (88.1)	5.51 (91.9)	1.43 2.33	1.74 0.39	0.82 0.96	x
A2		153.6	7.90 7.77 6.78	5.07 (55.5)	1.21 (20.6)							
B	(Cy)Pd**1'**$_n$Cl	150.6	8.41/(122.8) 7.32/(126.9)	4.86 (54.4)	1.81 (21.4)	5.06 (109.4)	5.61 (95.8)	4.49 (75.2)	1.80 1.51 (27.9)			x
a	(Cy)Pd**1'**$_2$Et	166.2	7.90 7.54 7.32	5.06		5.02 (115.0)	4.47 (80.2)	3.85 (70.6)	2.31 2.08	2.00 1.77	1.60	1.56 1.63
b		160.2	6.97 7.55 7.03			4.98 (113.4)	4.20 (81.6)	3.82 (72.2)	1.62 1.54		0.55	1.66 1.72
c		164.2	7.93 7.56 7.40		(5.09)	5.15 (111.0)	5.09 (80.7)	4.20 (72.1)	2.18 1.48	1.94 1.54	1.38	1.74 1.54
d		161.2	7.12/(122.2) 7.98/(129.8) 7.56/(123.1) 7.97/(129.6)	4.98 (53.8)	1.58 (20.9)	5.06 (110.1)	4.66 (81.1)	4.18 (72.3)	1.96 1.55 (27.4)	1.48 0.55 (26.9)	0.68 1.22 (19.7)	1.55 1.64
σ-complex		134.0	8.48 8.16 8.00 7.94 7.49 7.38 6.93			3.46	6.74 5.10		2.27 1.02 1.75 0.43			1.37 2.10

Table 5.3. NMR data of σ-allyl Pd complex species observed in a sample Pd**1'**$_2$Cl$_2$ + cyclohexenyl acetate + benzaldehyde + Et$_2$Zn.

Species		ligand **1'**				cyclohexenyl						ethyl
		$\delta(^{31}P)$ [ppm]	$\delta(^1H)/(\delta(^{13}C))$ [ppm]			$\delta(^1H)/(\delta(^{13}C))$ [ppm]						$\delta(^1H)$ [ppm]
			CH_{aromat}	CH	CH_3	-CH			-CH_2			
						A	B	C	D	E	F	
s1	(Cy)Pd**1'**$_n$	109.3	8.31 8.11 8.01 7.89 7.50 7.36 7.29			3.21	5.28.	6.60	2.95 2.68		1.66 1.19	2.99 2.82
s2	(Cy)Pd**1'**$_n$	106.1	8.31 8.11 8.01 7.89 7.50 7.36 7.29 7.11			1.65 3.28 5.30 3.27 1.31						x

Investigations using ligand (S_a,R_c,R_c)-1

Table 5.4. Summary of NMR data of the sample Pd**1**$_2$Cl$_2$ + Et$_2$Zn.

Species	ligand **1**				ethyl
	$\delta(^{31}P)$/[ppm]	$\delta(^{1}H)$/[ppm]			$\delta(^{1}H)$/[ppm]
		CH_{aromat}	CH	CH_3	
Pd**1**$_n$EtCl (int 1)	154.4	7.06 7.59 7.82	4.07	1.94	1.33 1.17
int 2	151.2				0.13
unknown complex	166.0	7.10 7.21 7.48 8.01 8.21	4.86	1.78	
Pd**1**$_2$	163.9	7.26 7.36 7.56 7.85	4.42	0.84	
1$_{ox}$	10.4	7.96 7.54 7.35	4.41		
unknown species	70.6	8.18 7.98 7.52 7.45	4.86	1.77	

Table 5.5. NMR data of different allyl-Pd complexes formed in a sample Pd**1**$_2$Cl$_2$ + cyclohexenyl acetate + Et$_2$Zn.

Species		ligand **1'**				cyclohexenyl						ethyl	
		$\delta(^{31}P)$ [ppm]	$\delta(^1H)/(\delta(^{13}C))$ [ppm]			$\delta(^1H)/(\delta(^{13}C))$ [ppm]						$\delta(^1H)/(\delta(^{13}C))$ [ppm]	
						-CH			-CH_2				
			CH_{aromat}	CH	CH_3	A	B	C	D	E	F	-CH_2	-CH_3
a	(Cy)Pd**1**$_2$Et	156.8	7.94 7.66 7.33	5.07 (54.0)	1.06 (20.6)	5.01 (110.5)	4.83 80.2	4.09 73.0	0.14 1.32 27.3	1.52 1.94 27.1	0.65 0.46 19.6	1.59 4.06	1.48 19.7
b	(Cy)Pd**1**$_2$Et	158.3	7.91 7.58 7.39			4.72 111.3	4.75 80.9	4.06 70.7	2.05 1.34	1.08 1.63	0.93 1.67	1.60 1.51	
A	(Cy)Pd**1**$_n$Cl	148.6	8.32 8.03 7.89 7.81 7.74 7.38 7.23	5.09 (54.8)	1.23	5.31 109.5	5.64 96.3	5.00 74.5	1.71 1.95	1.04 -0.19	0.39 0.49	x	

5.8 References

[1] V. Caprio, J. Williams, *Catalysis in Asymmetric Synthesis*, 2nd ed., Wiley, New York, **2009**.

[2] Yin, J. Liebscher, *Chem. Rev.* **2006**, *107*, 133-173.

[3] L. F. Tietze, H. Ila, H. P. Bell, *Chem. Rev.* **2004**, *104*, 3453-3516.

[4] I. P. Beletskaya, A. V. Cheprakov, *Chem. Rev.* **2000**, *100*, 3009-3066.

[5] C. E. I. Knappke, A. Jacobi von Wangelin, *Chemical Society Reviews* **2011**, *40*, 4948-4962.

[6] L. Sikk, J. Tammiku-Taul, P. Burk, *Organometallics* **2011**, *30*, 5656-5664.

[7] L. J. Goossen, D. Koley, H. L. Hermann, W. Thiel, *Organometallics* **2005**, *24*, 2398-2410.

[8] C. Amatore, G. Broeker, A. Jutand, F. Khalil, *J. Am. Chem. Soc.* **1997**, *119*, 5176-5185.

[9] A. L. Casado, P. Espinet, *Organometallics* **1998**, *17*, 954-959.

[10] G. Zanoni, A. Pontiroli, A. Marchetti, G. Vidari, *Eur. J. Org. Chem.* **2007**, *2007*, 3599-3611.

[11] W. Wang, T. Zhang, M. Shi, *Organometallics* **2009**, *28*, 2640-2642.

[12] N. T. Barczak, R. E. Grote, E. R. Jarvo, *Organometallics* **2007**, *26*, 4863-4865.

[13] M. Kimura, M. Shimizu, K. Shibata, M. Tazoe, Y. Tamaru, *Angew. Chem. Int. Ed.* **2003**, *42*, 3392-3395.

[14] G. Zanoni, S. Gladiali, A. Marchetti, P. Piccinini, I. Tredici, G. Vidari, *Angew. Chem. Int. Ed.* **2004**, *43*, 846-849.

[15] G. P. Howell, A. J. Minnaard, B. L. Feringa, *Organic & Biomolecular Chemistry* **2006**, *4*, 1278-1283.

[16] PdL2 is not meant to define the structure of a monomeric Pd(0) complex, but is only used to describe the (overall) ligand-to-Pd(0) ratio. It also includes the possibility of a mixture of different Pd(0) complex species or oligomerization

[17] E. Hartmann, R. M. Gschwind, *in preperation* **2012**.

[18] M. B. Schmid, K. Zeitler, R. M. Gschwind, *Chemical Science* **2011**, *2*, 1793-1803.

[19] M. Nishio, M. Hirota, Y. Umezawa, *The CH/π Interaction: Evidence, Nature, and Consequences*, Wiley, New York, **1998**.

[20] M. Nishio, *PCCP* **2011**, *13*, 13873-13900.

[21] S. Filipuzzi, P. S. Pregosin, M. J. Calhorda, P. J. Costa, *Organometallics* **2008**, *27*, 2949-2958.

[22] For some samples the reduction of Pd(II) to Pd(0) and the following addition of cyclohexenyl acetate causing a re-oxidation of Pd(0) to Pd(II) could be observed by a

temporary blackening of the reaction mixture immediately after the addition of Et_2Zn ($Pd^{II} \rightarrow Pd^0$) and a subsequent re-coloring of the solution from black to yellow ($Pd^0 \rightarrow Pd^{II}$)

[23] S. Filipuzzi, P. S. Pregosin, A. Albinati, S. Rizzato, *Organometallics* **2006**, *25*, 5955-5964.

[24] S. Filipuzzi, P. S. Pregosin, A. Albinati, S. Rizzato, *Organometallics* **2008**, *27*, 437-444.

[25] S. Filipuzzi, P. S. Pregosin, A. Albinati, S. Rizzato, *Organometallics* **2007**, *26*, 5446-5446.

[26] B. Böttcher, V. Schmidts, J. A. Raskatov, C. M. Thiele, *Angew. Chem. Int. Ed.* **2010**, *49*, 205-209.

[27] J. Mason, *Multinuclear NMR*, Plenum Press, New York and London, **1987**.

[28] J. G. Verkade, *Coord. Chem. Rev.* **1972**, *9*, 1-106.

[29] F. B. Ogilvie, J. M. Jenkins, J. G. Verkade, *J. Am. Chem. Soc.* **1970**, *92*, 1916-1923.

[30] R. J. Goodfellow, B. F. Taylor, *J. Chem. Soc., Dalton Trans.* **1974**, 1676-1684.

[31] Repetition of the experiment with a larger amount of Et_2Zn indicates that the run out of Et_2Zn is probably not the reason for the slow conversion of Pd**1**$_2$EtCl

[32] For the determination of the allyl-to-phosphorligand ratio CH signals of the allyl and of the phosphoramidite ligand(s) have been integrated.

[33] M. G. Pizzuti, A. J. Minnaard, B. L. Feringa, *J. Org. Chem.* **2008**, *73*, 940-947.

[34] J. Cossy, L. Tresnard, D. G. Pardo, *Eur. J. Org. Chem.* **1999**, *1999*, 1925-1933.

6 NMR Investigations on Highly Diastereoselective Csp^3-Csp^2 Negishi Cross-Coupling with 1,3-Substituted Cycloalkylzinc Compounds

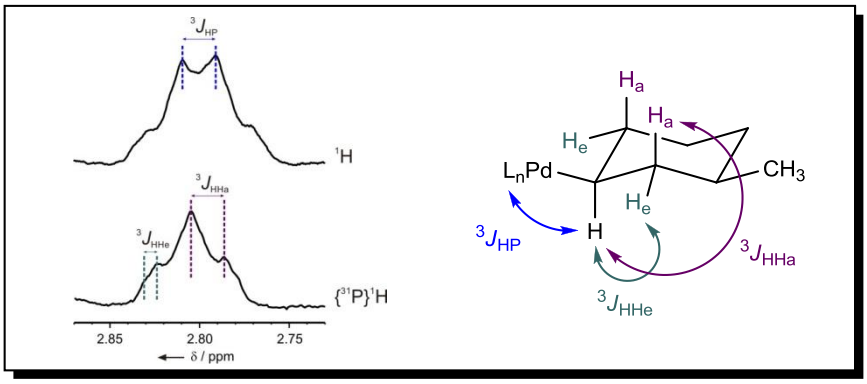

Tobias Thaler, Benjamin Haag, Andrei Gavruyshin, Katrin Schober, Evelyn Hartmann, Ruth M. Gschwind, Hendrik Zipse, Peter Mayer and Paul Knochel

T.T. and A.G. planned, conducted and analysed the experiments. B.H. and H.Z. planned and analysed the DFT calculations. B.H. conducted the DFT calculations. T.T., K.S., E.H. and R.M.G. planned and conducted the NMR experiments. K.S., E.H. and R.M.G. analysed the NMR experiments. P.M. performed the X-ray analysis.

Nature Chemistry, **2010**, *2*, 125-130

DOI: 10.1038/nchem.505

6.1 Abstract

Stereoselective functionalization of organic molecules is of great importance to modern synthesis. The accurate preparation of pharmaceutically active molecules is essential to ensure appropriate biological activity. Thereby, diastereoselective approaches are required for an efficient set-up of multiple stereocenters. In this chapter the remote stereocontrol of a highly diastereoselective Csp^3-Csp^2 Negishi cross-coupling reaction of a 1,3-substituted cyclohexylzinc reagent with aryl halides is discussed. Based on density functional theory (DFT) calculations the stereoselective step in this reaction and the intermediate complex structure was identified by NMR measurements.

6.5 Supporting Information

All reactions were carried out in heat gun-dried Schlenk flasks under argon atmosphere. d^8-THF was freshly distilled from CaH_2.

6.5.1 Preparation of 3-methylcyclohexylmagnesium chloride

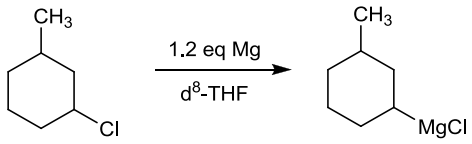

A three-necked 25 mL Schlenk flask was charged with magnesium powder (1.2 eq., 10.6 mmol, 0.260 g) and a catalytic amount of 1,2-diiodoethane (5 mol%). The solids were heated under stirring and reflux with a heat gun until the flask was filled with an iodine-colored gas-phase. After adding 7.4 mL d^8-THF the mixture was heated again to reflux until the color of the iodine vanished. A very strong evolution of ethane gas was observed. Afterwards, a solution of 3-methylcyclohexyl chloride (8.8 mmol, 1.17 g) in 2.6 ml d^8-THF was added dropwise and again the reaction mixture was heated under reflux. Important for the success of the reaction is the creation of hotspots with the heat gun for several short periods. The reaction was stirred further without heating (ca. 1-3 h) until a change of color from brownish-black to colorless-black signaled the end of the reaction.

6.5.2 GC analysis of the reaction mixture of 3-methylcyclohexylmagnesium chloride

The conversion of the reaction was monitored via GC analysis. For that purpose samples of the reaction mixture (0.2 mL each) were quenched with a few drops of water. After extracting the product with a few drops of diethyl ether, the organic phase was used for GC analysis. For reference, a blank sample with 3-methylcyclohexyl chloride in diethyl ether was analyzed.

6.5.3 Determination of the concentration of 3-methylcyclohexylmagnesium chloride

A titration of the reaction mixture to a solution of I_2 in THF until discoloration was performed to determine the concentration of 3-methylcyclohexylmagnesium according to:

$$c(\text{Grignard}) = \frac{n(I_2)}{V(\text{Grignard})}$$

6.5.4 Synthesis of 3-methylcyclohexylzinc chloride

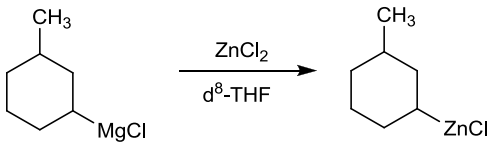

A 25 mL Schlenk tube was charged with $ZnCl_2$ powder (5 mmol, 0.682 g) and heated to 120°C in vacuum under stirring. After 1h dry $ZnCl_2$ was obtained as fine white powder. Afterwards 5 mL d^8-THF was added at 0°C (ice bath). For the transmetalation Grignard solution (0.5 mmol) was added to 0.55 mL of the $ZnCl_2$ solution (0.55 mmol, 1 M) at room temperature and stirred for another 10 minutes.

6.5.5 Sample preparation for NMR investigations

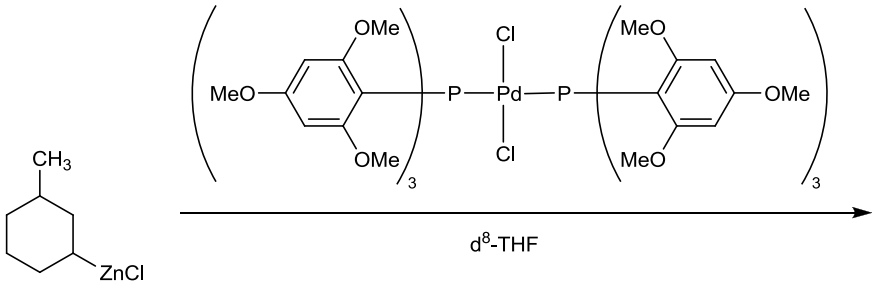

A Schlenk tube was charged with $(TMPP)_2PdCl_2$ (30 – 100 mol%, 0.15 – 0.5 mmol, 186.3 – 558.9 mg). After the addition of 0.4 mL d_8-THF the suspension was cooled to -10°C with an external cryostat (acetone bath). Subsequently 3-methylcyclohexylzinc chloride (0.5 mmol, 1.27 mL) was added slowly causing a color change from orange to brownish-red. For NMR investigation 0.7 ml of the reaction mixture were filtered into a cooled NMR tube.

6.5.6 NMR data collection and processing

NMR spectra were recorded on a Bruker Avance DRX 600 (600.13 MHz) spectrometer equipped with a 5 mm broadband triple resonance z-gradient probe. Temperature was controlled by a Bruker BVTE 3900 temperature unit. NMR data were processed and evaluated with TOPSPIN 2.1. ^{31}P spectra were calibrated using an external H_3PO_4-standard.

6.6 References

[1] D. Milstein, J. K. Stille, *J. Am. Chem. Soc.* **1979**, *101*, 4992-4998.

[2] K. Sonogashira, Y. Tohda, N. Hagihara, *Tetrahedron Letters* **1975**, *16*, 4467-4470.

[3] R. F. Heck, J. P. Nolley, *J. Org. Chem.* **1972**, *37*, 2320-2322.

[4] E. Negishi, A. O. King, N. Okukado, *J. Org. Chem.* **1977**, *42*, 1821-1823.

[5] N. Miyaura, A. Suzuki, *Chem. Commun.* **1979**, 866-867.

[6] C. E. I. Knappke, A. Jacobi von Wangelin, *Chem. Soc. Rev.* **2011**, *40*, 4948-4962.

[7] M. Hesse, H. Meier, B. Zeeh, *Spektroskopische Methoden in der organischen Chemie*, Thieme, Stuttgart, **2005**.

7 Investigations on Intermolecular Interactions of the Highly Efficient OLED Emitter *fac*-Ir(ppy)$_3$ in Solution

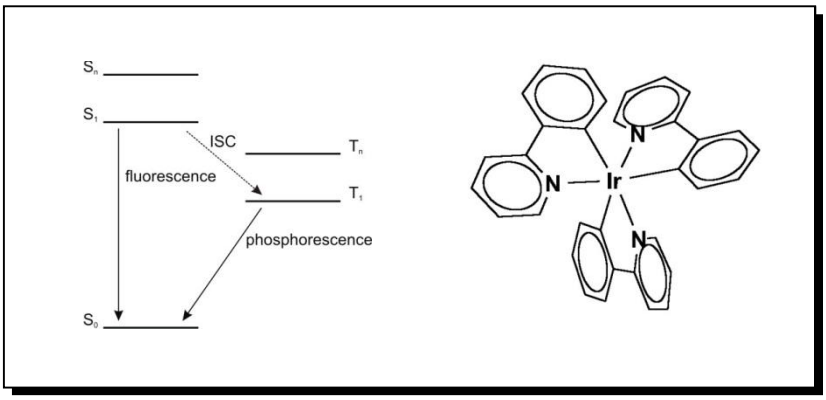

Evelyn Hartmann, Katrin Schober, Ruth M. Gschwind,
Thomas Hofbeck, Tobias Fischer, Hartmaut Yersin

This study was performed in collaboration with Thomas Hofbeck and Tobias Fischer of the group of Prof. Dr. Hartmut Yersin. The DOSY studies were performed in collaboration with Katrin Schober.

7.1 Abstract

Within the last decade an increasing interest in organo-transition metal compounds applied in electro-luminescent devices such as organic light emitting diodes (OLEDs) could be observed. One important advantage lies in their high efficiency as triplet emitters which are up to four times higher compared to pure organic compounds. An essential prerequisite for the actual spin-forbidden triplet-singlet relaxation pathway is the occurrence of spin-orbit couplings (SOCs) which are induced by the central metal. One of the most famous examples among organo-transition metal compounds are $Ir(ppy)_3$ and $[Ru(bpy)_3]^{2+}$. Different studies on the crystal structures of these complexes revealed that the complex structure is slightly distorted in order to optimize CH-π and π-π interactions. As a consequence of this structural distortion a dipole moment is induced leading to a twinning of these complexes in the crystal structures. However, despite exhaustive structural investigations the contributions of CH-π and π-π interactions compared to dipole-dipole interactions could not clearly be estimated so far. Since the SOC process not only depends on the metal but also on the complex structure, NMR investigations on $Ir(ppy)_3$ as a famous representative of triplet emitters were performed. The aggregation trend of $Ir(ppy)_3$ and its dependency on temperature and solvent was investigated by ^1H DOSY measurements. In addition the aggregation mechanism was addressed by disaggregation studies upon the titration of chlorbenzene.

7.2 Introduction

Organic light emitting diodes (OLEDs) embody the new generation of display screen technology applied in television, computer monitors or mobile phones. Since OLED displays work without backlight but directly emit light, they are brighter and provide a better color contrast compared to liquid crystal displays (LCDs). In addition OLEDs can be used on flexible substrates, which enables the fabrication of roll-up displays in fabrics or the preparation of illuminating wallpapers.

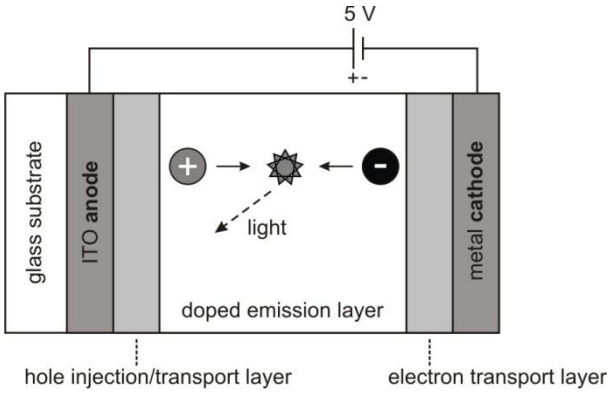

Figure 7.1. Basci set-up of an organic light-emitting diode (OLED).

An OLED device possesses a semiconducting and transparent anode and a metal cathode (see Figure 7.1). The anode, usually an indium tin oxide layer (ITO, a composition of SnO_2 and In_2O_3) is coated on a glass support. When an external potential is applied, electrons are injected from the cathode into the LUMOs of the adjacent electron transporting layer. At the opposite, holes are injected from the ITO anode into the HOMO of the adjacent hole transporting layer. Both charge particles – electron and hole – move towards each other in the direction of the recombination layer, where they can combine and form excitons, excited bound states of an electron and a hole. If this should happen near to emitter molecules which are doped in the recombination layer, the recombination leads to excited states of the emitter molecules which subsequently emit light when they return into the ground state.

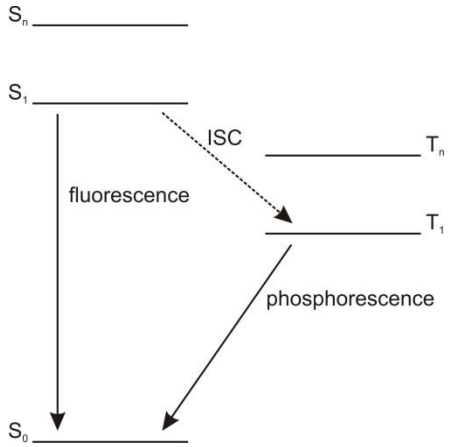

Figure 7.2. Jablonski energy diagram of a triplet emitter compound.

Among emitter materials organic-transition metal compounds have attracted much attention in the last years.[1-2] These so-called phosphorescent materials provide emission from the lowest excited triplet state to the singlet ground state which is actually a formally forbidden transition (see Figure 7.2). However, heavy metals, such as iridium or platinum induce spin-orbit couplings (SOC) which enable spin forbidden transitions. Besides the triplet→singlet phosphorescence processes SOCs also lead to intersystem crossings (ISC) from excited singlet states to the lower emitting triplet state. In contrast, for pure organic emitters the triplet excitons are lost as the transition between the excited triplet state and the singlet ground state is not possible without SOC. Since the recombination of electrons and holes lead to both singlet (25 %) and triplet (75 %) excitons, the triplet harvesting effect of organic transition metal compounds by ISC leads to quantum yields up to 100 % (75 % + 25 %) which is four times higher than achievable with pure organic, fluorescent singlet emitters (max. 25 %).

7.3 Results and Discussion

Complex *fac*-Ir(ppy)$_3$ (ppy = 2-phenyl pyridine anion) has become one of the most applied phosphorescence emitter in the last decades because of its relatively short-lived green emission and its high quantum yield of almost 100 % in a thin film.[3-6] The emission properties of organic-transition metal compounds strongly depend on complex environment and SOC efficiency.[1] Since the efficiency of the SOC process not only depends on the transition metal but also on the complex geometry, detailed structural investigations are of high importance for the development and improvement of new emitters. Investigations of the crystal structure of *fac*-Ir(ppy)$_3$ revealed that π-π stacking and CH-π interactions play an important role for intermolecular interactions.[7] However, distortions within the complex structure also induces a dipole moment which was calculated to 6.5 D for *fac*-Ir(ppy)$_3$. Moreover, a systematic twinning of such complexes could be observed in the crystal structures, which was explained by the attempt of cancelling out the induced dipoles.[8] Despite exhaustive structural investigations the contributions of dispersive and electrostatic interactions on the complex structure could not clearly be identified so far. Therefore, NMR investigations on *fac*-Ir(ppy)$_3$ in solutions were performed in order to gain some insight into interaction mechanisms in solution. For that purpose ^{1}H diffusion measurements in different solvents and at different temperatures have been performed.

7.3.1 Temperature and concentration dependency of complex aggregation

First the aggregation of *fac*-Ir(ppy)$_3$ in deuterated dichlormethane (DCM) and its temperature and concentration dependency was investigated. The complex was readily soluble and stable in DCM and a saturated sample (ca. 10 mmol·L^{-1}) was prepared for diffusion measurements.

Table 7.1. Hydrodynamic volume of ppy and *fac*-Ir(ppy)$_3$ by obtained ^{1}H DOSY measurements of a saturated sample in DCM at different temperature. Aggregation numbers were normalized to the monomeric volume at 300 K.

	Temperature [K]	Hydrodynamic volume [Å^3]	Aggregation number
ppy	300	206	1
fac-Ir(ppy)$_3$	300	733	1
	240	1432	2
	220	1542	2.1
	210	1934	2.6
	200	2442	3.3

At 300 K *fac*-Ir(ppy)$_3$ is monomeric and its experimental hydrodynamic volume of 733 Å^3 lies in the same order of magnitude as the complex volume of 627 Å^3 obtained from the crystal structure.[7] At 240 K the complex is already dimeric and with decreasing temperature the aggregation number further increases up to 3.3 at 200 K. Below 200 K diffusion measurements became unreliable because of precipitation of *fac*-Ir(ppy)$_3$.

Table 7.2. Experimental hydrodynamic volume of *fac*-Ir(ppy)$_3$ obtained by ^{1}H DOSY measurements in DCM with different concentrations. Aggregation numbers were normalized to the monomeric volume at 300 K.

Concentration [mmol L^{-1}]	Temperature [K]	Hydrodynamic volume [Å^3]	Aggregation number
10	300	733	1
10	240	1432	2
2	240	1592	2.2

In order to exclude that the observed aggregation was falsified by too high concentrations the sample was diluted to one fifth of the initial concentration (~2 mmol·L^{-1}). Nevertheless the complex is still dimeric at 240 K. Thus, the observed aggregation at low temperature is a real aggregation and unaffected by solubility effects.

7.3.2 Solvent dependency and aggregation mechanism

Next the influence of the solvent on complex aggregation was investigated. For that purpose samples using deuterated THF and toluene have been applied.

Table 7.3. Experimental hydrodynamic volume of *fac*-Ir(ppy)$_3$ obtained by ^{1}H DOSY measurements in different solvents at 300 K. Aggregation numbers were normalized to the monomeric volume in DCM.

Solvent	Hydrodynamic volume [Å^3]	Aggregation number
DCM	733	1
THF	766	1
Toluene	1443	2.0

Interestingly *fac*-Ir(ppy)$_3$ is monomeric in DCM and THF at 300 K, but in less polar toluene it is dimeric. This observation highly resembles the twinning phenomenon in the crystal structures which was explained by the interaction of induced dipole moments.[7-8] In order to test if dipole-dipole interactions are also dominant in solution, disaggregation studies were performed. For that purpose chlorbenzene was added to a sample of *fac*-Ir(ppy)$_3$ in DCM and diffusion measurements were carried out at 220 K, a temperature at which *fac*-Ir(ppy)$_3$ already aggregates. If aggregation was predominantly determined by CH-π

interactions and/or π-π stacking, chlorbenzene is assumed to compete with the analyte so that a significant disaggregation of *fac*-Ir(ppy)$_3$ should be observable.

Table 7.4. Experimental hydrodynamic volume of *fac*-Ir(ppy)$_3$ obtained by ^{1}H DOSY measurements in pure DCM and after the addition of chlorbenzene at 220 K. Aggregation numbers were normalized to the monomeric volume in DCM at 300 K.

Solvent	Hydrodynamic volume [Å^3]	Aggregation number
DCM	1542	2.1
DCM + Chlorbenzene	1308	1.8

The addition of chlorbenzene causes only a slight disaggregation of *fac*-Ir(ppy)$_3$ so that CH-π and π-π interactions as main aggregation mechanism can be excluded. Thus the disaggregation study confirmed the theory of dipole-dipole interactions as driving force for aggregation in solution.

7.4 Conclusion

Aggregation studies on the highly efficient triplet emitter *fac*-Ir(ppy)$_3$ by ^{1}H DOSY measurements were performed. The general tendency of *fac*-Ir(ppy)$_3$ to aggregate with decreasing temperature could be proven: At 300 K the complex is monomeric in DCM while at 240 K a dimerization of the complex was observed. A further decrease in temperature also causes a further aggregation. Moreover the independency of the observed aggregation from concentration was shown. Investigations on solvent dependency of the aggregation trend revealed that *fac*-Ir(ppy)$_3$ is monomeric in DCM and THF, while in less polar solvent toluene it is already dimeric at 300 K. The addition of chlorbenzene to a sample of dimeric *fac*-Ir(ppy)$_3$ in DCM at 220 K caused only slight disaggregation, which confirmed that complex aggregation was predominantly determined by dipole-dipole interactions and that CH-π and π-π interactions are only subordinate.

Needless to say further studies on the influence of aggregation on emission properties are still required. Nevertheless it is undisputed that distortions in complex structures, which also include aggregation effects, influence the SOC process in the emitter molecules and therefore the light emitting efficiency of a triplet emitter. Thus, the obtained results for the aggregation mechanism of *fac*-Ir(ppy)$_3$ in solution and the dependency of complex-aggregation on the used solvent is of high interest for the development of new matrices and the optimization of emitter properties in OLED dyes.

7.5 Supporting Information

7.5.1 Sample preparation

For NMR investigations *fac*-Ir(ppy)$_3$ was solved in deuterated solvent (5-6 mL) and transferred over a syringe filter (450 µm) into an Argon flashed NMR tube. Potential precipitation appearing upon decreasing temperature was removed with a syringe filter.

7.5.2 NMR data collection and processing

The NMR spectra were recorded on a Bruker Avance DRX 600 (600.13 MHz) spectrometer equipped with a 5 mm broadband triple resonance Z-gradient probe (maximum gradient strength 53.5 Gauss/cm). Temperature stability was controlled by a BVT 3000 unit. NMR data were processed and evaluated with Bruker Topspin 2.1.

Diffusion coefficients were obtained by ^{1}H diffusion NMR measurements using either a LED-sequence or a double-stimulated-echo pulse sequence developed by Jerschow and Müller[9] suppressing convection artefacts. Diffusion delays range between 35 and 80 ms. The experimentally obtained diffusion coefficients were corrected with respect to temperature and viscosity using TMS as internal standard according to the literature known procedure.[10-11] The corrected diffusion coefficients were used to calculate the hydrodynamic radii and volume using a shape factor of c = 4.28 for *fac*-Ir(ppy)$_3$ and c = 4 for ppy.

7.6 References

[1] H. Yersin, A. F. Rausch, R. Czerwieniec, T. Hofbeck, T. Fischer, *Coord. Chem. Rev.* **2011**, *255*, 2622-2652.

[2] H. Yersin, J. Strasser, *Coord. Chem. Rev.* **2000**, *208*, 331-364.

[3] T. Hofbeck, H. Yersin, *Inorg. Chem.* **2010**, *49*, 9290-9299.

[4] C. Adachi, M. A. Baldo, S. R. Forrest, M. E. Thompson, *Appl. Phys. Lett.* **2000**, *77*, 904-906.

[5] M. A. Baldo, S. Lamansky, P. E. Burrows, M. E. Thompson, S. R. Forrest, *Appl. Phys. Lett.* **1999**, *75*, 4-6.

[6] T. Sajoto, P. I. Djurovich, A. B. Tamayo, J. Oxgaard, W. A. Goddard, M. E. Thompson, *J. Am. Chem. Soc.* **2009**, *131*, 9813-9822.

[7] J. Breu, P. Stössel, S. Schrader, A. Starukhin, W. J. Finkenzeller, H. Yersin, *Chem. Mater.* **2005**, *17*, 1745-1752.

[8] J. Breu, H. Domel, A. Stoll, *Eur. J. Inorg. Chem.* **2000**, *2000*, 2401-2408.

[9] A. Jerschow, N. Muller, *J. Magn. Reson.* **1997**, *125*, 372-375.

[10] E. J. Cabrita, S. Berger, *Magn. Reson. Chem.* **2001**, *39*, 142-148.

[11] A. Macchioni, G. Ciancaleoni, C. Zuccaccia, D. Zuccaccia, *Chem. Soc. Rev.* **2008**, *37*, 479-489.

8 Summary

In the field of asymmetric synthesis palladium catalysis finds broad application and several name reactions such as Sonogashira and Stille coupling reactions or the Heck, Negishi and Suzuki cross-coupling, which was recently awarded with the Noble price in 2010, became standard tools in today's synthesis. The right choice of an appropriate chiral ligand is crucial for the stereoselectivity and the successful synthesis of enantiopure chemicals. Raising interest could be observed in the field of monodentate phosphorligands in the last years. Using a combination of two simple monodentate ligands instead of one complex bidentate ligand opened up a new period in asymmetric catalysis. The great success of monodentate ligands is explained by the formation of noncovalent ligand-ligand interactions in the coordination sphere of the metal center. Thus by such a self-assemble two monodentate ligands can imitate the structural features of a classical bidentate, chelating ligand. Among monodentate ligands phosphoramidites became a 'privileged class of ligands'. Despite several studies on diverse transition metal complexes there is still need for structural investigations on interaction mechanics of this class of ligands.

This thesis mainly focuses on the NMR spectroscopic structural investigation of phosphoramidite palladium complexes and the inter- and intraligand interaction patterns within these complexes. For the first time the pseudo-bidentate character of this class of ligands in solution was proven on *cis*-Pd complexes, which structurally highly resemble the corresponding crystal structures. Each investigated complex exhibited altogether four interaction sites, two inter- and two intraligand interaction sites and moreover the additivity of the formed interaction patterns was proven: Upon specific structurally changes within one of these interaction sites the residual interaction patterns are hardly affected and the general complex structure is retained. Moreover the coexistence of interactions - mainly based on CH-π and π-π interactions - and rotational processes was addressed. In the course of this study the role of the amine side chain NR(CH)Ar of phosphoramidite ligands is discussed which is supposed to form a planar interaction surface relevant for catalysis. We claim that interactions of this planar surface with the substrate lead to a precoordination of the substrate to the catalytic metal center. Depending on the configuration of the amine side chain the resulting interaction mode determines the relative orientation of the substrate towards the catalytic center and therefore controls the stereoselectivity.

The theory of interaction surfaces of both the biaryl backbone and the amine side chains of phosphoramidite ligands was also transferred to other complexes of different

transition metals. It was shown that the aggregation trends of phosphoramidite transition metal complexes is purely ligand dominated and independent of the transition metal or even the complex structure. This finding opened up the implementation of a new fast and easy method for the optimization of catalysis in terms of reaction temperature in an early development state. Furthermore it was shown that the validity of a ligand dominated aggregation is limited to phosphoramidites containing an NR(CH)Ar amine side chain which is capable to form an interaction surface essential for both aggregation and stereoselectivity in transition metal catalysis.

In the course of the investigations of intermolecular interactions a method is presented to quantify the free energy difference between two heterocomplexes $MLL'X_n$. Moreover, for the first time the separation of supramolecular CH-π and π-π interactions in the coordination sphere from stereoelectronic and electrostatic interactions close to the metal center is presented. Thus the energetically stabilization of one heterocomplex compared to another by pure noncovalent ligand-ligand interactions can be determined. The reliability of the presented method was proven on the example of two phosphoramidite Pd complexes. Complex structures and interaction patterns were characterized by ^{1}H chemical shift analyses and $^{1}H^{1}H$ NOESY measurements and in addition these results were correlated to the calculated stabilization energy.

Another part of the thesis deals with mechanistic studies on different coupling reactions using palladium catalysts. Based on $^{1}H^{31}P$ HMBC and a combination of various 2D NMR spectra structural investigations on intermediates of the Pd catalyzed Umolung reaction between 2-cyclohexenyl acetate and benzaldehyde are presented. The focus of these investigations lies on mechanistic differences between the employments of two diastereomeric phosphoramidite ligands providing different enantioselectivities. Besides various π-allyl palladium complexes the formation of σ-allyl complex species is described which is supposed to be the key intermediate for the Umpolung of the allyl from electrophilic to nucleophilic.

Aside from the structural investigations on phosphoramidite Pd complexes the remote stereocontrol of a highly diastereoselective C_{sp^3}-C_{sp^2} Negishi cross coupling reaction of a 1,3-substituted cyclohexyl zinc chloride with aryl halides catalyzed by $(TMPP)_2PdCl_2$ (TMPP: tris(2,4,6-trimethoxyphenyl)phosphine) was investigated. By a careful optimization of measuring parameters the stereoselective step and the crucial palladium intermediate could unambiguously be characterized by NMR. Based on DFT calculations it was shown that after a diastereoselective transmetalation of the cyclohexyl compound from zinc to

palladium exclusively the most stable palladium intermediate with all substituents in equatorial position is formed.

In respect of intermolecular interactions the aggregation behavior of the organo-transition metal complex *fac*-Ir(ppy)$_3$ was investigated. This compound is a famous and high efficient triplet-emitter applied in electro-luminescent devices such as organic light emitting diodes (OLEDs). The mechanistic insights into structure changing processes, which also include aggregation, are crucial for the development of new matrices and the optimization of emitter properties. Therefore, the dependency of aggregation on temperature, concentration and solvent was investigated by ^{1}H DOSY measurements. Based on these studies the aggregation mechanism of Ir(ppy)$_3$ by mainly dipole-dipole interactions with only a small percentage of CH-π and π-π stacking was identified, which was additionally confirmed by disaggregation studies.

In summary this thesis predominantly deals with the NMR spectroscopic investigation of different phosphoramidite palladium complexes and the interaction patterns within these complexes. The structural insight into inter- and intraligand interactions in palladium complexes using highly selective phosphoramidite ligands and the analyses of general structural motifs and interaction sites of this class of ligands deliver valuable information for the design and optimization of new catalysts. In addition the mechanistic studies on different Pd-catalyzed reactions such as the Umpolung reaction or the Negishi cross coupling essentially contributed to the elucidation of intermediate structures.

9 Zusammenfassung

Auf dem Gebiet der asymmetrischen Synthese findet die Palladium-Katalyse häufige Anwendung und etliche Namensreaktionen wie z.B. die Sonogashira und Stille Kupplung oder die Heck, Negishi und Suzuki Kreuzkupplung, welche erst kürzlich im Jahr 2010 mit dem Nobelpreis ausgezeichnet wurden, zählen bereits zu Standardmethoden in der heutigen Synthese. Die Wahl des richtigen chiralen Liganden ist ausschlaggebend für die korrekte Stereoselektivität und die erfolgreiche Synthese enantiomerenreiner Substanzen. In den letzten Jahren konnte ein wachsendes Interesse für einzähnige Liganden beobachtet werden. Der Gebrauch von zwei, strukturell einfachen, einzähnigen Liganden anstelle eines komplexen zweizähnigen Chelatliganden läutete den Anfang einer neuen Ära in der asymmetrische Katalyse ein. Der überragende Erfolg einzähniger Liganden wird durch die Bildung von nicht-kovalenten Ligand-Ligand-Wechselwirkungen in der Koordinationssphäre des Metallzentrums erklärt. Durch eine derartige Selbstanordnung können zwei einzähnige Liganden die strukturellen Eigenschaften eines klassischen zweizähnigen Chelatliganden nachahmen. Unter den einzähnigen Liganden gehören Phosphoramidite zu einer bevorzugten Ligandklasse. Allerdings besteht trotz vieler Studien zu verschiedenen Übergangsmetallkomplexen immer noch einen großer Bedarf an strukturellen Untersuchungen von Wechselwirkungsmustern dieser Ligandklasse.

Diese Arbeit konzentriert sich auf NMR-spektroskopische Strukturuntersuchungen von Phosphoramidit-Palladiumkomplexen sowie deren Inter- und Intraligand-Wechselwirkungsmustern. Zum ersten Mal wurde anhand von *cis*-Palladiumkomplexen, deren Strukturen stark denen der entsprechenden Kristallstrukturen ähneln, der pseudo-zweizähnige Charakter dieser Ligandklasse in Lösung nachgewiesen. Jeder untersuchte Komplex weist insgesamt vier Wechelwirkungsstellen auf, zwei Inter- sowie zwei Intraligand-Wechselwirkungen. Darüber hinaus wurde die Additivität dieser Wechselwirkungsmuster nachgewiesen: Bei einer strukturellen Modifikation einer Wechselwirkungsstelle bleiben die restlichen Wechselwirkungen nahezu unverändert und die allgemeine Komplexstruktur bleibt erhalten. Zusätzlich wurde die Dualität von Wechselwirkungen, welche überwiegend auf CH-π und π-π Wechselwirkungen beruhen, und Rotationsprozessen diskutiert. Im Zuge dieser Studie wurde ebenfalls die Rolle der Aminseitenkette NR(CH)Ar von Phosphoramiditen erörtert, welche vermutlich eine Wechelwirkungsfläche bildet, die auch für die Katalyse relevant ist. Wir behaupten, dass diese Fläche mit dem Substrat wechselwirkt und somit eine Präkoordination des Substrats zum katalytischen Zentrum bewirkt. Je nach Konfiguration der Aminseitenkette bestimmt

das daraus resultierende Wechselwirkungsmuster die relative Anordnung des Substrats zum katalytischen Zentrum und kontrolliert somit die Stereoselektivität.

Die Theorie der Wechselwirkungsflächen von sowohl Biarylrückgrat als auch Aminseitenkette von Phosphoramiditliganden wurde auch auf andere Komplexe verschiedener Übergangsmetalle übertragen. Es wurde gezeigt, dass die temperaturabhängige Aggregation von Phosphoramidit-Übergangsmetallkomplexen rein Ligand-bestimmt ist und somit von Übergangsmetall sowie von Komplexstruktur unabhängig ist. Diese Erkenntnis ermöglichte die Einführung einer neuen, schnellen und einfachen Methode zur Katalyseoptimierung bezüglich Reaktionstemperatur, welche bereits zu einem frühen Zeitpunkt des Optimierungsprozesses möglich ist. Darüber hinaus wurde gezeigt, dass die Gültigkeit dieser Ligand-dominierten Aggregation auf Phosphoramidite beschränkt ist, welche eine Aminseitenkette der Art NR(CH)Ar besitzen und somit eine Wechselwirkungsfläche ausbilden können, die sowohl für die Aggregation als auch für die Stereoselektivität in der Übergangsmetallkatalyse von grundlegender Bedeutung ist.

Im Hinblick auf die Untersuchung von intermolekularen Wechselwirkungen wurde eine neuartige Methode vorgestellt, die es erlaubt die freie Energiedifferenz zwischen zwei Heterokomplexen MLL'X_n quantitativ zu bestimmen. Darüber hinaus wurde zum ersten Mal die Unterscheidung von supramolekularen CH-π- und π-π-Wechselwirkungen in der Koordinationssphäre eines Übergangsmetallkomplexes von stereoelektronischen und elektrostatischen Wechselwirkungen am Metallzentrum gezeigt. Dadurch wird die Berechnung der Stabilisierungsenergie eines Heterokomplexes im Vergleich zu einem anderen Heterokomplex durch rein nicht-kovalente Ligand-Ligand-Wechselwirkungen ermöglicht. Die Anwendbarkeit der vorgestellten Methode wurde anhand von zwei Phosphoramidit-Palladiumkomplexen nachgewiesen. Komplexstrukturen sowie Wechselwirkungsmuster wurden durch ^{1}H chemische Verschiebungsanalysen und ^{1}H^{1}H NOESY Messungen charakterisiert und mit der berechneten Stabilisierungsenergie korreliert.

Ein weiterer Teil dieser Arbeit beschäftigt sich mit mechanistischen Studien zu unterschiedlichen Pd-katalysierten Kupplungsreaktionen. Basierend auf ^{1}H^{31}P HMBC und einer Kombination verschiedener 2D NMR-Spektren wurden Strukturuntersuchungen von Intermediaten der Pd-katalysierten Umpolungsreaktion von 2-Cyclohexenylacetat und Benzaldehyd untersucht. Der Schwerpunkt dieser Untersuchungen liegt auf den mechanistischen Unterschieden beim Einsatz diastereomerer Phosphoramiditliganden, welche sich in ihrer Enantioselektivität unterscheiden. Neben verschiedenen π-Allylpalladiumkomplexen wird die Bildung von σ-Allylkomplexspezies beschrieben,

welche sehr wahrscheinlich Schlüsselintermediate bei der Umpolung des Allyls von einem Elektrophil zum Nukleophil darstellen.

Neben Strukturuntersuchungen von Phosphoramidit-Palladiumkomplexen wurde auch die Stereokontrolle einer hochdiastereoselektiven Csp^3-Csp^2-Negishi Kreuzkupplung eines 1,3-substituierten Cyclohexylzinkchlorids mit Arylhalogeniden katalysiert von $(TMPP)_2PdCl_2$ (TMPP: Tris(2,4,6-trimethoxyphenyl)phosphan) untersucht. Durch die sorgfältige Optimierung der Messparameter konnte der stereoselektive Schritt und das entscheidende Palladiumintermediat eindeutig mit NMR-Spektroskopie charakterisiert werden. Basierend auf DFT-Rechnungen wurde gezeigt, dass nach einer diasteroselektiven Transmetallierung der Cyclohexylgruppe von Zink auf Palladium ausschließlich das stabilste Palladiumintermediat mit allen Substituenten in äquatorialer Position gebildet wird.

Im Hinblick auf intermolekulare Wechselwirkungen wurde auch das Aggregationsverhalten des Organo-Übergangsmetallkomplexes *fac*-$Ir(ppy)_3$ untersucht. Dieser Komplex ist ein bekannter und hocheffizienter Triplet-Emitter, der in elektrolumineszierenden Einheiten wie organischen Leuchtdioden (OLEDs) zum Einsatz kommt. Der mechanistische Einblick in strukturverändernde Prozesse, welche auch die Aggregation miteinschließen, ist grundlegend für die Entwicklung neuer Matrizen und die Optimierung von Emittereigenschaften. Daher wurde die Abhängigkeit der Aggregationstendenz von Temperatur, Konzentration und Lösungsmittel mit Hilfe von ^{1}H DOSY Messungen untersucht. Anhand dieser Studien konnte nachgewiesen werden, dass die Aggregation von *fac*-$Ir(ppy)_3$ hauptsächlich über Dipol-Dipol-Wechselwirkungen mit nur einem gewissen Anteil an CH-π- und π-π-Wechselwirkungen abläuft, was zusätzlich durch Desaggregationsstudien bestätigt wurde.

Zusammenfassend handelt diese Arbeit überwiegend von NMR-spektroskopischen Untersuchungen verschiedener Phosphoramidit-Palladiumkomplexe und den Wechselwirkungsmustern innerhalb dieser Komplexe. Der strukturelle Einblick in sowohl Inter- als auch Intraligand-Wechselwirkungen in Palladiumkomplexen bei der Verwendung hochselektiver Phosphoramiditliganden und die Analyse von allgemeinen Wechsel-wirkungsmotiven dieser Ligandklasse bietet wertvolle Informationen für die Entwicklung und Optimierung neuer Katalysatoren. Darüber hinaus haben die mechanistischen Untersuchungen der Pd-katalysierten Umpolungsreaktion und der Negishi Kreuzkupplung essentiell zur Aufklärung von Intermediatstrukturen beigetragen.